HZDR-066

TOPFLOW-EXPERIMENTS ON DIRECT CONDENSATION AND BUBBLE ENTRAINMENT

Tobias Seidel, Dirk Lucas, Matthias Beyer

Wissenschaftlich Technische Berichte
HZDR-066 · ISSN 2191-8708

WISSENSCHAFTLICH-
TECHNISCHE BERICHTE

HZDR
HELMHOLTZ
ZENTRUM DRESDEN
ROSSENDORF

Wissenschaftlich-Technische Berichte

HZDR-066

Tobias Seidel, Dirk Lucas, Matthias Beyer

TOPFLOW-Experiments on Direct Condensation and Bubble Entrainment

Druckausgabe: ISSN 2191-8708

Elektronische Ausgabe: ISSN 2191-8716

Qucosa: http://fzd.qucosa.de/startseite/

2016

Herausgegeben vom

Helmholtz-Zentrum Dresden - Rossendorf

Bautzner Landstraße 400

01328 Dresden

Germany

Technischer Fachbericht

TOPFLOW-Experimente zur direkten Kontaktkondensation und zum Blasenmitriss

Technical Report

TOPFLOW-Experiments on Direct Condensation and Bubble Entrainment

Reaktorsicherheitsforschung-Vorhaben-Nr./
Reactor Safety Research-project No.: 150 1411

Vorhabenstitel: **TOPFLOW-Experimente, Modellentwicklung und Validierung zur Qualifizierung von CFD-Codes für Zweiphasenströmungen**

Project Title: **TOPFLOW experiments, development and validation of models qualifying of CFD codes for two-phase flows**

Autoren / Author(s): **T. Seidel, D. Lucas, M. Beyer**

Dienststelle der Autoren /
Performing Organisation: **Helmholtz-Zentrum Dresden-Rossendorf**
Institut für Sicherheitsforschung

Berichtsdatum / Publication Date: **Januar 2016**

Berichts-Nr. / Report-No.: **HZDR-066**

Gefördert durch:

Bundesministerium
für Wirtschaft
und Energie

aufgrund eines Beschlusses
des Deutschen Bundestages

Das diesem Bericht zugrundeliegende Vorhaben wurde mit Mitteln des Bundesministeriums für Wirtschaft und Energie unter dem Förderkennzeichen 150 1411 gefördert. Die Verantwortung für den Inhalt dieser Veröffentlichung liegt bei den Autoren.

Berichtsblatt

1. ISBN oder ISSN 2191-8708	2. Berichtsart Technischer Fachbericht
3. Titel TOPFLOW-Experimente zur direkten Kontaktkondensation und zum Blasenmitriss	
4 Autor(en) [Name(n), Vorname(n)] T. Seidel, D. Lucas, M. Beyer	5. Abschlussdatum des Vorhabens 31.12.2015
	6. Veröffentlichungsdatum Januar 2016
	7. Form der Publikation Broschüre
8. Durchführende Institution(en) (Name, Adresse) Helmholtz-Zentrum Dresden-Rossendorf Institut für Fluiddynamik Bautzner Landstr. 400 01328 Dresden	9. Ber.Nr. Durchführende Institution HZDR-066
	10. Förderkennzeichen 150 1411
	11. Seitenzahl 69
13. Fördernde Institution (Name, Adresse) Bundesministerium für Wirtschaft und Energie (BMWi) 11019 Berlin	12. Literaturangaben
	14. Tabellen
	15. Abbildungen
16. Zusätzliche Angaben	
17. Vorgelegt bei (Titel, Ort, Datum)	
18. Kurzfassung Die direkte Kontaktkondensation zwischen Wasserdampf und Wasser spielt ebenso wie ein Mitriss von Dampfblasen unter die Wasseroberfläche bei verschiedenen Störfallszenarien für Leichtwasserreaktoren eine Rolle. Ein Beispiel ist die Notkühlwassereinspeisung in ein Zweiphasengemisch, deren Betrachtung u.a. zur Beurteilung von Thermoshock-Phänomenen wichtig ist. Dieser Bericht dokumentiert Experimente, die an einem flachen Testbassin innerhalb des TOPFLOW-Drucktanks mit dem Ziel durchgeführt wurden, Daten für die CFD-Modellentwicklung und –validierung zu generieren. Dabei wurden drei verschiedene Konfigurationen betrachtet: Kondensation an einer stratifizierten Oberfläche unterkühlten Wassers, Kondensation an einem unterkühlten Wasserstrahl und eine Kombination der beiden Vorgänge in Verbindung mit Blasenmitriss. Die Dokumentation umfasst alle Details des experimentellen Aufbaus, der konkreten Versuchsbedingungen (Versuchsmatrizen), der Durchführung der Experimente, der eingesetzten Messtechnik sowie der Datenaufbereitung. Weiterhin werden einige ausgewählte Ergebnisse präsentiert.	
19. Schlagwörter Experiment, CFD, Zweiphasenströmung, Kondensation, Blasenmitriss	
20. Verlag	21. Preis

Document Control Sheet

1. ISBN or ISSN 2191-8708	2. type of document Technical Report
3. title TOPFLOW-Experiments on Direct Condensation and Bubble Entrainment	
4. author(s) (family name, first name(s)) T. Seidel, D. Lucas, M. Beyer	5. end of project 31.12.2015
	6. publication date January 2016
	7. form of publication Booklet
8. performing organization(s) (name, address) Helmholtz-Zentrum Dresden-Rossendorf Institut für Fluiddynamik Bautzner Landstr. 400 01328 Dresden	9. originator's report no. HZDR-066
	10. reference no. 150 1411
	11. no. of pages 69
13. sponsoring agency (name, address) Federal Ministry for Economic Affairs and Energy (BMWi) 11019 Berlin	12. no. of references
	14. no. of tables
	no. of figures
16. supplementary notes	
17. presented at (title, place, date)	
18. abstract Direct Contact Condensation between steam and water as well as bubble entrainment below the water surface play an important role in different accident scenarios for light water reactors. One example is the emergency core cooling water injection into a two-phase mixture. It has to be considered for example to evaluate potential pressurized thermal shock phenomena. This report documents experiments conducted in flat basin inside the TOPFLOW pressure chamber aiming on the generation of a database useful for CFD model development and validation. It comprises 3 different setups: condensation at a stratified flow of sub-cooled water, condensation at a sub-cooled water jet and a combination of both phenomena with steam bubble entrainment. The documentation includes all details on the experimental set up, on experimental conditions (experimental matrices), on the conduction of the experiments, on measuring techniques used and on data evaluation procedures. In addition, selected results are presented.	
19. keywords experiment, CFD, two-phase flow, condensation, bubble entrainment	
20. publisher	21. price

Contents

1 Introduction

In nuclear reactor safety research, multiphase flows play an important role especially during hypothetical accidents with pressure loss. For the proper prediction of non-adiabatic flows, the correct modelling of phase transfer is necessary. Modelling the phase transfer is a specially challenging task, because it is not only dependent on phase distribution but also on temperature profiles and interfacial area density. In Direct Contact Condensation processes, the mixing in the liquid phase mainly governs the rate of condensation in each part of the interfacial area, because the thermodynamic properties of saturated steam do not allow temperature gradients, which leads to nearly zero resistance for condensation in the gas phase. Therefor the turbulence field of the liquid phase, which determines the turbulent heat diffusion, is most important for all condensation processes.

One exemplary application is the Pressurized Thermal Shock scenario. In a hypothetical Small Break Loss of Coolant Accident in a Pressurized Water Reactor, the temperature in the primary system is at around 300 °C at the beginning. In the course of the accident, cold water is injected from accumulators through the Emergency Core Cooling (ECC) system. The Reactor Pressure Vessel wall may be exposed to thermal stress, because the injected water is cold. Processes around the injection nozzle determine the loads on the primary loop and RPV walls. Hot water and steam surround the cold-water jet and therefore mixing and condensation processes determine the cold-leg output temperature. Especially in scenarios with an injection into a partly covered cold leg as shown in Figure 1.1, the condensation and the entrainment of steam beneath the water surface determines the heat-up.

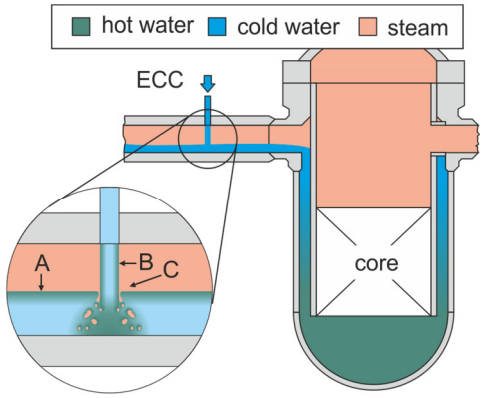

Figure 1.1: Pressurized thermal shock scenario with partly covered cold leg

In order to use Computational Fluid Dynamics (CFD) simulations for future safety assessment and design purposes, the associated models need further development and validation. Experiments for CFD-development have to meet a high standard of reproducibility, measurement certainty and temporal and local resolution. The pressure tank technology of the TOPFLOW facility allows conducting such experiments at reasonable effort.

The Direct Condensation and Entrainment Installation for Steam Experiments (DENISE) was built to meet these needs. Because of the complexity of the concurrent condensation and entrainment, the flow domain was split into three various parts. Stratified condensing flow and jet flow through steam atmosphere were studied separately, while their combination leads to bubble entrainment.

2 Experimental facility

2.1 Experimental Program

Direct Contact Condensation was investigated at three different configurations in the same facility:

A) Free surface flow

B) Liquid jet

C) Gas entrainment of a liquid jet that penetrates a free surface

Experiments were conducted at up to 50 bar pressure, because fluid dynamic properties strongly depend on the system pressure and the connected steam saturation temperature. During the hypothetical scenario, the reactor system pressure is supposed to fall from operation pressure down to saturation pressure which is about 70 bars. Further pressure decrease in the course of the accident is possible. Emergency core cooling may be active during the whole depressurization process.

In order to develop and validate CFD-models for condensation heat transfer during these scenarios it is necessary to cover a wide range of thermodynamic properties with experiments and to record the resulting distributions of temperature, velocity, void and turbulence in a high temporal and spatial resolution. These experiments need have to be stationary, reproducible and the instrumentation should deliver high accuracy with low measurement uncertainty.

2.2 TOPFLOW facility and pressure tank technology

The thermal hydraulic test facility TOPFLOW (Transient TwO Phase FLOW test facility) is one of the major research facilities at Helmholtz-Zentrum Dresden-Rossendorf and with the pressure tank it makes it possible to meet the above mentioned requirements at reasonable effort.

An electrical steam generator with a power of 4 MW is the heat source and the heat sink consists of a blow-down tank to quench the exhaust media (see figure 2.1). These are the two main infrastructural components of TOPFLOW (see Schaffrath[1], Prasser[2] and Beyer[3]). Between these two ends, the flow may pass through various test rigs, which makes TOPFLOW a multi-purpose test facility. The facility working parameters are 7 MPa maximum pressure and the corresponding saturation temperature of

[1] Schaffrath, A., Krüssenberg, A.-K., Weiss, F.-W., Hicken, E. F., M. Beyer, H. Carl, J. Schuster, P. Schütz, M. Tamme. (2001). TOPFLOW - a new multipurpose thermalhydraulic test facility for the investigation of steady state and transient two-phase flow phenomena. Kerntechnik, 66/4, pp. 209-212.

[2] Prasser, H.-M., Beyer, M., Böttger, A., Carl, H., Lucas, D., Schaffrath, A., Schütz, P., Weiß, F.-P., Zschau, J. (2005). Influence of the pipe diameter on the structure of the gas-liquid interface in a vertical two-phase pipe flow. Nuclear Technology, Vol. 152, pp. 3-22.

[3] Beyer, M., Carl, H. (2004). Betriebshandbuch für die Mehrzweck-Thermohydraulikversuchsanlage TOPFLOW. Forschungszentrum Rossendorf, Wissenschaftlich-Technische berichte, FZR-405, Juli 2004, ISSN 1437-322X.

286 °C. The maximum steam mass flow is about 1.4 kg/s and the maximum water flow into the test section circuit is 50 kg/s.

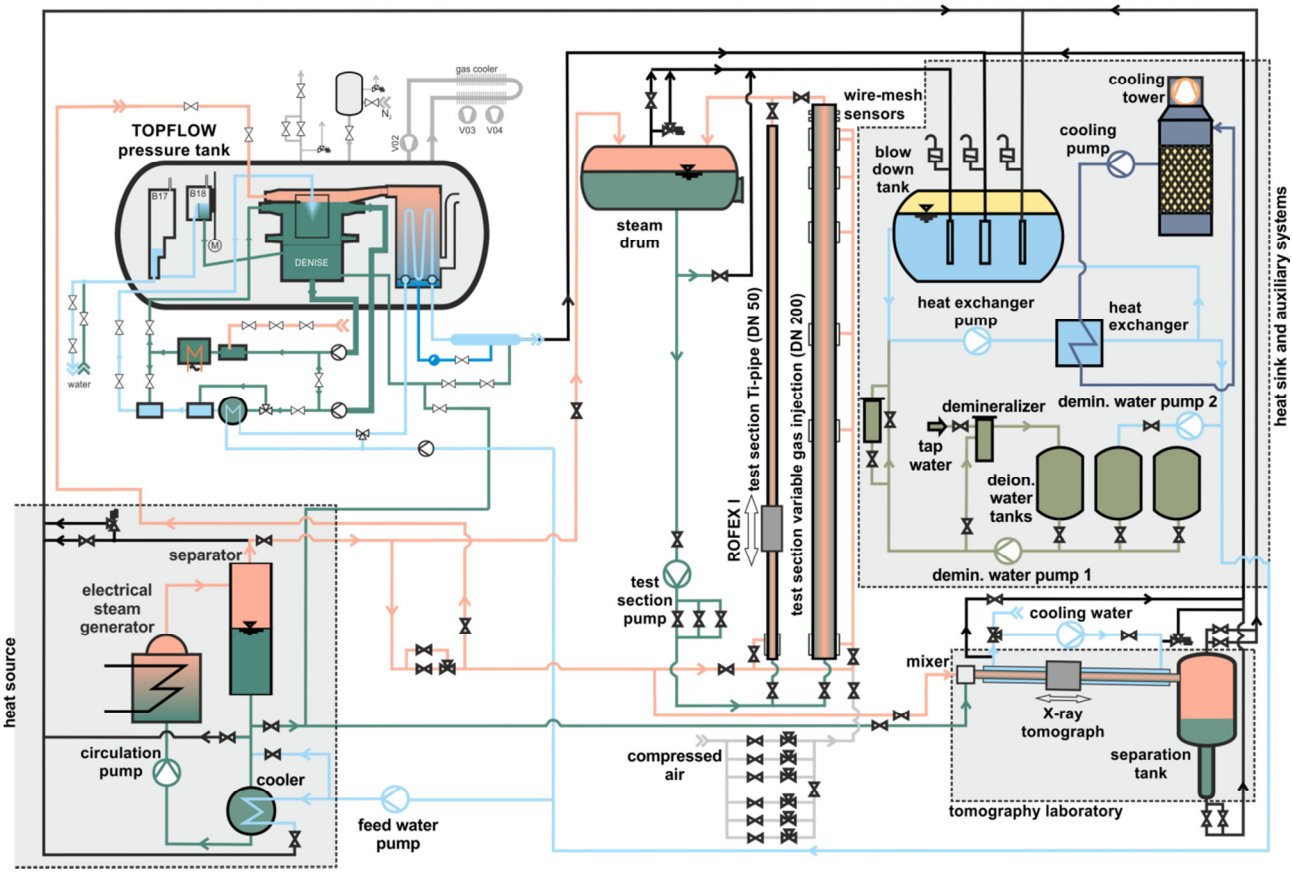

Figure 2.1: TOPFLOW test facility principle flow plan

Figure 2.1 shows the main components and circuits of the TOPFLOW facility, which are used for the experiments. The saturated steam for these tests was generated in the steam generator circuit (see the bottom left corner in Fig. 2.1). The main component of this system is an electrical heater. It consists of 24 directly heated stainless steel pipes, supplied from a power transformer. In these pipes, a maximum of 15% of the circulating water evaporates. The power of the steam generator can be adjusted coarsely into 9 modes between 0.5 and 3.9 MW by a switch on the transformer and it is set precisely by the cooler. After the separation, the steam flows to the test rigs controlled by 2 parallel units, each consisting of a flow meter and a regulating valve. The mass flow diverted from the steam generator circuit (steam or saturated water) is compensated with feed water from the blow down tank.

Figure 2.2: TOPFLOW pressure Tank B04

The mass flow diverted from the steam generator circuit (steam or saturated water) is compensated with feed water from the blow down tank. The entire facility is filled with chemically demineralized water with conductivity smaller than 5 µS/cm.

Experiments with steam and water at power plant typical boundary conditions implicate to deal with two main constraints: the high pressure and the high temperature. Usually these harsh boundary conditions limit the measuring techniques strongly. In order to broaden range of applicable instrumentation, a special operation technique, the pressure tank technology, was developed at HZDR. It makes it possible to perform high-pressure steam/water experiments under pressure equilibrium.

The pressure tank is 6.5 m long, with a diameter of 2.45 m and a volume of ca. 32 m³ (see figure 2.2). It can be pressurized with nitrogen up to 5 MPa using a nitrogen-supply unit (Fig. 2.3) to maintain the system pressure.

Figure 2.3: Nitrogen supply unit

The temperature of the inner tank atmosphere has to be kept below 60 °C for safety reasons by using an effective thermal insulation of the test rig itself and an air circulation system, which is connected to a gas/air cooler. In order to protect all the electronic devices inside the tank, the temperature has to stay below 50 °C.

For steam-water experiments, a special heat exchanger condenses the exhaust steam from the test section directly in the pressure chamber. This condenser, called W05 (see figure 2.4), is open to the test section steam on one side and to the ambient nitrogen pressure inside the pressure tank on the other side.

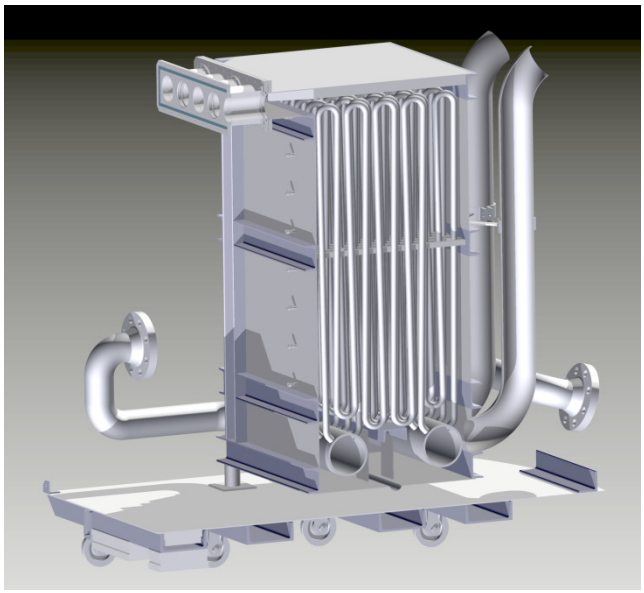

Figure 2.4: Cross section view of steam condenser W05

Using vertical cooling pipes, a steam-nitrogen stratification builds up inside, passively uncovering as much heat exchanger surface as necessary to condense the steam completely.

2.3 Test Section Design specifications

In the following section, some principle considerations are explained concerning the design and the operation of the facility.

Basically the experiments could have been conducted in transient or stationary operation. For the comparison to CFD simulations stationary boundary conditions are preferred, because it simplifies the model development approach.

The fundamental flow direction of the steam was chosen along the pressure tank axis in the direction toward the condenser in order to have straight flow and best degassing on the stratified surface. The water inlet is directed co-currently to the steam flow for stratified experiments and from the top through a special jet nozzle injector for jet flow. There are two water outlets, one opposite to

the stratified inlet for co-current flow and one at the bottom center of the basin for symmetrical boundary conditions at jet injection.

A flat design of the main flow domain was chosen, because of the better observability with cameras. A depth of the flat part of 50 mm represents an optimum to minimize 3D-effects and wall effects.

Three series with different basic flow characteristics were conducted in one experimental basin. The basin was operated for the test series A to C as shown in figure 2.5.

The general dimensions of the basin of 1 m width and 1 m height was adapted to the available space inside the pressure tank. Below the flat test section there is a small water tank as buffer reservoir for the circulation pumps. Window sizes are determined by the size of possible gas entrainment plumes, therefor the basic size of the windows is 500 mm width and 700 mm height. The observation angle of the camera and mirrors is determined in a way, that the stratified water surface inside is observed slightly from below. The basin is not in the center of the tank, because of accessibility. The distance between high-speed camera box (in the right of figure 2.6) and DENISE basin is bigger than the distance to the infrared camera box (in the left) so that there is space for a man climbing to the back of the pressure tank for installation purposes.

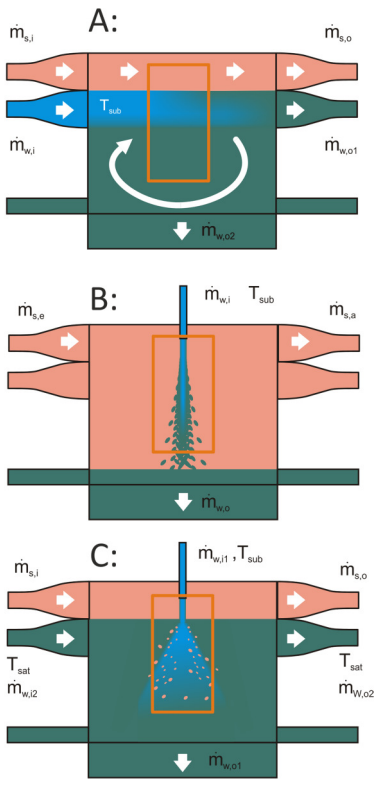

Figure 2.5: Three different flow conditions in one basin

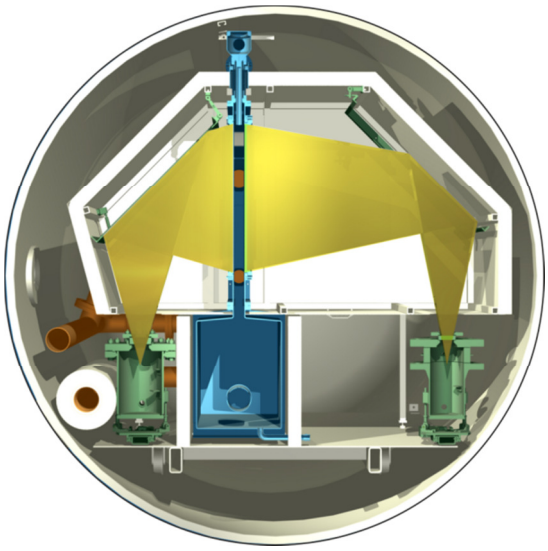

Figure 2.6: Cross section view of pressure tank (B04) with DENISE basin (B15) and camera view rays

2.4 Circuit diagram

The circuit diagram shown in figure 2.7 is most important to understand the boundary conditions of the experiments and the recorded data in the facility control system. A list of all the containers, mixers and heat exchangers is given in Table 2.1 while pumps, fans and valves can be found in table 2.2. The purpose of every part of the installation can be taken from the tables but in principle, there is a regulated steam flow from the electrical heater circuit to the condenser at the top and a closed water loop driven by pumps P16 and P18 at the bottom of figure 2.7. The temperature of the circulating water may be regulated by the cooler W08, the heater W07 and the injection of steam into M03.

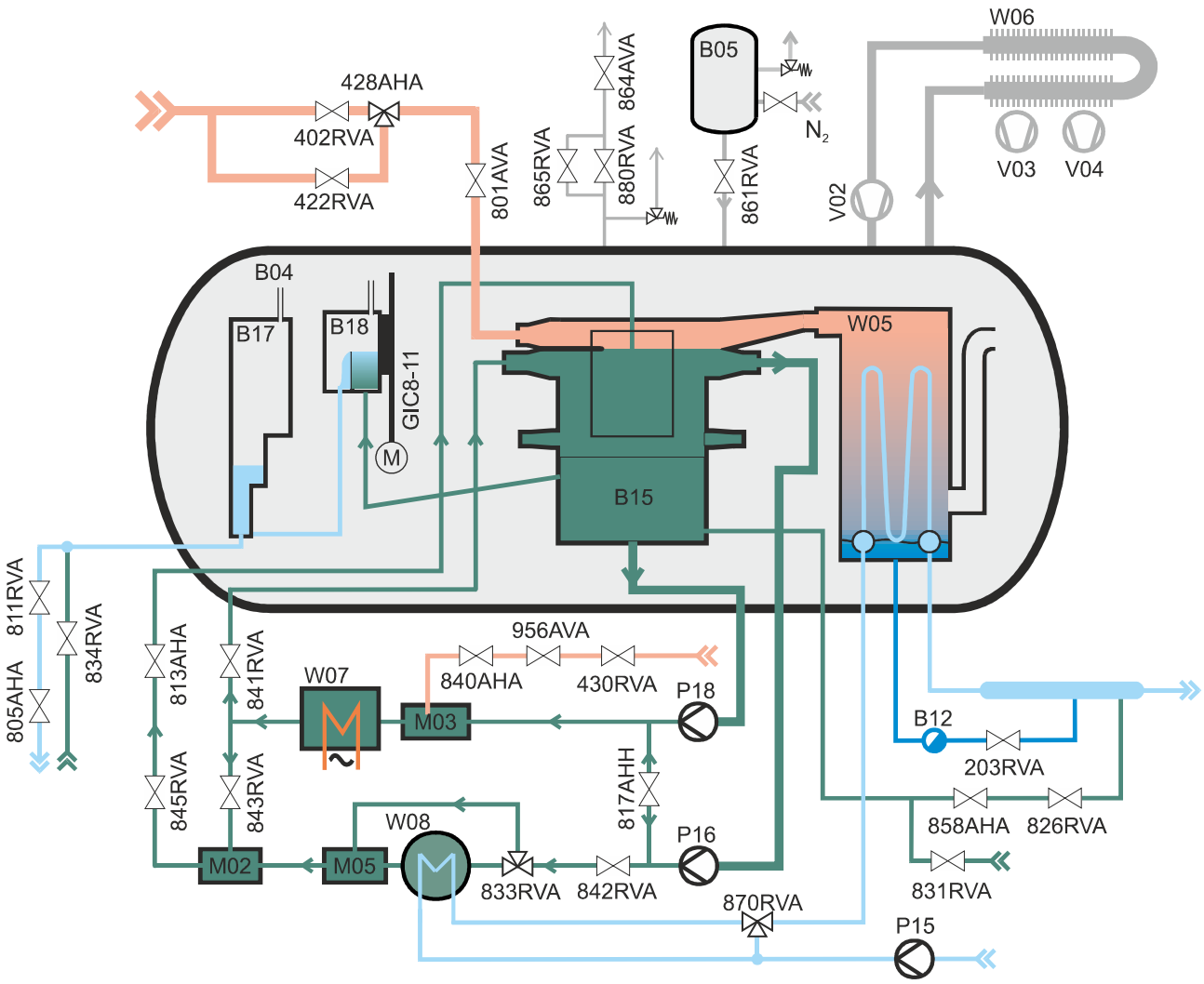

Figure 2.7: Piping of pressure tank with basin and supporting components

Table 2.1: List of containers, mixers and heat exchangers

ID	name	purpose	Approx. volume
B04	Pressure tank	maintain pressure in Experiment	31.7 m³
B05	Air vessel	Holding gas at higher pressure than B04 and make it available for regulation	2 m³
B15	DENISE basin	Contains the experimental domain	0.25 m³
B18	Overflow vessel	Contains a weir that can be used as overflow from B15 to B17	0.001 m³
B17	Collection tank	Collects the water that flows out of B18 as long as the valves below are closed. With the special form it can be used for volume flow measurement at different regions.	0.051 m³
B12	Condensate collection tank	Collects condensate from W05	0.25 m³
W05	Test steam condenser	Condenses the steam that exits the test section	1.6 m³
W06	Gas cooler	Cools down the pressurized gas atmosphere against the environment	1.13 m³

Table 2.1: List of containers, mixers and heat exchangers

ID	name	purpose	Approx. volume
W07	Electrical heater	Heats up the water in the test circuit with max. 30 kW	0.023 m³
W08	Water cooler	Cools down the water in the test circuit against cooling water	0.83 m³
M02	Mixer 02	Mixes water from the cooling and the heating side of the test circuit	0.007 m³
M03	Steam heater	Injects steam into the water circuit in order to heat it up	0.115 m³
M05	Mixer 05	Mixes the water out of W08 with the bypass water	0.009 m³

Table 2.2: List of pumps, fans and valves

ID	Name/type	purpose
P15	Cooling water pump	Circulates the cooling water through W08 and W05
P16	Test section pump “side”	Pumps water from the side outlet of the test section to the heating and cooling lines
P18	Test section pump “bottom”	Pumps water from the bottom outlet of the test section to the heating and cooling lines
V02	Gas cooling circulation fan	Circulates the gas from the coolers back to B04
V03/04	Secondary cooling fans	Circulate ambient air over the secondary side of W06
203RVA	Condensate regulation valve	Regulate the level in B12
402RVA	Steam regulation valve	Regulates the high steam mass flow rates through FIC4-04
422RVA	Steam regulation valve	Regulates the low steam mass flow rates through FIC4-05
428RVA	Steam three-way valve	Selects if steam mass flow rate is regulated within the low or the high range
430RVA	Steam regulation valve	Regulates the steam injection to M03
801AVA	Pneumatic steam isolation valve	Isolates the tank B04 from the steam line in cases of emergency
805AHA	Water isolation valve	Isolates the drainage line of B17
811RVA	Water regulation valve	Regulates the flow of B17 and the level respectively
813AHA	Pneumatic water isolation valve	Isolates the inlet of the test section
817AHH	Manual water isolation valve	Isolates the two pressure sides of P16 and P18 (always open in these experiments!)
826RVA	Water regulation valve	Regulates the drainage line of B15 and the water level in B15 respectively
831RVA	Water regulation valve	Regulates the water inflow to B15
833RVA	Water three-way valve	Regulates how much of the primary water flows through W08 and how much through the bypass
834RVA	Water regulation valve	Regulates the water inflow to B17
840AHA	Steam isolation valve	Isolates M03 from the steam line
841RVA	Water regulation valve	Regulates flow to the side inlet of B15
842RVA	Water regulation valve	Regulates the flow from P16 to W08 (or M03)
843RVA	Water regulation valve	Regulates the flow from W07 to M02
845RVA	Water regulation valve	Regulates the flow from M02 to the jet injection nozzle

Table 2.2: List of pumps, fans and valves

ID	Name/type	purpose
858AHA	Water isolation valve	Isolates the drainage line of B15
861RVA	Gas pressure regulation valve	Regulates the inflow of gas from B05 to B04 to increase the pressure
864AVA	Gas isolation valve	Isolates the gas outlet line of B04
865RVA	Gas pressure regulation valve	Regulates the outflow of gas from B04 to decrease the pressure (until 20 m³/h)
880AVA	Gas pressure regulation valve	Regulates the outflow of gas from B04 to decrease the pressure (above 20 m³/h)
956AVA	Pneumatic steam isolation valve	Isolates the mixer M03 from the steam line in cases of emergency

2.5 Construction drawings

A set of construction drawings can be found in appendix A. The main overview drawing, called 00_DENISE.pdf gives a structure to all the other drawings. The position number in the table of this drawing is also the number of the more detailed drawing below. As an example, position number 3 is the main basin called “DENISE-Behälter (B15)” so the drawing of this part is called “03_DENISE-Behälter (B15).pdf”. The same system applies to the hierarchy below. Note that the alternative name of “DENISE-Behälter” is “B15”, which is the container name in table 2.1 and in figure 2.7. All experimental relevant components are drawn – some support components as pipe fixings and insulation are not drawn.

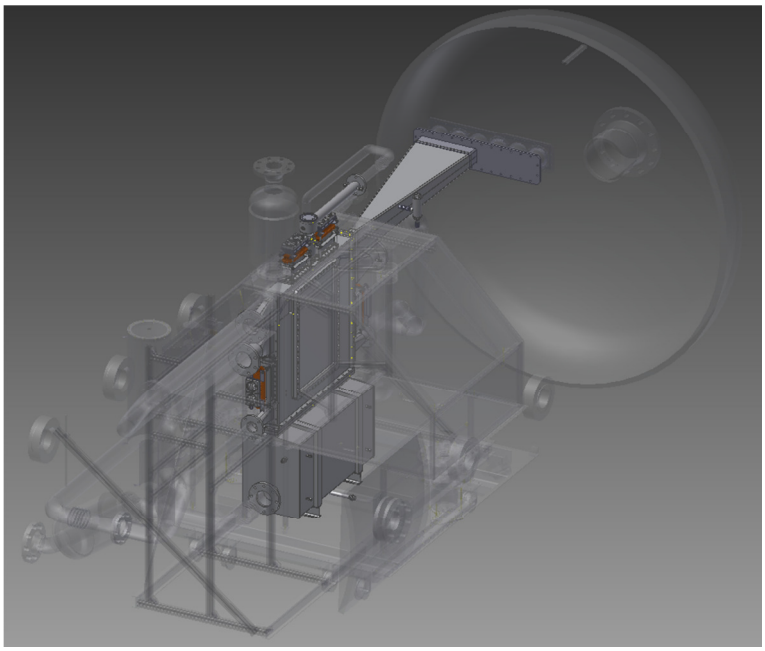

Figure 2.8: Content of the STEP-file 3D construction data

For even further detailed construction information an export of the 3D construction data called DENISE.stp is placed in appendix A (see figure 2.8). Please note, that it is not possible to model every last detail but the model may be useful if a special distance is not given in the drawings. Some parts were only used in several experimental series. In the model all parts are at their usage position, which means especially for piping, that different models are in the same position but were not installed at the same time. Furthermore it is not possible to model and draw all the construction tolerances. The DENISE basin itself is mainly a welding construction made from sheet material of 4 mm thickness. The welding process may lead to some thermal strain distortion.

In order to support the simulation process of the experimental data, an additional model was made of the internal fluid domain with all the relevant details. An overview of the main dimensions is given in

figure 2.9. A unified coordinate system is given in red color. The model 3D data is also stored as FluidDomain.stp in appendix A.

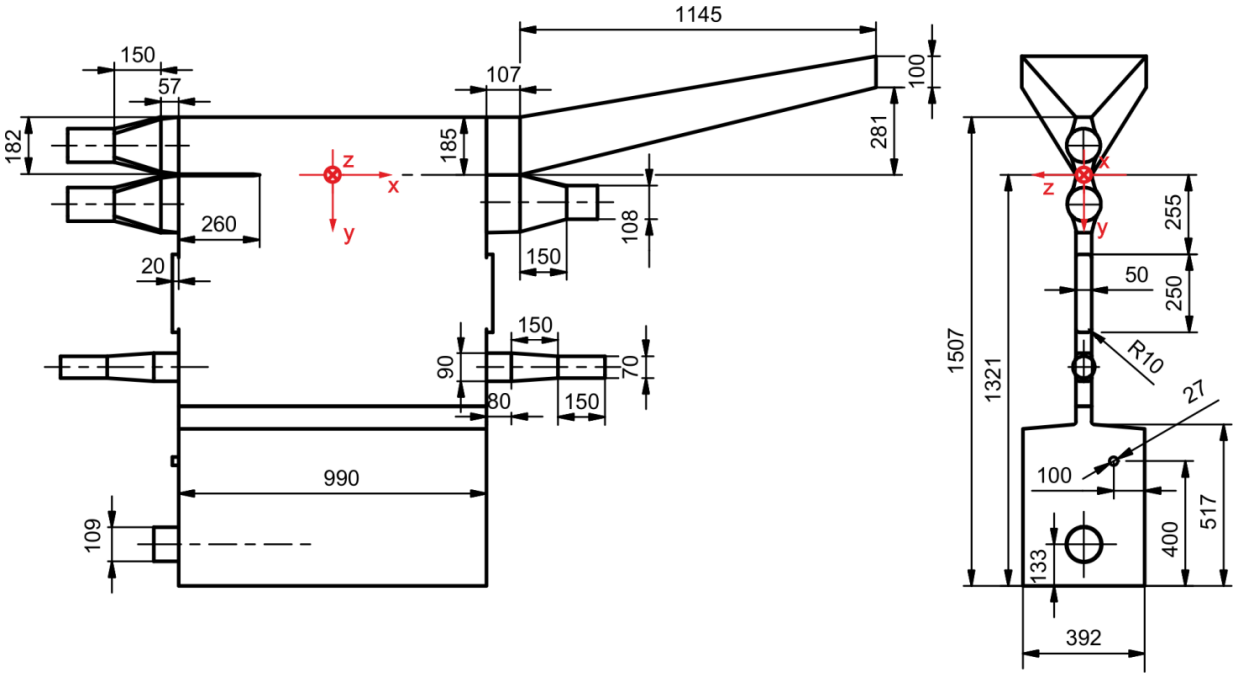

Figure 2.9: Fluid-Domain with dimensions and coordinate system

The jet nozzle is a straight pipe, because it is best comparable to other experiments and the developed pipe flow is a well described boundary condition for comparison with CFD. Because of space constrains, a 90-degree flow direction change is necessary. In order to get best developed flow out, the bend was installed before the reduction to the nozzle diameter and a flow straightener was introduced (see figure 2.10).

To get some impressions of the facility, in figures 2.11 to 2.13 some photos are given. Figure 2.11 shows the state of the basin itself at the first tightness test at the TOPFLOW facility. All possible openings were closed and the basin was filled with water at a pressure of about 0.5 bars in order to find possible leaks. Installed into the pressure tank, during the commissioning of several measurement systems and application of thermal insulation, it is shown in figure 2.12. After the completion of all experiments, DENISE was placed outside of the pressure tank shown in figure 2.13. The thermal insulation of the installation is best visible in this picture.

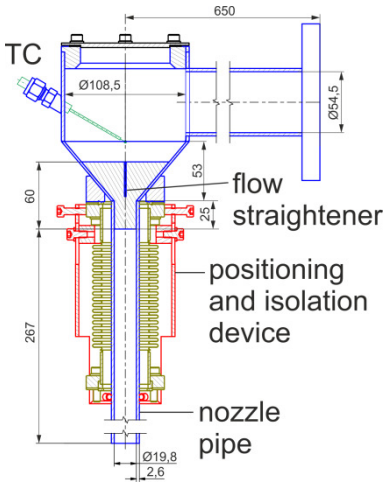

Figure 2.10: Jet injection nozzle

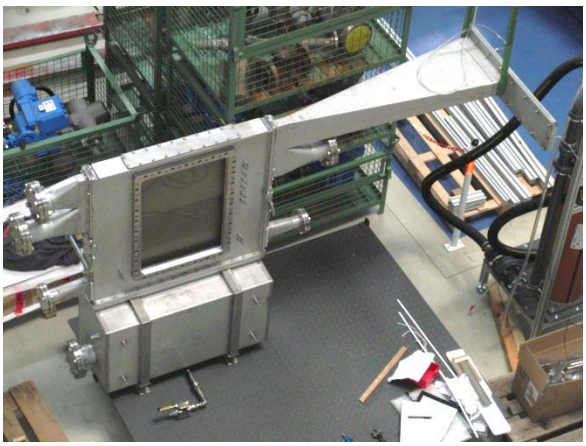

Figure 2.11: Basin B15 during the first tightness test.

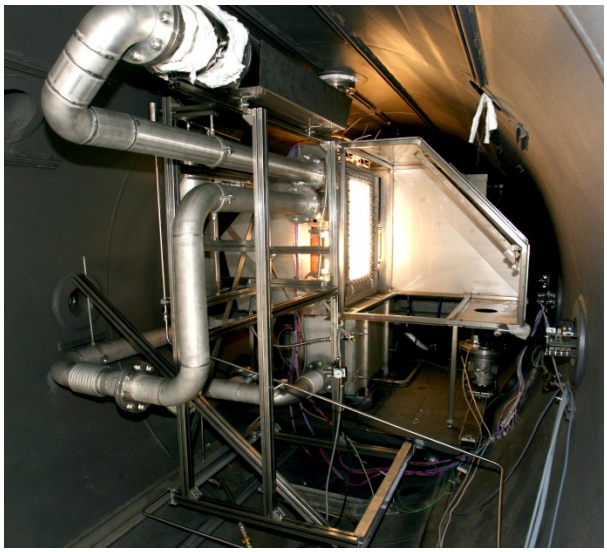

Figure 2.12: DENISE installation during commissioning inside the pressure tank.

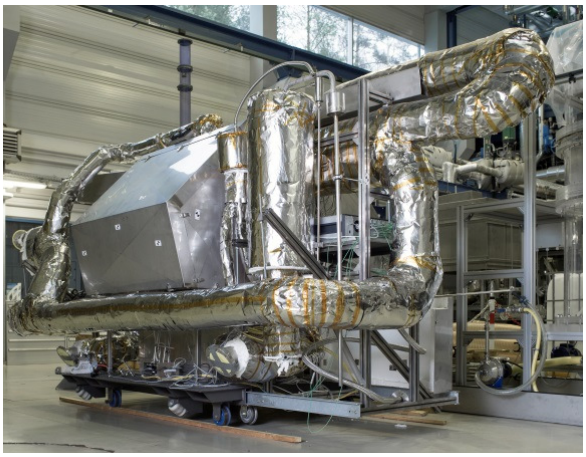

Figure 2.13: DENISE installation after experiments outside the pressure tank

3 Measurement technique

Various measurement systems were used. The TOPFLOW-facility control system controlled, monitored and recorded the fluid dynamic boundary conditions of experiments. An optical high-speed camera recorded the flow structure, phase distribution and surface roughness through a glas window.

Two different systems recorded the temperature distributions. A special fast thermocouple acquisition electronics registered fast changes of fixed thermocouples and an infrared camera observed the wall opposite to the window of the high speed camera.

In experiment series B, the infrared observation was replaced by moveable thermal and pressure lances for recording conditions inside the jet.

3.1 Facility control system data

In the control system of the TOPFLOW-facility, different measurement devices are connected. Most transducers scale a measured physical value (pressure, temperature, concentration etc.) and transform it into a standard 4 to 20 mA current output signal. Beside the transducers, measurement channels include an A/D converter. The electronic devices are combined in groups and connected to Interbus modules, which manage the communication among each other and with an OPC server. This server stores the measured data and delivers information for visualization and controlling. Additionally, it serves as a data source for the operational data logging system. The calibration and scaling data of each Sensor is stored here as well. Therefore the output file of the data logging system contains the final scaled and calibrated measurements.

Every device has a unique name – for example “TIC6-62” and a location id (in this case 25) listed in table 3.1 together with a location description, type, unit, deviation, device make, calibration range and calibration date. The position of the location ids can be taken from figure 3.2 and for more comprehensive information from the R&I-plan in appendix C. Please note here, that the piping and instrumentation changed a bit between series A and B/C. Mainly, the flow meters FI8_47 and FI8_46 (position 18 and 29) were added after series A and the jet injection nozzle was connected to the circulation.

The facility control system records continuously with a rate of 1 Hz. The raw signals of every measurement-day are stored in a Diadem-file (format R64) and a copy in an Excel-file. The first row of the files contains the unique name and all the rows below have the Signal values in ascending time order.

The information on boundary conditions of the experiments can be taken from the hourly plot of selected measurement positions in appendix B. The plots of every day contain two pages per hour with a temporal overlap of 30 minutes. Figure 3.1 shows an exemplary pair of data sheets. The first (left in the figure) is called “raw” in the heading and mainly shows unprocessed data directly from the measurement. The different plots present pressures (top), mass flow rates, water level and temperature of the gas phase (bottom left) and of the liquid phase (bottom right). The Signals are indicated by color and can be best understood by comparing to table 3.1 below.

The different experiments are identified by their trigger number shown in the plots as two vertical lines. The Trigger number is written on the line of the experiment start.

The other page holds plots of calculated signals as described in section 3.7. On top there is a plot of three different logical signals stacked above each other, which means that for the first signal (called “Stationary”), a value of 0 means false and 1 means true. The second signal (called “GasIsSteam”) is 1 for false and 2 for true - and so on. The second plot shows different signals that are used to process “FI_Cond”. Since this is based on the measurement of FI8_46 and FI8_47 which was installed after series A, this plot does not exist for the first experiments. In the third plot of the calculated data sheets, four different methods to calculate the condensation mass flow rate are compared. Additionally, the signal “Q_loss” is plotted in the unit kW but on the same diagram. Finally the bottom plot shows the raw and corrected signal of FI8_47 as described in section 3.7 in detail.

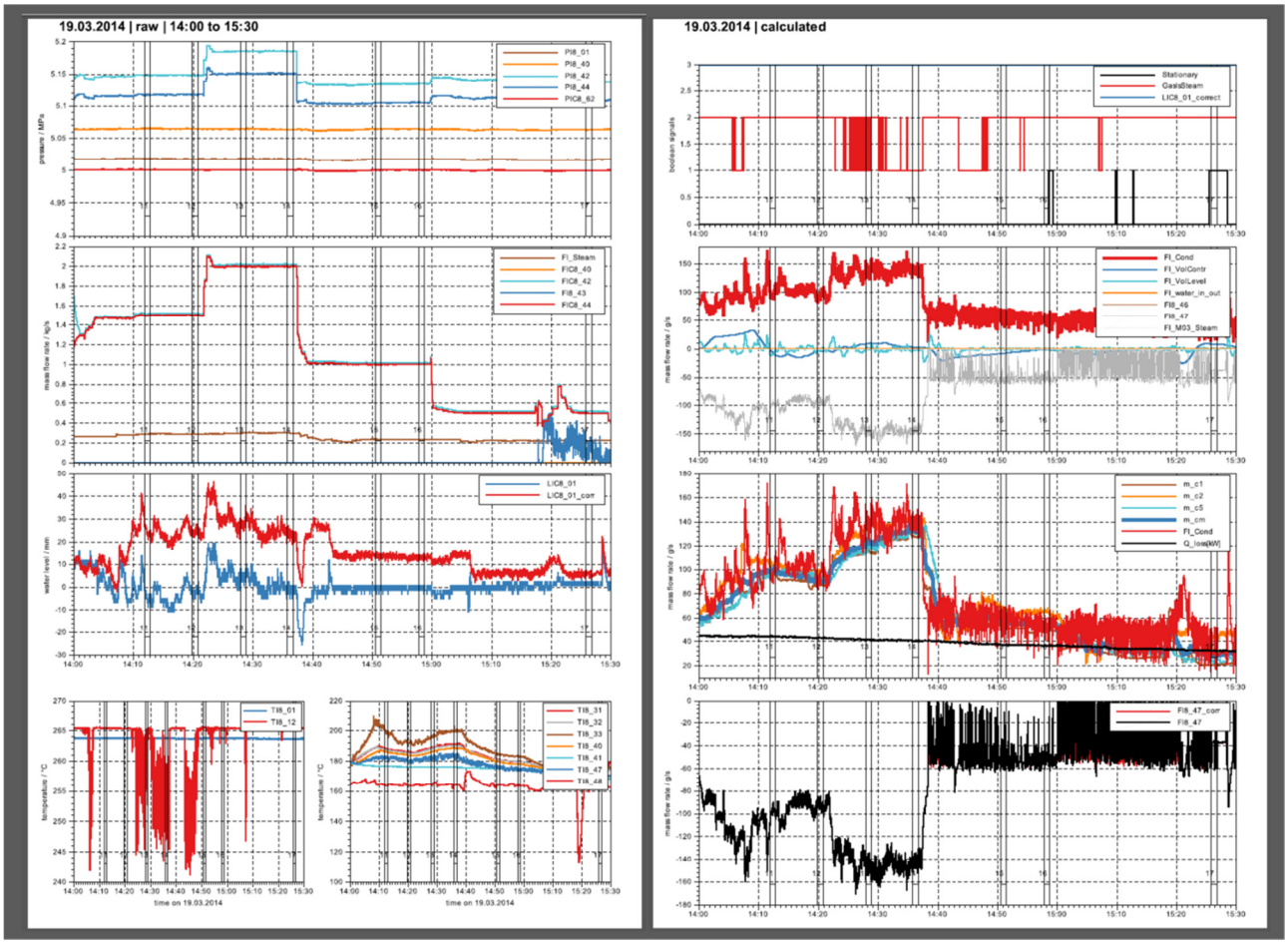

Figure 3.1: Example of data sheet content for a duration of 1.5 hours

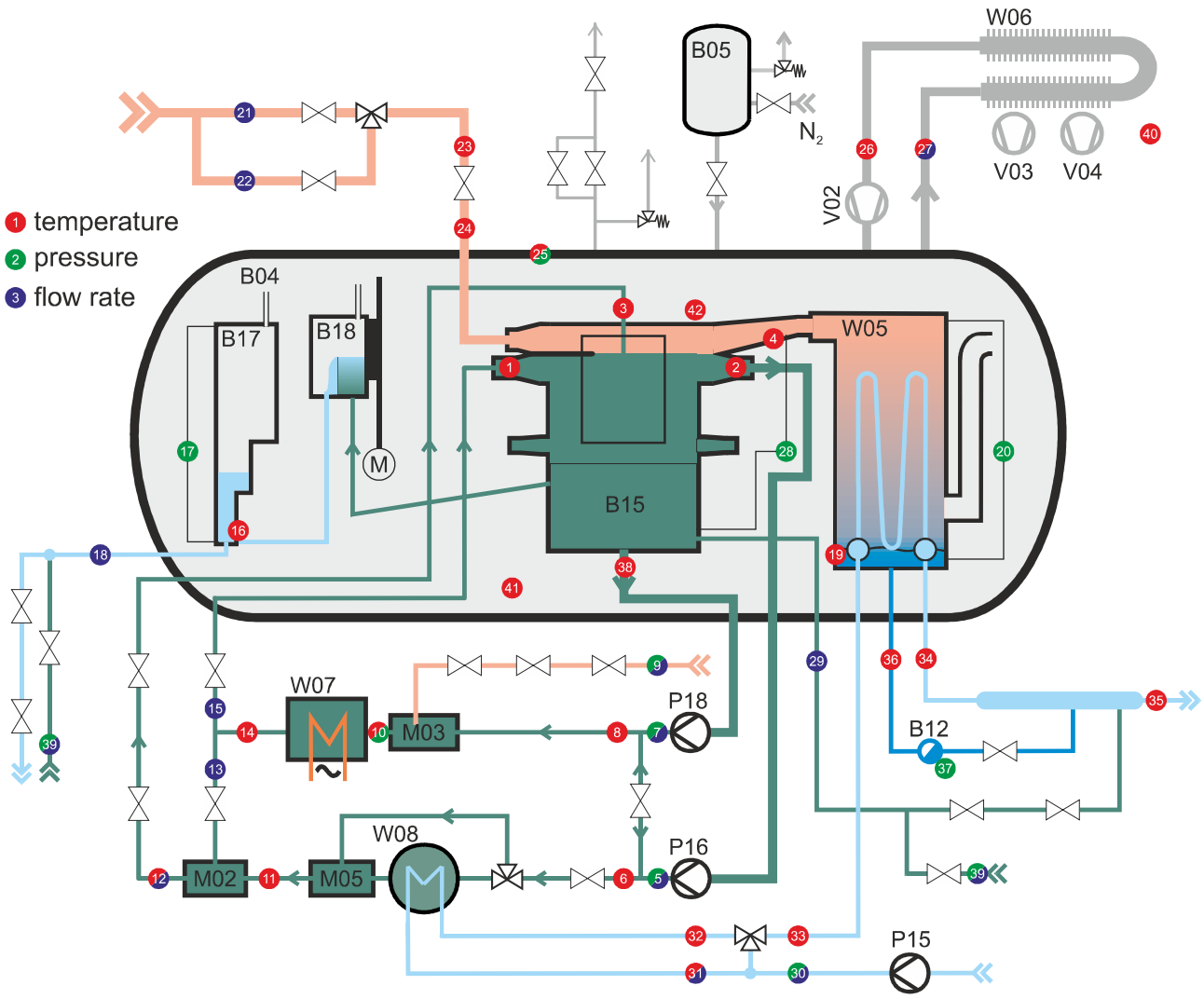

Figure 3.2: Measurement positions (ID) in the piping of the pressure tank

Table 3.1: List of measurement positions in the facility control system

Signal Name	ID	location	type	unit	deviation	Device make	Calibration range	Calibration Date
TI8_33	1	water input stratified	temperature	°C	0,5 K	Reckmann TC NiCrNi 0,5 mm	0 .. 270 °C	15.11.2013
TI8_31	2	water output stratified	temperature	°C	0,4 K	Reckmann TC NiCrNi 0,5 mm	0 .. 270 °C	10.12.2013
TI8_48	3	water input jet	temperature	°C	0,2 K	Reckmann TC NiCrNi 0,5 mm	0 .. 270 °C	04.12.2013
TI8_12	4	gas overflow to condenser	temperature	°C	0,3 K	Reckmann TC NiCrNi 0,5 mm	0 .. 270 °C	22.01.2013
PI8_40	5	water after P16	pressure absolute	MPa	0,5 percent	Fisher Rosemount 3051TA	100 .. 6000 kPa	22.07.2009

Table 3.1: List of measurement positions in the facility control system

Signal Name	ID	location	type	unit	deviation	Device make	Calibration range	Calibration Date
FIC8_40	5	after P16	mass flow rate	kg/s	0,2 percent	Krohne Coriolis OPTIMASS 8300C	0,06 .. 6,45 kg/s	16.10.2007
TI8_40	6	after bypass	temperatur e	°C	0,2 K	Emerson TC NiCrNi 1,5 mm	0 .. 300 °C	29.11.2013
PI8_42	7	water after P18	pressure absolute	MP a	0,2 percent	Fisher Rosemount 3051TA	100 .. 6000 kPa	10.08.2009
FIC8_42	7	after P18	mass flow rate	kg/s	0,2 percent	Krohne Coriolis OPTIMASS 8300C	0,64 .. 6,38 kg/s	17.10.2007
TI8_47	8	after bypass	temperatur e	°C	0,2 K	Reckmann Typ K, 1.5 mm, 1/1KX	0 .. 270 °C	14.10.2013
FI4_09_SB	9	heating steam to M03	mass flow rate	kg/s	0,6 percent	Rosemount Venturi ISO 5167-1 / MU 3095	0,03 .. 0,22 kg/s	22.05.2002
FI4_09_SH	9	heating steam to M03	mass flow rate	kg/s	0,3 percent	Rosemount Venturi ISO 5167-1 / MU 3095	0,21 .. 2,7 kg/s	22.05.2002
PI4_08	9	heating steam at FI4-09	pressure	bar	1 percent	Rosemount MU 3095 Tri Loop	0 .. 80 bar	factory
TI8_41	10	water after M03	temperatur e	°C	0,3 K	Reckmann TC NiCrNi 1,5 mm	0 .. 270 °C	10.10.2013
PI8_44	10	water after M03	pressure absolute	MP a	0,3 percent	Fisher Rosemount 3051TA	100 .. 9999,7 kPa	22.07.2009
TI8_45	11	after M05	temperatur e	°C	0,4 K	Reckmann Typ K, 1.5 mm, 1/1KX	0 .. 270 °C	26.11.2013
TI8_44	12	after M02	temperatur e	°C	0,4 K	Reckmann Typ K, 1.5 mm, 1/1KX	0 .. 270 °C	26.11.2013
FIC8_44	12	at pipe 152-HKW-50	mass flow rate	kg/s	0,2 percent	Krohne Coriolis OPTIMASS	0,06 .. 6,38 kg/s	17.10.2007

Table 3.1: List of measurement positions in the facility control system

Signal Name	ID	location	type	unit	deviation	Device make	Calibration range	Calibration Date
						8300C		
FI8_43_MAS	13	inlet in M02 in pipe 154-HKW-50	mass flow rate	kg/s	1,5 percent	Rosemount Vortex 8800D	0,5 .. 7,25 kg/s	23.07.2007
TICS8_43	14	after W07	temperature	°C	0,3 K	Reckmann Typ K, 1.5 mm, 1/1KX	0 .. 290 °C	23.10.2013
TICS8_43_2	14	after W07	temperature	°C	0,4 K	Reckmann Typ K, 1.5 mm, 1/1KX	0 .. 290 °C	17.10.2013
FI8_41	15	at pipe 153-HW-50	mass flow rate	kg/s	0,15 percent	Krohne Coriolis OPTIMASS 8300C	0,65 .. 6,45 kg/s	16.10.2007
TI8_06	16	bottom of B17 near inlet/outlet	temperature	°C	0,2 K	Reckmann TC NiCrNi 0,5 mm	0 .. 270 °C	16.01.2013
LIC8_02	17	in B17	level	m	1 percent	Fisher Rosemount 3051CD	0 .. 2 m	25.06.2013
PDI8_01	17/28	between B15 and B17	pressure difference	kPa	0,5 percent	Rosemount 3051CD	0 .. 50 kPa	26.06.2013
FI8_46_I	18	filling/drainage B17	mass flow rate	kg/s	0,1 percent(abs)	Krohne Coriolis OPTIMASS 6400 F	-2 .. 2 kg/s	25.05.2013
TI8_11	19	condensate in bottom of W05	temperature	°C	0,3 K	Reckmann Typ K, 1.5 mm, 1/1KX	0 .. 290 °C	29.11.2012
LI8_03_N	20	in W05	level	m	1 percent	Fisher Rosemount 3051CD	0 .. 20 m	26.06.2013
FIC4_04_I	21	steam to testsections	mass flow rate	kg/s	1,1 percent	Rosemount ISA 1932 Düse /MU 3095	0,16 .. 1,6 kg/s	Jan. 2009
FIC4_05_I	22	steam to testsections	mass flow rate	kg/s	1,1 percent	Rosemount ISA 1932 Düse /MU 3095	0,016 .. 0,16 kg/s	Jan. 2009
TI8_01	23	steam before B04 in pipe 100-D-100	temperature	°C	0,2 K	Reckmann Typ K, 1.5 mm, 1/1KX	35 .. 300 °C	21.11.2013
TI8_04	24	steam before B04 in pipe	temperature	°C	0,2 K	Reckmann Typ K, 1.5	35 .. 300 °C	18.11.2013

Table 3.1: List of measurement positions in the facility control system

Signal Name	ID	location	type	unit	deviation	Device make	Calibration range	Calibration Date
		100-D-100				mm, 1/1KX		
PI8_01	24	steam at inlet to B04	pressure absolute	MPa	0,2 percent	Fisher Rosemount 3051TA	100 .. 6000 kPa	24.06.2013
TIC8_61	25	gas atmosphere top of B04	temperature	°C	0,1 K	Jumbo Pt100	0 .. 100 °C	27.07.2010
PIC8_62	25	in pressure tank B04	pressure absolute	MPa	0,1 percent	Fisher Rosemount 3051TA	100 .. 6000 kPa	25.06.2013
TI8_03	26	before V02 in atmosphere cooling system	temperature	°C	0,2 K	Pförtner Pt100	0 .. 100 °C	04.12.2013
TI8_05	27	before W06 in atmosphere cooling system	temperature	°C	0,1 K	Reckmann Typ K, 1.5 mm, 1/1KX	0 .. 100 °C	15.05.2013
FI8_01	27	B04 atmosphere cooling system	volume flow rate	Pa	5 percent	Smar LD 301 Torbar	-	-
LIC8_01	28	in B15	level	m	1 percent	Fisher Rosemount 3051CD	0 .. 20 m	25.06.2013
FI8_47_I	29	filling/drainage B15	mass flow rate	kg/s	0,1 percent(abs)	Krohne Coriolis OPTIMASS 6400 F	-2 .. 2 kg/s	06.07.2013
FI8_51	30	after P15	mass flow rate	kg/s	1 percent	Rosemount Vortex 8800CW	2,5 .. 38 kg/s	27.04.2004
PI8_51	30	water after P15	pressure absolute	MPa	0,5 percent	Fisher Rosemount 3051TA	100 .. 700 kPa	factory
TI8_50	31	secondary water to W08	temperature	°C	0,1 K	Rössel Pt100	0 .. 400 °C	03.12.2013
FI8_52	31	secondary water to W08	mass flow rate	kg/s	0,1 percent	Krohne Coriolis OPTIMASS 2300C	6 .. 72 kg/s	12.01.2009
TI8_55	32	secondary water after W08	temperature	°C	0,2 K	Reckmann Typ K, 1.5 mm, 1/1KX	0 .. 150 °C	07.11.2013
TI8_51	33	after bypass line	temperature	°C	0,1 K	Pförtner Pt100	0 .. 400 °C	28.11.2013

Table 3.1: List of measurement positions in the facility control system

Signal Name	ID	location	type	unit	deviation	Device make	Calibration range	Calibration Date
TI8_52	34	water output of W05	temperature	°C	0,1 K	Pförtner Pt100	0 .. 400 °C	13.11.2013
TI8_53	35	collected water output of B15	temperature	°C	0,1 K	Pförtner Pt100	0 .. 150 °C	29.11.2013
TI8_21	36	condensate output of condenser W05	temperature	°C	0,3 K	Reckmann Typ K, 1.5 mm, 1/1KX	35 .. 100 °C	21.11.2013
LIC8_04_D	37	in B12	level	m	1 percent	Smar LD 301 D21IV000B10 Z	-10 .. 30 m	26.06.2013
TI8_32	38	bottom output of B15	temperature	°C	0,3 K	Reckmann TC NiCrNi 0,5 mm	0 .. 270 °C	10.12.2013
PIC5_02	39	pressure after P02	pressure	MPa	1 percent	Smar LD 301M51	0 .. 10000 kPa	factory
FI4_06	39	water from P02	mass flow rate	kg/s	0,15 percent	Krohne Coriolis OPTIMASS 8300C	0,25 .. 4,26 kg/s	01.03.2011
FI8_31	39	water to B04 in pipe 129-HW-20	mass flow rate	kg/s	0,05 percent	Micromotion Coriolis F100	0,45 .. 4,53 kg/s	28.07.2011
TI6_03	40	environment temperature (for cooling conditions)	temperature	°C	1,5 K	PT100	0 .. 100 °C	factory
TI8_68	41	bottom of testsection on platform	temperature	°C	0,3 K	Reckmann Typ K, 1.5 mm, 3/3	0 .. 300 °C	29.11.2012
TI8_67	42	top below the insulation cap	temperature	°C	0,2 K	Reckmann Typ K, 1.5 mm, 3/3	0 .. 300 °C	29.11.2012

3.2 Temperature measurement inside the experimental facility

Additionally to the thermocouples in the facility control system, 28 thermocouples were installed in the DENISE installation and connected to a special high-pressure resistant digital acquisition system shown in figure 3.3 which operates at high recording frequency of 500 Hz. The positions of all thermocouples are shown in the overview drawing in appendix D. **It is important to distinguish the different recording systems of thermocouples!** The ones marked in red in the overview were recorded by the facility control system as described in section 3.1 above at 1 Hz rate. The thermocouples marked blue were connected to the high speed recording system described here. A detailed list of the thermocouple positions and their application is given in NamesAndPositions.pdf in appendix D. The table consists of columns:

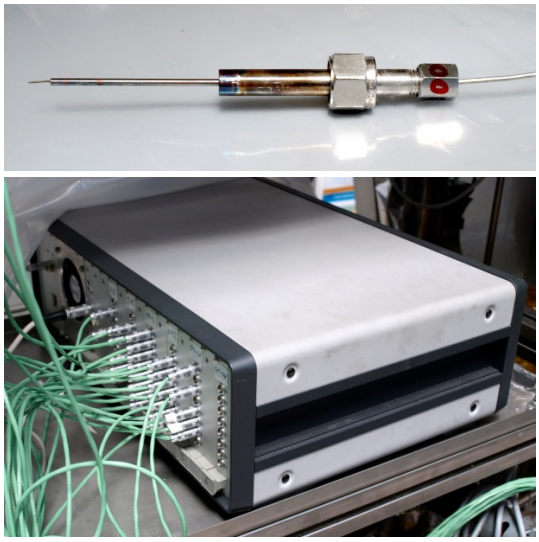

Figure 3.3: Thermocouple sensor (top) and high speed acquisition electronics (bottom)

- Pos#: is the number of the position shown in the drawing
- TC-ID: is the unique thermocouple identifier and also the recording channel in the file
- R&I number: is the name of the thermocouple if it is connected to the facility control system
- Abs. position (x,y,z): is the place of the thermocouple tip in the coordinate system shown in figure 2.9
- Position of sensor and position of tip: is an additional description where to find the TC
- Valid in series (A,B,C): is a logic identifier if the TC was installed at this position in the according series. Some technical conditions lead to TC being unavailable in certain settings.

The sensors are NiCr-Ni type K Sheathed Thermocouple Assemblies made by Reckmann with a diameter of 1.5 mm and a hammered tip of 500 µm and a measurement range of 0 to 300 °C. They are mounted in the facility using a graphite sealed sensor shown in figure 3.3. A capillary pipe with an inner diameter of 1.6 mm

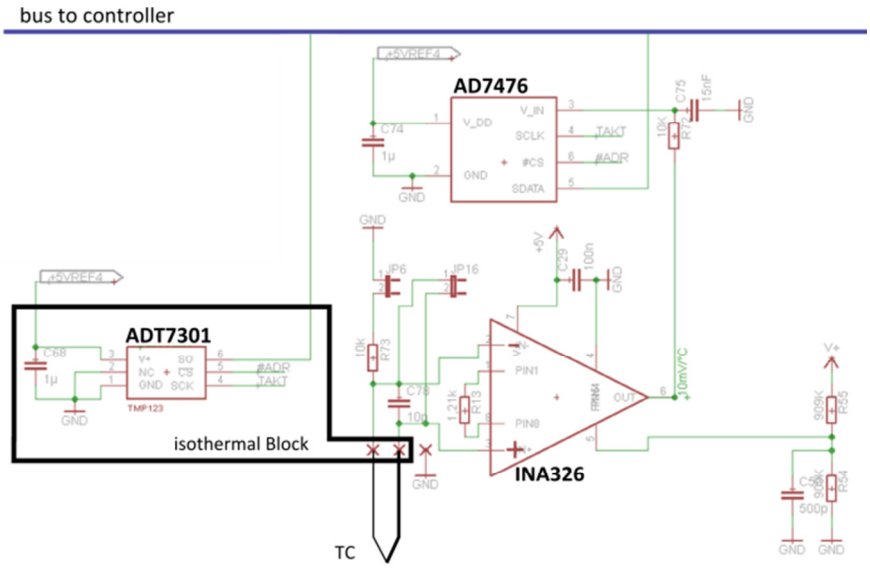

Figure 3.4: Structure of one channel in the high speed acquisition electronics with one TC connected to a cold junction

supports the thermocouple until 5 mm from the tip. The tip of the thermocouple is left blank and unsupported in order to guarantee maximal temporal responsiveness and minimal influence of the wall and sensor base temperature.

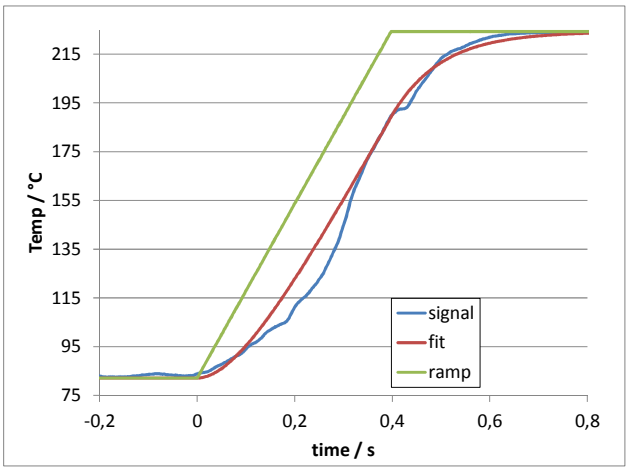

Figure 3.5: Dynamic behavior test of thermocouple tip

In the acquisition electronics, every recording channel consists of the three parts shown in figure 3.4. The thermocouple is connected to a cold junction with an isothermal block together with a digital temperature sensor ADT7301. This records the cold junction temperature at every time step. The thermocouple voltage is then amplified with an instrumentation amplifier INA326. The resulting signal is digitized with a 12 bit analog digital converter AD7476 and recorded as well.

The cold junction compensation is calculated afterwards using both signals and the calibration accordingly.

In order to quantify the temporal response time by the damping of the thermocouple tip, a fast change of temperatures was taken from the data and analyzed. It is the response signal of the thermocouple 3038, which is installed in the upper temperature and pressure lance (described in section 3.5). This thermocouple moved out of the cold water jet at 82 °C back into the pure steam at 224 °C. Because of the small geometry of the tip and relatively fast movement of the lance, this would result in theoretical ramp slope of 357 K/s (shown in green in figure 3.5). A theoretical PT1 damped ramp was fitted to the signal and the resulting damping time factor T1 was found at 100 Milliseconds. This temporal damping has to be considered when analyzing the dynamics of fast processes.

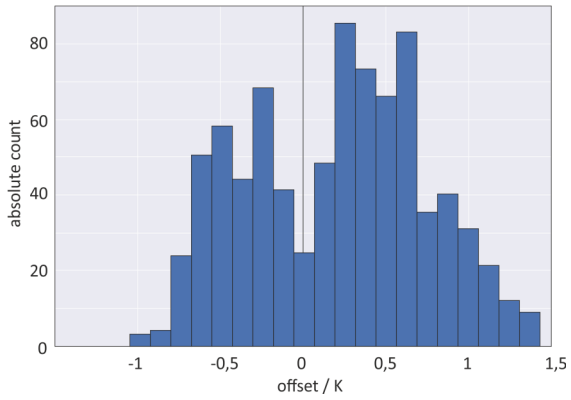

Figure 3.6: Histogram of differences between steam saturation and measured temperature in steam

In order to check the consistency of the whole measurement chain including the stability of calibration, it is a good approach to assess thermocouples that are definitely covered by steam at a known pressure. Because of the isothermal property of pure steam, the estimated temperature from the table can be compared to the measured signal. Taking all the 77 measurements where the water level is more than 600 mm below the upper lid and the gas is steam; all 10 thermocouple signals above the water level were evaluated. Figure 3.6

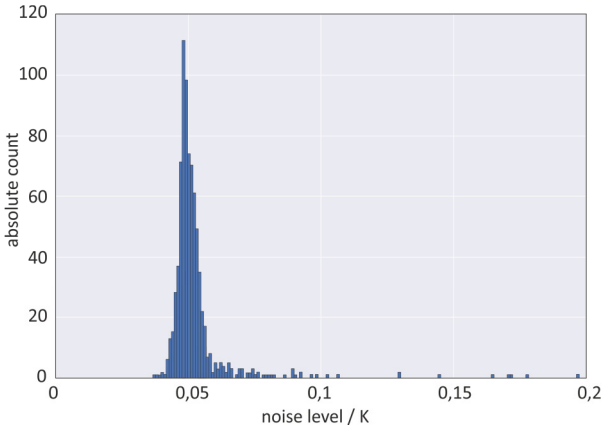

Figure 3.7: Histogram of thermocouple signal noise

shows the histogram of all mean temperature differences to saturation. The average difference is 0.20 K and the standard deviation is 0.53 K, which are usual values for thermocouples.

The constant conditions of a steam atmosphere can also be used to quantify the temperature signal noise, generated by the acquisition electronics. Figure 3.7 shows a histogram of the standard deviation of the measurement described above. The mean noise level is as low as 0.054 K, which results from the oversampling of four times the frequency and the use of low noise electronics.

See Appendix I for the description how to access the data.

3.3 High-Speed-Camera

The most important instrumentation of the DENISE experiments is the high speed camera. In the following section, the technical details about the camera itself are given together with a description of the necessary support systems: lens, windows, mirrors and illumination.

Figure 3.8: IDT Y3 high speed camera

Figure 3.9: AOS Q-VIT high speed camera

Two different cameras were used during the experiments. An IDT MotionPro Y3 camera (figure 3.8) with a NIKKOR 50 mm F1.8 lens was used in series A and an AOS Q-VIT (figure 3.9) with a Kowa LM25XC 25 mm F2.0 lens for series B and C. The respective camera is always installed in a pressure box inside the pressure tank. This box is connected to the ambient pressure with pipes and a cooling system supplies cold air for the camera to avoid overheating. As shown in figure 3.10, the camera does not see the basin directly but via a set of front surface mirrors. The first mirror (red in the figure) is there to increase the object distance and to prevent the camera from being in a hot area inside the insulation cap (marked white). The other two mirrors in the high speed camera view (marked green and blue) were only used in series B and C. They make it possible to observe the flow domain from different directions at the same time in order to reconstruct 3D phenomena. An exemplary image of an air-water plunging jet experiment is shown in figure 3.11. The vertical mirrors are visible on the left and right side.

Finally, the camera sees the flow though a 13 mm thick borosilicate glass window fixed to the basin (see construction drawing for more details). In order to use the mirrors correctly, the position has to be measured. A special calibration measurement was used for this. A well-known pattern of black and white squares was placed on the outside of the glass window. Since the vertical mirrors were at different positions during series B and C, the Calibration was made twice. The two images called "2014_02_28_MirrorCalibration_for_A_and_C.bmp" and "2014_08_13_MirrorCalibration_for_B.bmp" are contained in appendix E. The pattern for series A and C has a square size of 20 mm and the other of 10 mm. The numbers on the patterns are for identifying identical squares in different views.

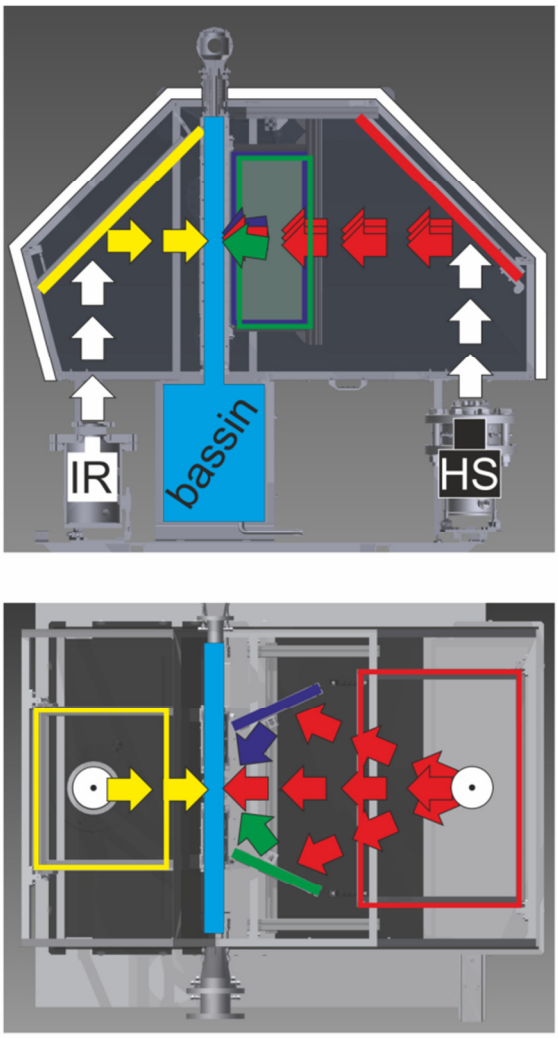

Figure 3.10: Observation directions from the camera boxes via mirrors to the DENISE basin

On top and on the narrow sides of the basin, a set of four illumination devices (shown in figure 3.12) are fixed to bring enough light into the fluid for very short exposure times needed in high speed observation. Every device consists of eight high power LEDs mounted on a cooling block and a specially designed polished stainless steel reflector to guide most parts of the light into the basin. Lenses are not applicable because the refractive index of the ambient nitrogen changes with different pressure levels. A set of stacked windows with a small gas gap works as temperature insulation and another window serves as tightness insulation to the basin. The LEDs are Bridgelux BXRA-C2002 type with a luminous flux of 2200 lm each so a total flux of about 70400 lm was directed into the basin. The effective illuminance in 1.3 m distance was measured for the LED devices and figure 3.12 shows the effect of the reflector.

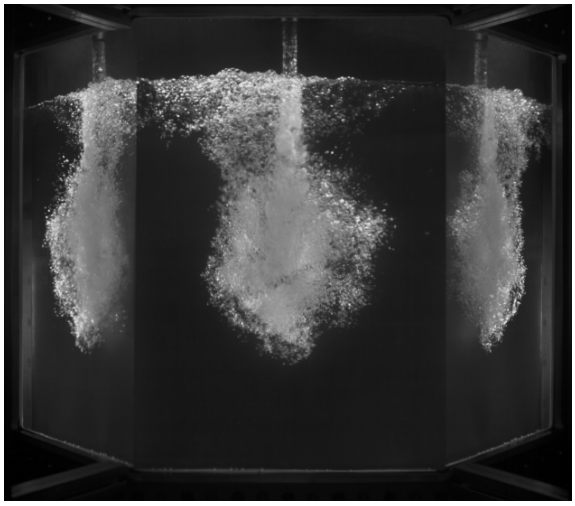

Figure 3.11: High speed camera image observing a nitrogen-water plunging jet experiment via mirrors

See Appendix I for the description how to access the data.

The stored image data is different for the two cameras. For the IDT camera in series A, every experiment is stored as a series of bmp-files in a subfolder structure of "[experimental day]/ HSC/ [ExpID]_Tr[Trigger number] /[ExpID]_[image number].bmp". With the second camera, the data is

stored in raw format of the AOS software in the form "[experimental day]/ HSC/ [ExpID]_Tr[Trigger number] .raw3". For the overview of image data, statistics for every video was extracted. In appendix E is a folder containing jpg-files showing different statistical approaches to every pixel in the image:

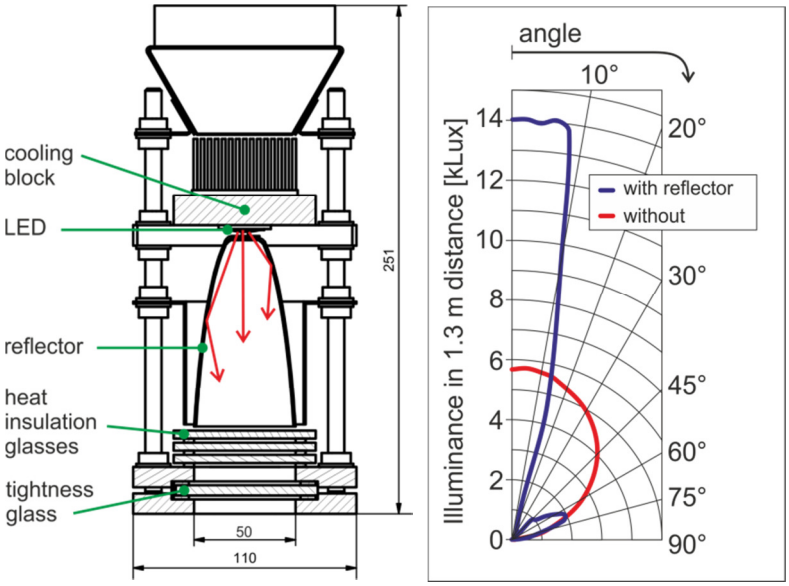

Figure 3.12: LED illumination system with reflectors (left) and illuminance measurement with and without reflector (right)

- AVG_*.jpg files show the average value of each pixel over the whole video. It is the same as a long time exposure image.
- FST_*.jpg files show the first image of each video.
- MAX_*.jpg files show the maximum value of each pixel
- MIN_*.jpg files show the minimum value of each pixel
- MED_*.jpg files show the median value of each pixel
- P05_*.jpg files show the 5% Percentile value of each pixel, this is sometimes more useful than the minimum, because the minimum depends very much on single events like dark bubbles.
- P95_*.jpg files show the 95% Percentile value of each pixel, this is sometimes more useful than the maximum, because the maximum depends very much on single events like bright droplets or bubbles.

The "VideoData.xlsx" file in appendix E contains a list of all experiments with high speed video recording and a set of columns containing:

- "NoFrames" is the total number of frames in the stack
- Width and height are the dimensions of each picture
- fps is the recording speed in frames per second
- shutter is the shutter speed in µs, please note that the maximum possible shutter speed is the inverse of the recording speed but it is not necessarily identical
- filename, date, trigger number and Experimental ID called ExpID

Figure 3.13: Infrared camera

3.4 Infrared camera

Analogue to the high-speed camera, an infrared camera is installed in a pressure proof box inside the pressure tank and observes a part of the test section via a mirror (see yellow mirror

in figure 3.10 above). The camera type is Infratec VarioCAM hr head 640 with a 30 mm Carl Zeiss lens (shown in figure 3.13). The camera has a calibration range from 0 to 300 °C and a frame rate of 10 Hz. With its resolution of 640x480 px it observes a field of view of 662x497 mm, which results in an object resolution of 1.03 mm/px. Thermal radiation is recorded at a spectral range of 7.5 to 14 µm with a resolution of 30 mK. Please note, that all shown IR-images are flipped vertically in order to simplify comparisons to high speed camera observations.

The camera observes a 1 mm thin sheet of stainless steel coated with a special high temperature resistive and high infrared emissive paint. The emissivity of the paint was measured beforehand with a result of ε=0.93. Measurement side effects of the infrared observation are a combination of unknown pathway temperature and density resulting in a lower signal and multiple reflections inside the isolation cap.

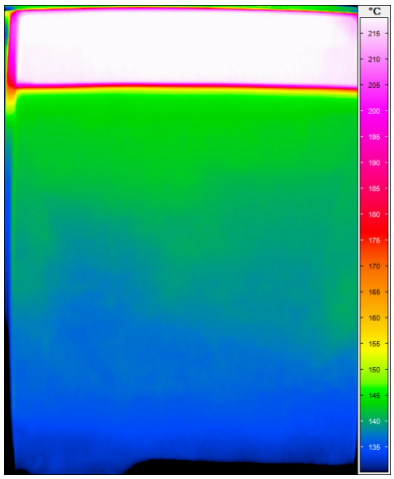

Figure 3.14: A05 raw

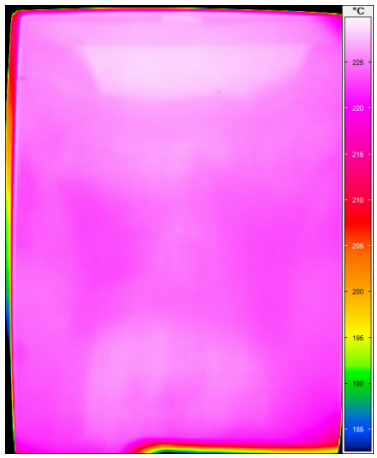

Figure 3.15: 50 bar steam

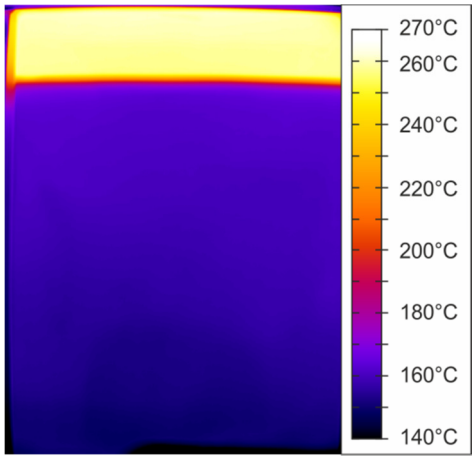

Figure 3.16: A05 corrected

The raw data of a measured infrared temperature distribution of experiment A05 (14.8.2013, Trigger 22) is shown in figure 3.14. It is visible, that the steam-filled top of the basin is at around 215 °C while it should be at 264 °C saturation temperature of steam at 50 bar pressure. The inlet temperature should be around at 164 °C for this experiment but the area below the steam-water interphase at the top left is about 145 °C. An infrared image of the well-known steam atmosphere at 50 bars pressure is shown in figure 3.15. The temperature should be constant at 264 °C but it is more or less equal around 225 °C. To correct this image well, as shown in figure 3.16 it is important to understand the distribution and to imagine the slightly reflecting observed surface as a mirror as well. As shown in figure 3.17, the infrared camera (IR) is directed upwards to the infrared mirror (yellow rays). This mirror changes the imaginary viewpoint of the camera to the position IR' (blue rays) and brings the coated surface of the basin into the field of view. Most parts of the infrared radiation are produced by this surface itself (ϵ = 93%) but the remaining 7 % of the rays are reflected from this surface. The rays are reflected like the viewpoint of the camera is reflected to position IR'' (red rays). In the view of IR'' mainly is the IR-mirror again, which leads to a final change of viewpoints to IR''' (green rays). In this view from the top of the cap, the coated hot surface is in the top part, which leads to a self-view and therefore to a hot trapezoid in the resulting image. Also in the view IR''' is the bottom part of the cap and the infrared camera box itself (slightly visible round shape in the center). The lower part of view IR'' is directed towards the cap interior, which is also mostly reflecting the hot surface again.

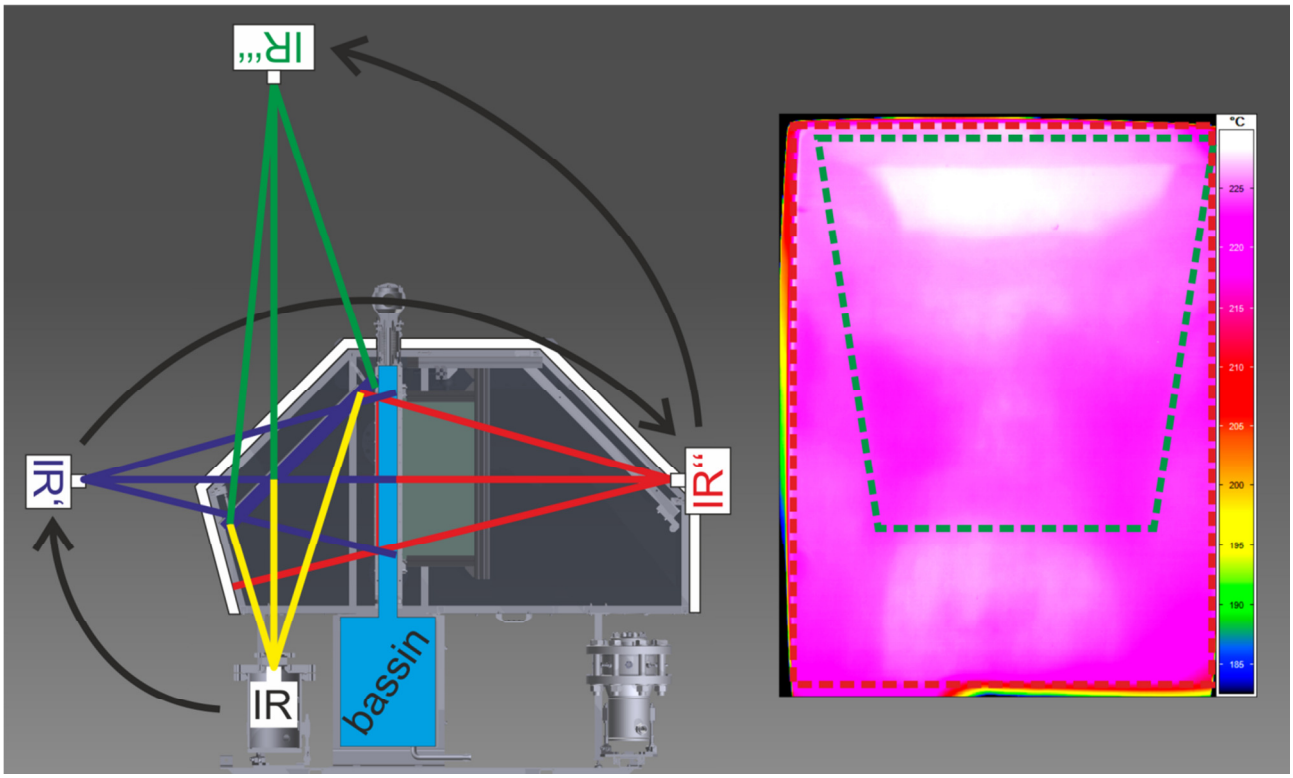

Figure 3.17: Schematic of the infrared observation with virtual mirrored views (in different colors) and thermogram of 50 bars steam experiment

Figure 3.18 shows a schematic how the infrared radiation is altered between the observed object and the camera. The surface reflects two kinds of rays and emits its own temperature. One part of the reflection is coming from the environment of the whole setup, which is at a temperature of about 40 to 50 °C. The rest of the reflection is a self-reflection of the surface itself as described above. So the overall emission of the object can be expressed as

$$\Phi_0 = \epsilon \cdot \Phi(T_{obj}) + \rho \cdot \Phi(T_{avg}) + (1 - \epsilon - \rho) \cdot \Phi(T_{env}) \quad (1)$$

While Φ is the radiation according to Stefan-Boltzmann law $\Phi(\mathrm{t}[°\mathrm{C}]) = \sigma \cdot (\mathrm{t} + \mathrm{T}_0)^4$.

The radiation is then attenuated by the observation path and the window of the camera-box window. The high and varying moisture content of the high pressure nitrogen atmosphere inside the pressure tank brings some difficulties with it, but since some of the temperatures visible in the images are known, the effects may be calibrated in-situ.

$$\Phi_1 = \tau_{path} \cdot \Phi_0 + (1 - \tau_{path}) \cdot \Phi(T_{path}) \quad (2)$$

$$\Phi_2 = \tau_{glass} \cdot \Phi_1 + (1 - \tau_{glass}) \cdot \Phi(T_{glass}) \quad (3)$$

In the end, the infrared camera can observe radiation differences between its own emission and the incident radiation. To calibrate the self-reflection properties of the observation, the 50 bar steam experiment was used. It is known, that the temperature of the surface is homogenous distributed at steam temperature of 264 °C. Using the previously measured ϵ =0.93 and the known properties of the steam experiments, ρmay be calculated for every pixel in the image – it is shown in figure 3.19.

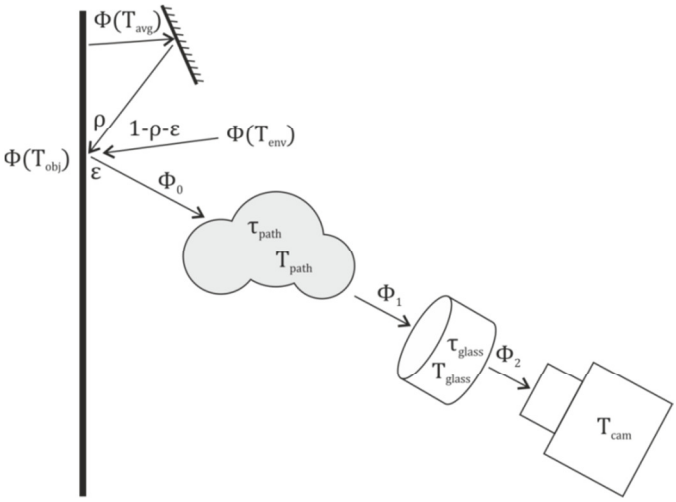

Figure 3.18: Schematic representation of the infrared observation path.

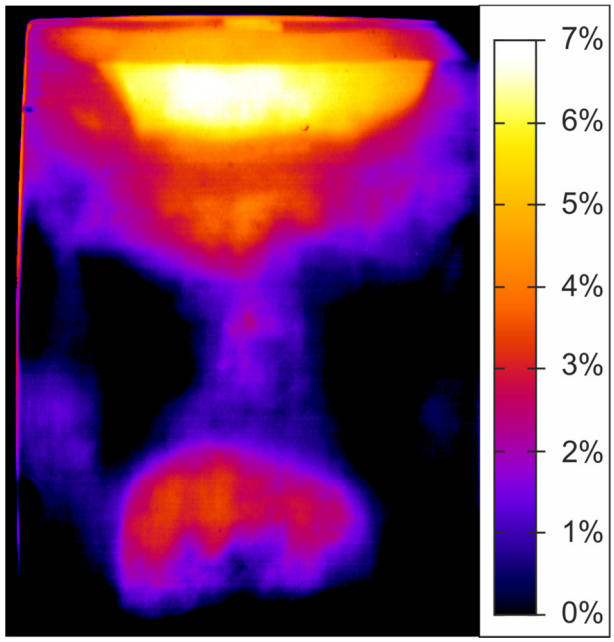

Figure 3.19: Refraction characteristics ρ of the infrared image

The properties $\tau_{path}$and T_{path}can only be calibrated in-situ using known temperatures in the experiment. Finally, the temperature distribution of experiment A05 can be corrected and the average image is shown in figure 3.16.

3.5 Thermal pressure lances

In order to measure the temperature and dynamic pressure distribution inside the condensing jet and since the infrared camera observation of the jet experiments would be useless; the infrared window was replaced for experimental series B. It is replaced by a plate holding two gears (shown in figure 3.20) that make it possible to move a lance with a pressure and temperature sensor through the jet. The temperature sensor is a thermocouple connected to the high speed acquisition system described in section 3.2 above. Dynamic pressure measurement is done by guiding a capillary impulse pipe with an open tip. The pipe is connected to a BD-Sensors DMP 331 pressure transducer (0 .. 400 mbar range) inside the pressure tank atmosphere and the signal is recorded by a BD-Simex PAC-99X I16 acquisition system. The recoding frequency is 1 Hz if the trigger signal is off and 10 Hz if the experiment is running. Triggers numbers are always counting up every day, so in order to find a pressure signal one has to count up. In order to distinguish dynamic from static pressure, it is necessary to subtract the pressure value from outside of the jet from all of the values.

Figure 3.20: Lances and moving gears

Every lance is connected to two stepping motors of the make Orientalmotor, a PK268PDA-L for longitudinal movement (motor 1 in figure 3.21) and a PK264DA for turning (motor 2). Every stepping motor has a reference position switch inside the gear in order to know the absolute position. In the startup procedure, the motor first moved the lance to the associated reference position and then to the position zero. For motor 1 this is the position most outside of the basin (center of the pressure pipe is 5 mm from the wall and thermocouple is 2.5mm from the wall) and the vertical position for motor 2. The stepping motors are controlled by software that recorded all the positioning commands and the following movement in a csv-File for each experiment. In this software, the motors have the following notation: A1 = top lance motor 1, A2 = top lance motor 2, A3 = bottom lance motor 1 and A4 = bottom lance motor 2. Motors 2 (A2 and A4) are only used to adjust the lances to the center of the jet. In every experiment, the motor control waits for the common trigger signal like all the other measurement systems. After the trigger signal rose, the bottom lance starts to move stepwise towards the jet center as shown in figure 3.22. Ten steps of 5 mm take about 90 s and the movement backwards takes 38 s. Afterwards, the top lance starts moving in 16 steps of 2 mm distance. After every stepwise movement, the lance stops for 5 s in order to record stationary data of the flow and to have a good statistical base. It is possible, that step-losses occur in the motors. This was detected and the position was restored by driving to the reference switch. In the normal case the position of the lance is known very exactly because the high gear reduction results in resolution of 10 µm per step.

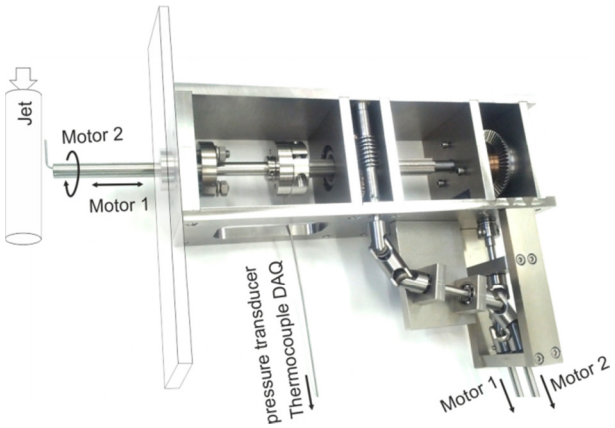

Figure 3.21: Temperature and dynamic pressure lance with gearbox and connections to stepping motors

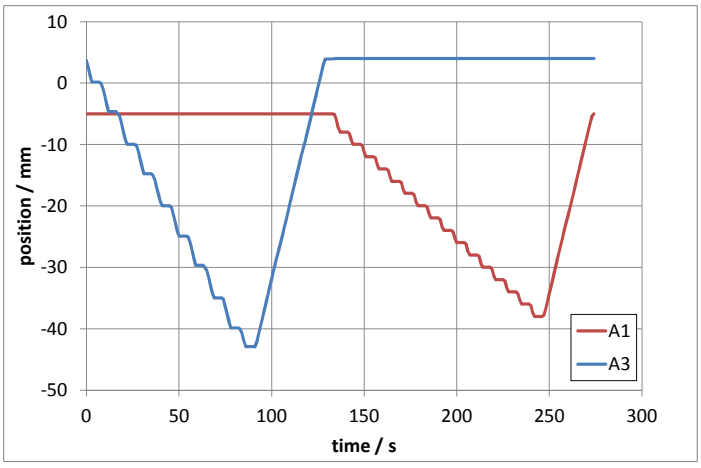

Figure 3.22: Exemplary position/time plot of the two lance axes

After combining all available measurements, profile plots can be produced. Figures 3.23 and 3.24 show dynamic pressure and normed temperature profiles for an experiment with the following parameters: p=25 bar, T_{in} = 174 °C, steam/water, m_{in}=1.5 kg/s.

The results of lance measurements can be found in appendix H. The file Lancestatistics.csv contains statistical properties of the moments when the lances stopped to measure for about 5 seconds. The columns contain the lateral Position through the jet (latPos), the number of Points measured (count), the average value of the Points (mean), the standard deviation (std), minimal and maximal values (min/max), the several percentiles (2%, 5%, 9%, 25%, 50%, 75%, 91%, 95%, 98%), the sensor (TorP={T1=temperature top, T3=temperature bottom, P1=pressure top ,P3=pressure bottom})

and the experimental ID (ExpID including date and Trigger number). Furthermore diagrams like figures 3.23 and 3.24 have been made for all experiments in appendix H. It has to be noted, that small differences in the temperature measurement in experiments with low sub-cooling may lead to big disturbances in normed temperature (outside of the plausible rage of 0 to 1).

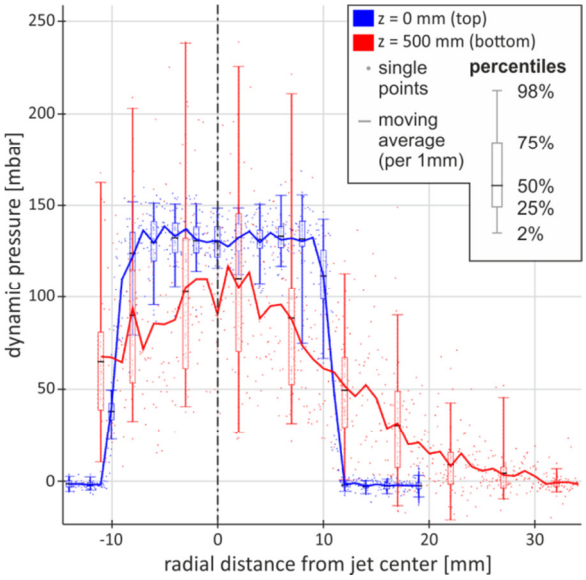

Figure 3.23: Dynamic pressure profile

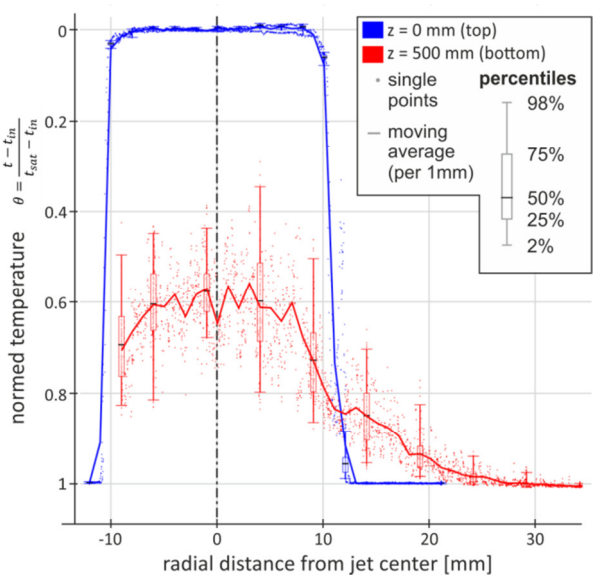

Figure 3.24: Normed Temperature profile

3.6 Synchronization of the different measurement systems

Figure 3.25 shows how all the different measured systems are connected to a common trigger signal coming from the so called Clock Box, which is controlled directly from the operators PC. There are three different types of signals. So called “Enable” signals are activated for the whole time of the experiment. The stepping motor controller, PAC pressure recording system and the facility control system gets one of these signals (blue line). “Trigger” signals are have a positive flank in the moment when the measurement system is supposed to start recording a single measurement. The systems with the high frequency like high speed camera, infrared camera and thermocouple electronics use this signal (red line). The high speed camera also receives a signal called “Sync” (orange line) to synchronize the internal frequency to the external. Since all the measurement systems have different recording frequencies, the Clock Box also uses a different trigger rate for every measurement system. Therefore it is guaranteed, that the measurement data is recorded at the same time.

For that reason, the trigger number is also used to identify every experiment. For every day, the number of trigger events is counted up in the facility control system. The files of the other systems are then named according to the date and this trigger number.

Every experimental matrix point has a so called “ExpID” number, which only depends on the boundary conditions but it can have more than one combination of date and trigger, because several measurements were performed in a row with different measurement settings (e.g. HSC frequency) and some experiments are repeated on a different day to check reproducibility. The ExpID has the form “A01” to “A59” for series A stratified experiments, “B01” to “B90” for series B jet experiments and

"C01" to "C97" for series C entrainment experiments. Some of the trigger events are unrelated to experimental matrix points. They are usually called "pre01" and ascending, which means that they are used to test the measurement system after the startup or if anything interesting is happening in the facility.

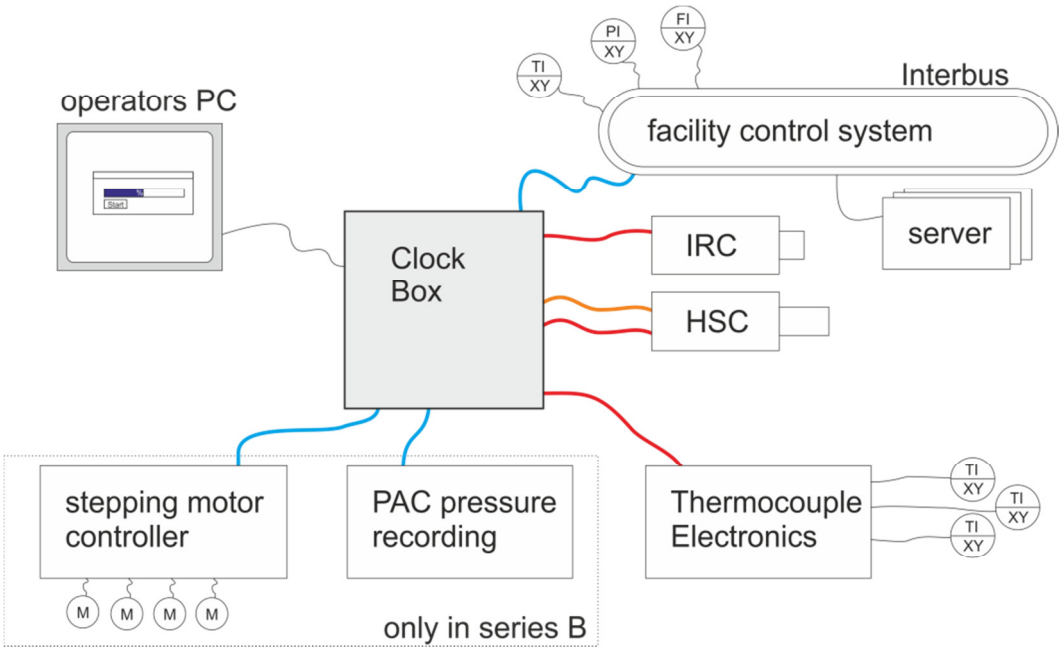

Figure 3.25: Synchronization with an electronic Clock box connected to all measurement systems

3.7 Derived Data

In order to understand more in depth what happens during the experiments and to get more than the directly measured data from the facility control system, several signals were calculated combining raw measured data and thermo-physical properties from the database. Similar to the raw data, derived signals have unique names to identify them. The open source Matlab–alternative called Scilab was used to calculate the results. The scripts to calculate the signals are attached to appendix F. In the following section, the most important derived signals are described.

FI_Steam is a combined signal of FIC4_04 and FIC4_05. Steam mass flow rate to the pressure tank is measured in the TOPFLOW facility in two different ranges (see table 3.1 and image 3.2 for further information). If the valve 428_AHA is opened, the steam flows through FIC4_04 to measure high flow rates and if it is closed through FIC4_05 for low rates. The signal FI_Steam analyses the valve position to select, which flow meter to use.

T_Sat is the saturation temperature calculated from IAPWS IF97 thermal properties and using the pressure signal of PIC8_01.

bGasIsSteam is a logical value, which is 1 if the gas atmosphere is steam and 0 if not. It is calculated by comparing the temperature TI8_12 to the temperature T_Sat. If the absolute difference is lower than 2 K, gas is anticipated to be steam.

LIC8_01_correct is a corrected version of water level LIC8_01 inside the DENISE basin. It uses the raw unscaled version of the pressure transducer LIC8_010 in the unit kPa, temperatures TI8_32 and TI8_33 for the average density of the water in the basin, TIC8_61 for the water density in the impulse

lines, TI8_12 and T_Sat for the density of the gas atmosphere and the constant vertical distance between pressure impulse pipe connections top and bottom dL_8_01(=1.51 m).

$$LIC8_{01_{corr}} = \frac{dL_{8-01} \cdot \left(\rho_{avg_{impulsePipes}} - \rho_{gas}\right) - \frac{p_{LIC8-01}}{g}}{\rho_{avg_{bassin}} - \rho_{gas}}$$

bStationary is the logical signal combing the dynamic history of certain signals. The signals are treated with a weak low-pass (T_{lowp}) or moving average (T_{avg}) filter to neglect noise on the signal, differentiated, compared to a maximum absolute allowed value (dS_{max}). The value of a differentiated signal has to be smaller for a certain time (t_{stay}) in order to be stationary. The following signal dynamics are combined in bStationary:

- Jet inlet temperature TI8_48 (T_{avg} = 120 s, dS_{max} = 0.005 K/s, t_{stay} = 60 s)
- Jet mass flow rate FIC8_44 (T_{avg} = 60 s, dS_{max} = 0.5 g/s, t_{stay} = 100 s)
- Bottom outflow rate FIC8_42 (T_{avg} = 60 s, dS_{max} = 0.5 g/s, t_{stay} = 100 s)
- Side outflow rate FIC8_40 (T_{avg} = 60 s, dS_{max} = 0.5 g/s, t_{stay} = 100 s)
- Water level LIC8_01_corr (T_{lowp} = 400 s, dS_{max} = 0.03 mm/s, t_{stay} = 60 s)

FI8_47_corr is a correction of flow rate FI8_47 of water in or out of container B15. The installed flow rate measurement fails if the rate is very small (usually below 50 g/s). This operation is common in the experiments, because this feed and drainage line was used to compensate the condensation mass flow and to keep the level in the basin constant. To correct the flow rate, it is compared to the simulated flow rate that corresponds to the pressure drop and the valve characteristics in the drainage line. If the measured rate is below 70 g/s and the difference to the anticipated value is above a certain threshold, the simulated value is used instead of the measured.

FI_M03_Steam is a correction similar to FI8_47_corr for the flow rate of steam to the steam heater M03 measured by FI4_09. If FI4_09 is blow 30 g/s it is replaced by the valve-simulation.

FI_water_in_out is a cumulative flow rate signal used in the mass balance of the whole experiment. It is the sum of signals FI8_46_I, FI8_47_corr and FI_M03_Steam.

FI_VolContr is the mass flow rate of water that the basin can capture at the same water level because the water volume shrinks by decreasing temperature and vice versa. Since the volume of water in the circulation loop and in the basin is about 0.73 m³, small gradients in average temperature can cause relative big changes in water level.

FI_VolLevel is the mass flow rate of water that the basin captures by increasing the water level. It is needed because the balance in FI_Cond (below) uses the assumption of a constant water level.

FI_Cond is the combination of above mentioned mass flow rates. The mass balance can be used to assume, that the mass flow rate of the condensed steam, is the difference between the inward and outward water flow and the two correction flow rates FI_VolContr and FI_VolLevel. Therefore FI_Cond is the most direct way to measure the condensation mass flow rate.

Q_loss is an estimation of the heat losses from the test installation to the surroundings. It is a sum of the heat that is given off by heat exchanger W06 (using flow rate FI8_01 and difference of temperatures TI8_05 and TI8_03), the heat-up of the nitrogen atmosphere (differentiated average of

TI8_03 and TI8_05) and a Nusselt-approximation of heat losses from the pressure tank B04 to the environment. It is used in the heat balances m_c1, m_c2 and m_c5 below.

m_c1 is an alternative approach to quantify the condensation mass flow rate using an energy balance of the inflow and outflow of circulating water. The steam condensation leads to heat-up which can be used to conclude the amount of condensation.

m_c2 is another alternative that uses the balance of steam that flows in at the one side and the heat-up of the cooling-water in the steam condenser. The temperature difference between TI8_51 and TI8_52 is used to quantify the heat transfer in the condenser. Since the mass flow rate through the condenser is very high, the temperature difference has a very big influence on the resulting heat flow, therefore an in-situ calibration offset was applied to TI8-52. The average difference between the two temperatures was evaluated for all the experiments without steam inside the condenser and with a small temperature difference between TI8_12 and TI8_51 (<3K). The average offset is 0.168 K

(**m_c3** and **m_c4** are approached that are not used in the end)

m_c5 is a variant of quantifying the condensation mass flow rate by balancing the heat flow of cooling and heating devices W07, W08 and M03.

***_dev** is a series of signals containing the deviation (aka measurement uncertainty) of derived signals. For every aforementioned derived signal and every single time-step, the propagation of uncertainty is calculated according to the recommendations of ISO/BIPM “Guide to the expression of uncertainty in measurement” JCGM 100:2008.

m_cm is the best-estimate of the condensation mass flow rate and uses the weighted average of FI_Cond, m_c1, m_c2 and m_c5. The weight factors are the inverse square roots of the respective measurement uncertainty, which leads to the smallest possible uncertainty of the resulting signal.

m_cmax is the maximum possible condensation rate based on the heat capacity of the injected cold water to heat up until saturation.

More detailed information about derived data can be found in the Scilab scripts available in appendix F.

4 Experiments

This chapter focuses on the experiment procedures. This includes the preparation and conduction to the experiments and the discussion how to read the results and what to expect from the data basis.

4.1 A - Stratified Flow Experiments

The first series of experiments is on stratified flows. Subcooled water was injected directly below the water level at one side of the basin and the steam condensed on the cooled surface directly. In the same time, the hot layer of condensate stratifies at the same surface because of buoyancy, which hinders the condensation.

4.1.1 Experiments specification and procedures

Figure 4.1 shows the differences in the experimental setup compared to the other set of experiments. The jet injection nozzle is not installed yet, so the side injection into the basin is connected to the pipe from 813AHA instead of 841RVA as in the other series (compare the R&I plans in appendix C for further details).

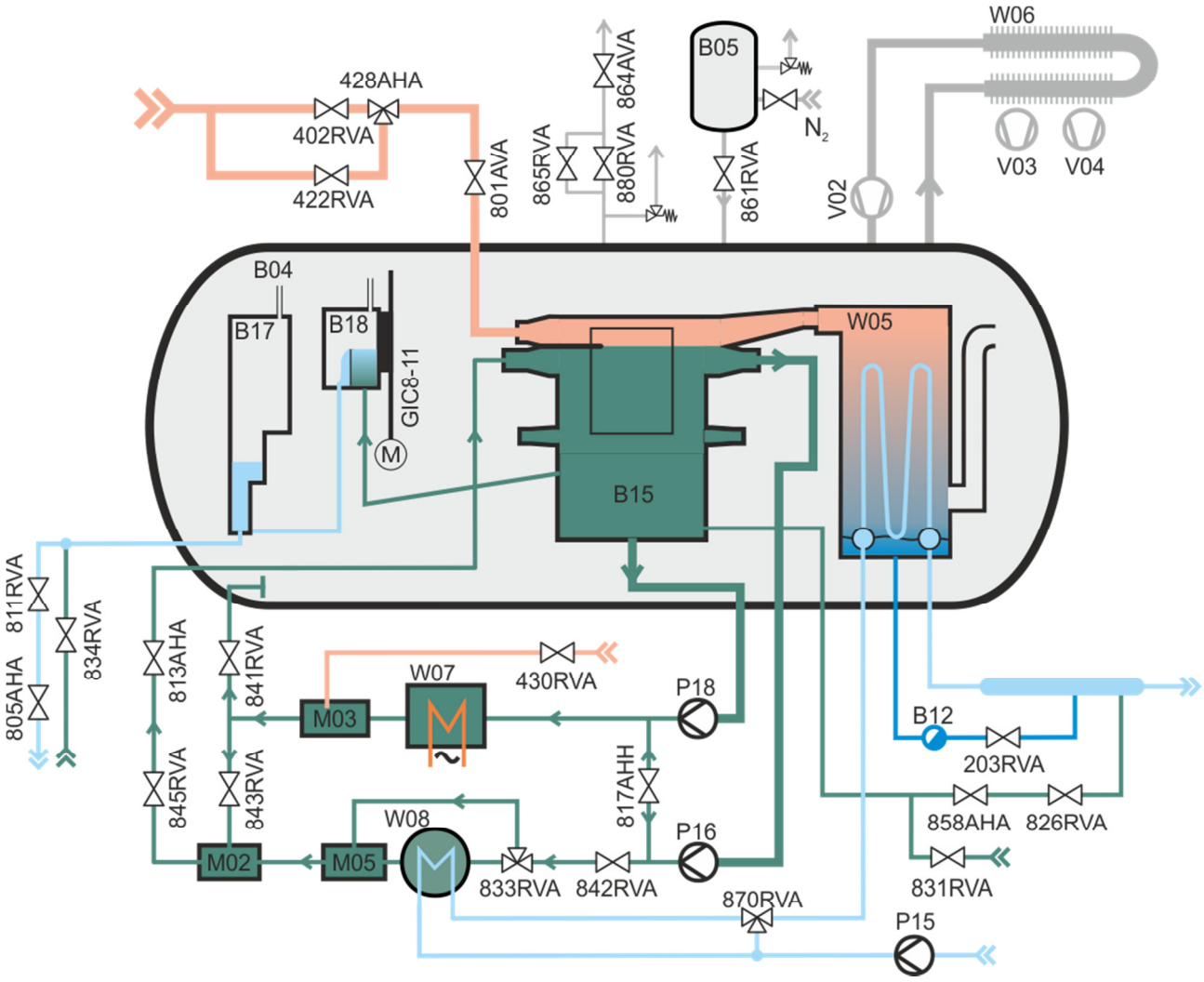

Figure 4.1: Alternative piping of pressure tank with basin and supporting components for series A

The order of W07 and M03 is opposite because of historical reasons and valves 840AHA and 956AVA were also installed after the experiments. The same is the case for flow meters FI8_46 and FI8_47, which were installed after the experience of series A. Therefore the condensation mass flow rate was measured by using the overflow container B18 and the collection and leveling container B17 in a discontinuous operation mode.

There are two different flow directions in the basin. Input of water is always from the side (green line top left into B15) but output may be at the top to P16 (aka complete co-current flow) or at the bottom of B15 to P18 (aka partly counter-current flow). In the second case, a part of the flow near the interface is flowing in counter current to the steam flow.

After pumps P16 and P18, the connecting line is always open in the experiments (817AHH is open). It depends on the experimental conditions whether the recirculating flow is directed through the heating (M03 and W07) or the cooling (W08) section of the facility. For heating, the water flows through the electrical heater W07 and the through steam injection mixer M03. For temperatures very near to saturation, the condensation inside M03 did not work well and the resulting steam in the line disturbed the flow meters behind M03 and lead to significant water level increase.

4.1.2 Experimental matrix

The experimental matrix design is aimed to supply a broad range of experiments with the given setup. Table 4.1 shows the actual measured values of boundary conditions averaged over the duration of the particular triggered time. The columns date, trigger and ExpID are there to identify the experiment as described in section 3.6. The flow rates are FIC8-40 (outflow at the bottom to P18), FIC8-42 (outflow at the top to P16), FIC8-44 (inflow at the top) and FI_Steam (combined flow rate of steam using FIC4-04 and FIC4-05 as described in section 3.7). Also water level LIC8-01, pressure PIC8-62 and inflow temperature TI8-33 is in the table. Figure 4.2 gives an overview of the available data on co-current flow (when FIC8-42 is 0 kg/s).

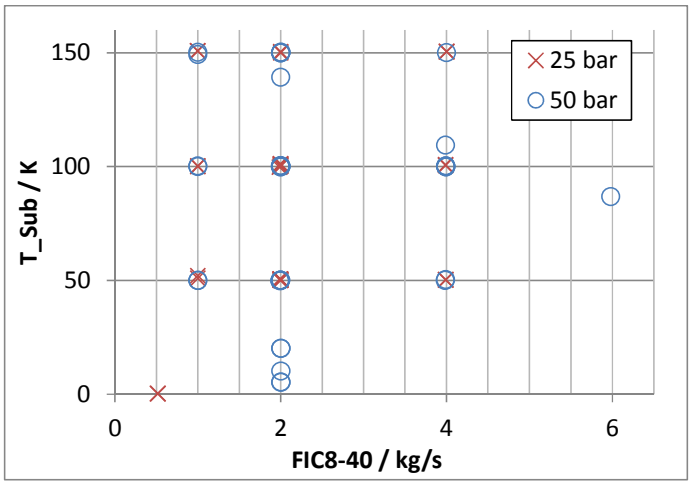

Figure 4.2: Co-current flow matrix A

Table 4.1: List of experiments in series A with measured boundary conditions

date (YYYY_MM_DD)	Trig-ger	ExpID	FIC8-40 / kg/s (P18)	FIC8-42 / kg/s (P16)	FIC8-44 / kg/s (in)	LIC8-01 / mm	PIC8-62 / MPa	TI8-33/ °C	FI_Steam / kg/s
2013_07_11	6	A05	1,981	0,000	1,998	-2,8	5,00	165,6	0,148
2013_07_11	7	A07	4,002	0,000	4,024	5,4	5,00	167,7	0,152
2013_07_11	8	A06	1,007	0,000	1,014	-0,3	5,00	165,2	0,149
2013_07_11	11	A09	0,003	2,005	1,996	0,0	5,00	165,1	0,152

Table 4.1: List of experiments in series A with measured boundary conditions

date (YYYY_MM_DD)	Trig-ger	ExpID	FIC8-40 / kg/s (P18)	FIC8-42 / kg/s (P16)	FIC8-44 / kg/s (in)	LIC8-01 / mm	PIC8-62 / MPa	TI8-33/ °C	FI_Steam / kg/s
2013_07_11	12	A12	2,004	0,000	2,012	-1,4	5,00	213,8	0,153
2013_07_11	13	A03	1,992	0,000	1,998	1,8	5,00	260,8	0,158
2013_07_11	14	A04	0,003	0,000	0,000	-4,7	5,00	262,9	0,153
2013_07_11	15	A35	1,947	0,000	1,949	1,5	5,00	114,5	0,154
2013_07_31	4	A23	0,003	1,011	0,993	-1,5	2,50	124,1	0,252
2013_07_31	5	A23	0,003	1,010	0,995	-0,9	2,50	126,5	0,252
2013_07_31	6	A24	0,003	2,000	1,992	-0,6	2,50	124,2	0,249
2013_07_31	7	A24	0,003	2,000	2,032	1,1	2,50	124,1	0,252
2013_07_31	8	A24	0,003	2,000	1,991	-0,4	2,50	124,0	0,249
2013_07_31	9	A24	0,003	2,000	1,991	-4,7	2,50	123,4	0,249
2013_07_31	10	A25	0,003	4,000	3,991	0,4	2,50	124,1	0,252
2013_07_31	11	A25	0,003	3,999	3,989	-0,6	2,50	124,2	0,251
2013_07_31	12	A22	3,990	0,000	4,003	0,3	2,50	123,6	0,250
2013_07_31	13	A22	3,990	0,000	4,003	-0,5	2,50	123,8	0,250
2013_07_31	14	A20	1,989	0,000	1,988	-0,2	2,50	124,6	0,252
2013_07_31	15	A20	2,001	0,000	2,005	-0,6	2,50	124,1	0,252
2013_07_31	17	A21	1,000	0,000	1,001	-1,1	2,50	124,2	0,253
2013_07_31	18	A21	1,000	0,000	1,001	0,3	2,50	124,3	0,252
2013_07_31	19	A33	0,199	2,000	2,198	-1,9	2,50	124,3	0,252
2013_07_31	20	A33	0,196	2,000	2,193	-1,1	2,50	124,2	0,254
2013_07_31	21	A37	0,405	1,995	2,398	1,0	2,50	124,0	0,253
2013_07_31	22	A37	0,398	1,999	2,396	1,6	2,50	123,9	0,251
2013_07_31	23	A38	0,996	2,008	3,007	-1,7	2,50	124,2	0,250
2013_07_31	24	A38	1,001	2,006	3,007	-1,2	2,50	124,2	0,250
2013_07_31	25	A39	2,005	1,998	4,010	-0,1	2,50	124,2	0,249
2013_07_31	26	A39	2,008	2,002	4,015	-0,7	2,50	124,0	0,252
2013_07_31	28	A40	0,003	6,002	5,994	-3,4	2,50	124,1	0,252
2013_08_01	1	A26	1,000	0,000	1,002	-1,7	2,50	173,4	0,251
2013_08_01	3	A26	1,000	0,000	1,003	-0,8	2,50	172,3	0,251
2013_08_01	4	A27	1,994	0,000	2,000	4,1	2,50	173,9	0,251
2013_08_01	5	A27	1,993	0,000	2,001	-0,3	2,50	173,7	0,253
2013_08_01	6	A28	3,991	0,000	4,008	2,3	2,50	174,2	0,252
2013_08_01	7	A28	3,991	0,000	4,007	-0,8	2,50	174,1	0,251

Table 4.1: List of experiments in series A with measured boundary conditions

date (YYYY_MM_DD)	Trig-ger	ExpID	FIC8-40 / kg/s (P18)	FIC8-42 / kg/s (P16)	FIC8-44 / kg/s (in)	LIC8-01 / mm	PIC8-62 / MPa	TI8-33/ °C	FI_Steam / kg/s
2013_08_01	8	A34	2,001	0,194	2,201	-1,1	2,50	174,2	0,250
2013_08_01	9	A34	1,999	0,203	2,206	-1,2	2,50	174,0	0,253
2013_08_01	10	A41	0,003	4,011	3,998	1,8	2,50	174,0	0,251
2013_08_01	12	A41	0,003	4,010	3,999	1,5	2,50	174,0	0,250
2013_08_01	13	A01	1,954	0,000	2,153	20,8	2,50	224,3	0,250
2013_08_01	14	A01	1,976	0,000	2,220	2,1	2,50	224,3	0,251
2013_08_01	15	A02	0,003	0,000	0,000	-46,8	2,50	222,9	0,253
2013_08_01	16	A36	2,000	0,000	2,000	-0,9	2,50	74,3	0,251
2013_08_01	17	A36	2,000	0,000	2,000	2,5	2,50	73,9	0,252
2013_08_01	18	A42	1,000	0,000	1,001	0,9	2,50	73,7	0,252
2013_08_01	19	A42	0,999	0,000	0,999	0,0	2,50	73,5	0,250
2013_08_01	21	A43	4,001	0,000	4,005	-1,3	2,50	73,8	0,246
2013_08_01	22	A43	4,001	0,000	4,010	-0,6	2,50	73,9	0,252
2013_08_01	23	A44	0,003	4,010	3,998	0,2	2,50	74,1	0,252
2013_08_01	24	A44	0,003	4,010	4,000	-1,0	2,50	74,0	0,252
2013_08_01	25	A45	0,003	5,999	5,990	0,6	2,50	74,2	0,249
2013_08_01	28	A45	0,003	6,000	5,992	0,4	2,50	74,0	0,251
2013_08_09	2	A29	1,998	0,000	2,001	1,6	2,50	123,7	0,402
2013_08_09	3	A29	1,997	0,000	2,002	-1,1	2,50	123,4	0,401
2013_08_09	5	A31	1,998	0,000	1,998	-2,1	2,50	123,1	0,604
2013_08_09	6	A31	1,997	0,000	2,002	-2,8	2,50	124,2	0,598
2013_08_09	7	A32	1,999	0,000	2,005	-0,1	2,50	173,9	0,600
2013_08_09	8	A32	1,998	0,000	2,005	-0,3	2,50	174,3	0,603
2013_08_09	9	A30	1,998	0,000	2,005	0,1	2,50	174,3	0,399
2013_08_09	10	A30	1,998	0,000	2,005	-1,1	2,50	174,1	0,398
2013_08_09	11	A14	1,998	0,000	2,010	-1,3	5,00	164,1	0,395
2013_08_09	12	A14	1,997	0,000	2,008	-1,7	5,00	164,1	0,398
2013_08_09	13	A16	1,997	0,000	2,008	-2,1	5,00	163,7	0,599
2013_08_09	14	A16	1,998	0,000	2,008	-1,7	5,00	164,0	0,594
2013_08_09	15	A17	1,992	0,000	2,006	-0,6	5,00	214,4	0,605
2013_08_09	16	A17	1,990	0,000	2,003	-0,2	5,00	214,2	0,595
2013_08_09	18	A15	1,994	0,000	2,006	-0,2	5,00	214,3	0,402
2013_08_09	19	A15	1,993	0,000	2,007	0,5	5,00	214,1	0,396

Table 4.1: List of experiments in series A with measured boundary conditions

date (YYYY_MM_DD)	Trig-ger	ExpID	FIC8-40 / kg/s (P18)	FIC8-42 / kg/s (P16)	FIC8-44 / kg/s (in)	LIC8-01 / mm	PIC8-62 / MPa	TI8-33/ °C	FI_Steam / kg/s
2013_08_12	2	A07	3,993	0,000	4,009	3,4	5,00	164,3	0,261
2013_08_12	3	A07	3,993	0,000	4,011	-0,3	5,00	163,9	0,250
2013_08_12	4	A07	3,993	0,000	4,016	-0,3	5,00	164,3	0,248
2013_08_12	5	A05	1,995	0,000	2,007	-1,2	5,00	164,0	0,251
2013_08_12	6	A05	1,995	0,000	2,006	0,1	5,00	164,2	0,253
2013_08_12	7	A06	0,999	0,000	1,005	-0,6	5,00	164,2	0,248
2013_08_12	9	A06	0,998	0,000	1,004	0,2	5,00	164,0	0,254
2013_08_12	10	A10	0,003	4,001	3,995	-0,7	5,00	164,3	0,248
2013_08_12	11	A10	0,003	4,000	3,995	-1,0	5,00	164,0	0,249
2013_08_12	12	A09	0,003	2,000	1,998	-1,4	5,00	164,0	0,248
2013_08_12	13	A09	0,003	2,000	1,997	-0,5	5,00	164,0	0,251
2013_08_12	14	A08	0,003	1,000	0,996	-1,0	5,00	163,9	0,249
2013_08_12	15	A08	0,003	1,000	0,994	-0,4	5,00	164,2	0,252
2013_08_12	16	A18	0,198	2,000	2,197	-1,3	5,00	164,0	0,249
2013_08_12	17	A18	0,196	2,000	2,194	-1,2	5,00	164,4	0,249
2013_08_12	18	A46	0,397	2,000	2,396	-0,6	5,00	164,3	0,249
2013_08_12	19	A46	0,397	2,000	2,395	-1,2	5,00	164,1	0,248
2013_08_12	20	A47	1,000	2,000	3,003	-0,5	5,00	164,0	0,250
2013_08_12	21	A47	0,998	2,000	3,002	0,5	5,00	164,1	0,251
2013_08_12	22	A48	1,996	2,000	4,002	-0,5	5,00	164,1	0,249
2013_08_12	23	A48	2,001	1,999	4,007	-0,6	5,00	163,9	0,251
2013_08_12	24	A48	2,000	2,000	4,008	-1,2	5,00	164,1	0,248
2013_08_12	26	A49	0,003	6,000	6,001	-1,8	5,00	164,1	0,250
2013_08_12	28	A49	0,003	6,000	5,999	-0,5	5,00	164,0	0,250
2013_08_12	29	A54	0,003	6,000	5,997	0,1	5,00	114,0	0,248
2013_08_12	30	A54	0,003	6,000	5,996	-0,7	5,00	114,1	0,250
2013_08_12	31	A53	0,003	4,000	3,996	-0,3	5,00	114,2	0,248
2013_08_12	32	A53	0,003	4,000	3,996	-1,9	5,00	114,2	0,248
2013_08_13	3	A52	3,999	0,000	4,003	-0,8	5,00	114,1	0,250
2013_08_13	4	A52	3,998	0,000	4,010	-0,2	5,00	114,1	0,252
2013_08_13	5	A35	1,999	0,000	2,006	-0,2	5,00	114,3	0,248
2013_08_13	6	A35	1,998	0,000	2,004	1,2	5,00	114,3	0,253
2013_08_13	7	A51	0,998	0,000	1,003	-0,5	5,00	113,9	0,250

Table 4.1: List of experiments in series A with measured boundary conditions

date (YYYY_MM_DD)	Trig-ger	ExpID	FIC8-40 / kg/s (P18)	FIC8-42 / kg/s (P16)	FIC8-44 / kg/s (in)	LIC8-01 / mm	PIC8-62 / MPa	TI8-33/ °C	FI_Steam / kg/s
2013_08_13	8	A51	0,998	0,000	1,003	-0,2	5,00	115,0	0,249
2013_08_13	9	A55	1,998	0,000	2,005	0,5	5,00	124,9	0,251
2013_08_13	11	A56	3,988	0,000	4,012	2,7	5,00	161,9	0,250
2013_08_13	12	A57	5,980	0,000	6,023	-1,7	5,00	177,3	0,250
2013_08_14	3	A13	3,983	0,000	4,008	0,1	5,00	214,1	0,253
2013_08_14	4	A13	3,990	0,000	4,015	0,0	5,00	213,9	0,252
2013_08_14	5	A12	1,998	0,000	2,008	-0,3	5,00	214,0	0,247
2013_08_14	6	A12	1,998	0,000	2,007	-0,3	5,00	214,2	0,249
2013_08_14	7	A11	1,001	0,000	1,003	-1,4	5,00	214,4	0,252
2013_08_14	8	A11	1,002	0,000	1,005	-0,7	5,00	214,2	0,249
2013_08_14	10	A50	0,003	4,001	3,993	-0,1	5,00	214,4	0,249
2013_08_14	12	A50	0,003	4,000	3,993	-0,5	5,00	214,1	0,251
2013_08_14	13	A19	0,202	2,001	2,197	-1,0	5,00	213,7	0,253
2013_08_14	14	A19	0,204	2,000	2,198	-0,3	5,00	211,6	0,248
2013_08_14	15	A03	2,000	0,000	2,015	4,8	5,00	258,9	0,252
2013_08_14	16	A03	2,000	0,000	2,015	9,2	5,00	259,0	0,248
2013_08_14	17	A58	2,000	0,000	2,014	43,0	5,00	254,0	0,248
2013_08_14	20	A59	2,000	0,000	2,020	7,6	5,00	244,0	0,248
2013_08_14	21	A59	2,000	0,000	2,021	0,8	5,00	244,1	0,251
2013_08_14	22	A05	2,000	0,000	2,008	1,2	5,00	163,9	0,251
2013_08_14	24	A05	2,000	0,000	2,008	-2,0	5,00	164,3	0,246
2013_08_14	25	A07	3,990	0,000	4,008	1,8	5,00	163,9	0,252
2013_08_14	26	A07	3,990	0,000	4,011	0,3	5,00	164,2	0,249
2013_08_14	27	A35	2,000	0,000	2,005	0,2	5,00	113,9	0,250
2013_08_14	28	A35	2,000	0,000	2,005	-0,1	5,00	114,0	0,249

4.1.3 Results

In figure 4.3, some high speed camera snapshots are compared. All pictures are taken from experiments with 2 kg/s water flow from left (trough FIC8-40) to right (through P16 and FIC8-40). Different pressures, inlet sub-cooling and steam mass flow rates are compared. It is visible, that the waviness of the stratification layer mainly depends on the steam velocity. Different values of the inlet sub-cooling seems not to have big influence on the interphase structure.

Figure 4.4 shows a similar comparison with the same steam mass flow rate but different water inlet flow rates. Since the density of water is much higher and much less dependent on the temperature,

different interphase structures cannot be identified here. Interphase waviness in principle depends on the velocity difference between the phases and the turbulence near the interphase. When the water inlet mass flow rate is increased, the turbulence in the water phase increases but the velocity difference decreases. The differences are too small and act against each other so they are not visible.

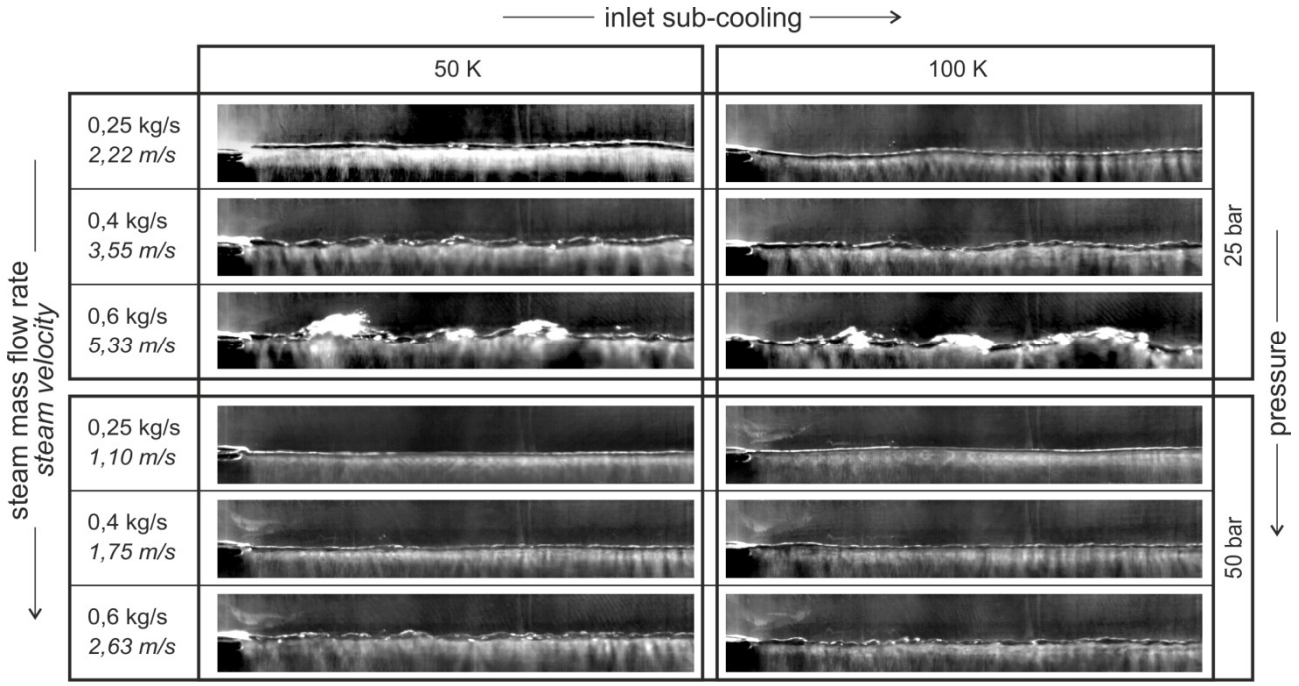

Figure 4.3: Snapshots of selected surfaces captured by the high speed camera at 2 kg/s water mass flow rate

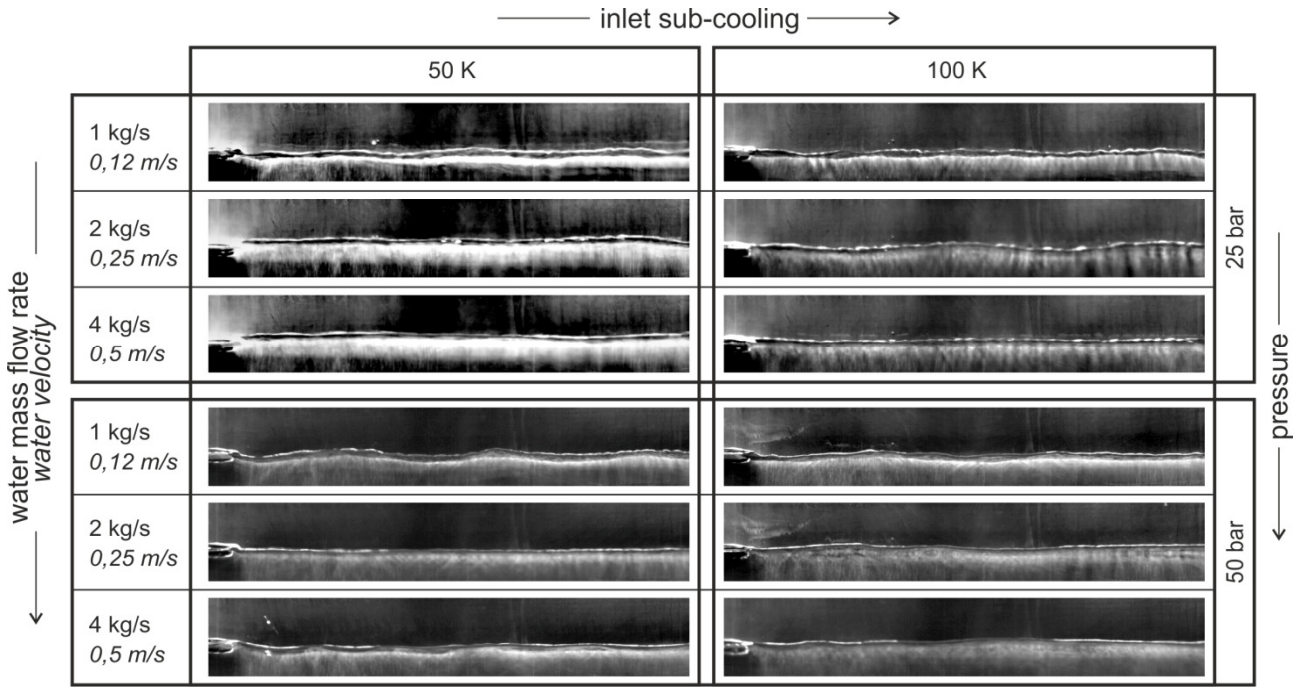

Figure 4.4: Snapshots of selected surfaces captured by the high speed camera at 0.25 kg/s steam mass flow rate

In Figure 4.7 temperature profiles are compared for the co-current flow experiments. The flow inside the basin can be assumed to be as shown with idealized streamlines in figure 4.5. The layer of condensate and heated water due to condensation is too thin in most cases to see a significant difference in the temperature profiles measured by the thermocouples. Another set of experiments

was conducted as shown in figure 4.6 with the water outlet at the bottom of the basin. In these cases it is expected and observed, that a recirculation vortex forms opposite to the water injection into the basin and at the position of the thermocouples. Therefore, warmer water is trapped in the eddy and this is measured and visible in figure 4.8.

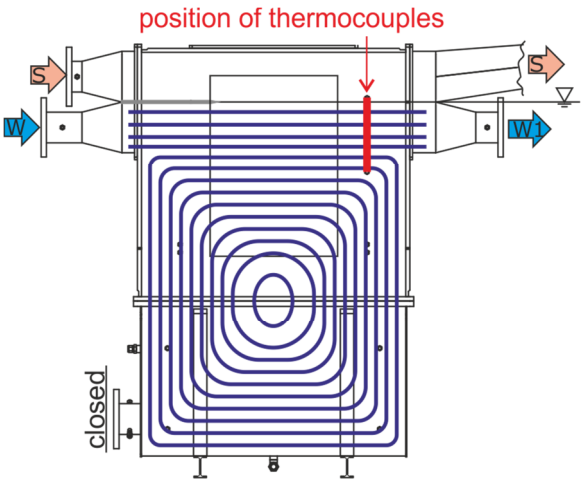

Figure 4.5: Idealized streamlines of fully co-current flow in series A

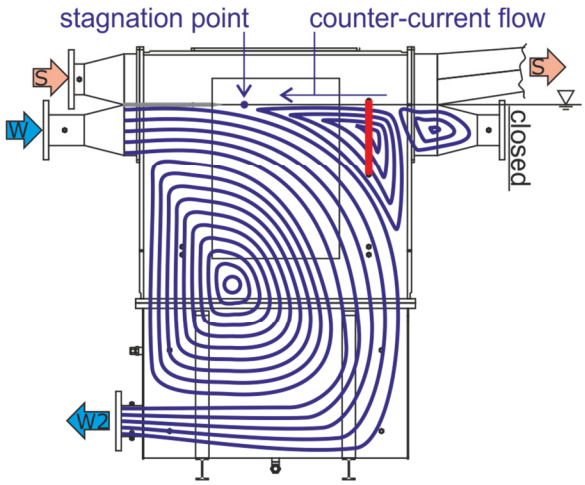

Figure 4.6: Idealized streamlines of partly counter-current flow in series A

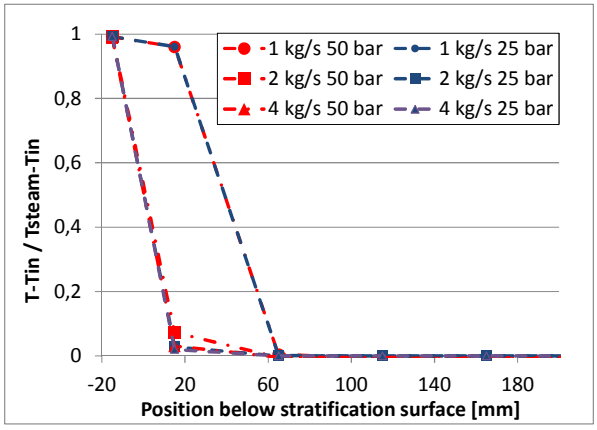

Figure 4.7: Temperature profiles of co-current flow

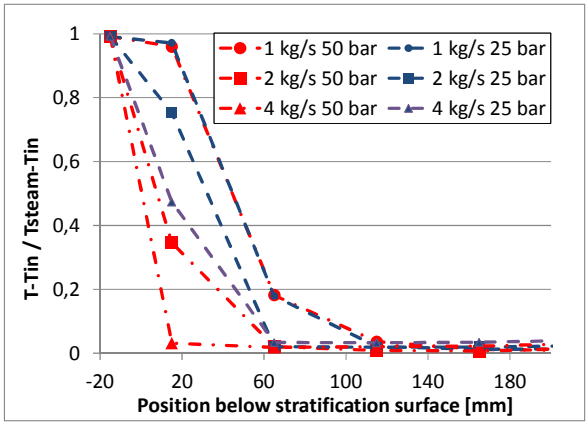

Figure 4.8: Temperature profiles of counter-current flow

In figure 4.9 the infrared image of an experiment at 50 bars and 1 kg/s inlet mass flow rate is shown together with the plot of normalized temperature $\theta = \frac{T - T_{in}}{T_{steam} - T_{in}}$ over depth below the interphase. It can be observed that a layer of about 60 mm thickness forms near the interphase over the whole facility length – even upstream to the inlet on the left of the image. Defining the condensate layer thickness where $\theta > 0.5$ makes it possible to compare different experiments as shown in figure 4.10 for all experiments with 1 kg/s inlet mass flow rate. Here it is visible, that the layer thickness depends on the inlet sub-cooling at similar inlet mass flow rate. In figure 4.11 the difference between inlet and outlet condensate layer thickness is plotted over inlet sub-cooling. Here an increase can be observed at low sub-cooling and low inlet layer thickness. For higher sub-cooling, the difference is not significant.

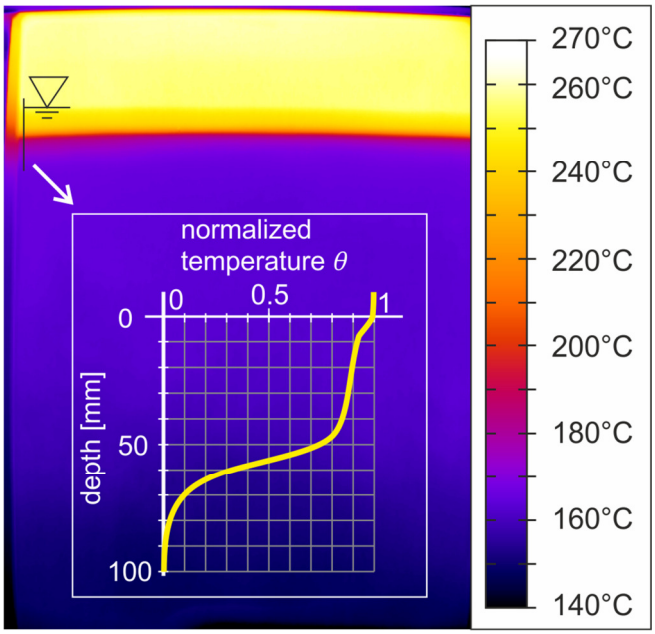

Figure 4.9: IR Temperature distribution of experiment 2013_08_13_Tr08_A51 with plot of normalized temperature over water depth near the inlet (left)

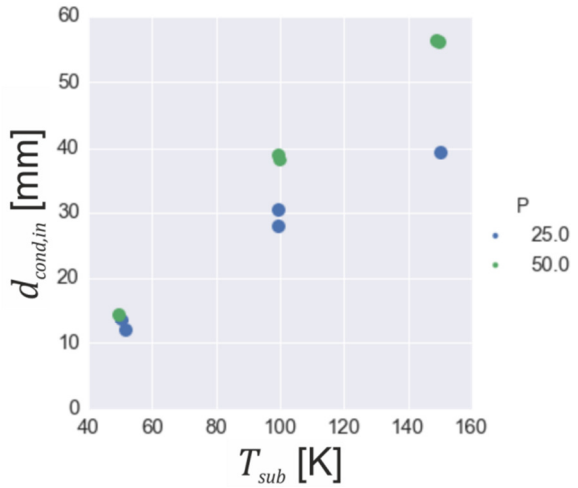

Figure 4.10: Condensation layer thickness of steam experiments with 1 kg/s inlet mass flow rate

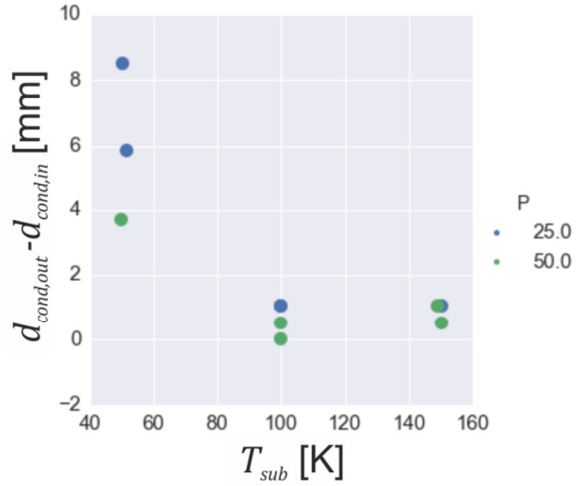

Figure 4.11: Condensation layer thickness increase between inlet and outlet (of IR-window) for the 1 kg/s experiments

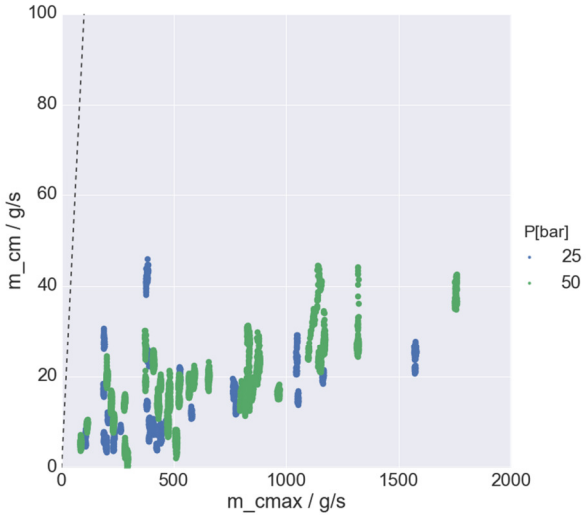

Figure 4.12: Comparison of measured condensation mass flow rate with maximum possible values m_cmax for all experiments in series A (line shows identity)

In figure 4.12 the measured condensation rate m_cm as described in section 3.7 above is plotted over the maximum possible mass flow rate of condensation m_cmax. Only about 2.5 % of the condensation potential can be observed in the measurements and so the rates are very low, which makes it also very difficult to evaluate them and the effects of condensation.

4.2 B – Jet Flow Experiments

The last experiments in chronological order are the jet flow series. The aim is to observe the jet during condensation, how the surface roughness increases and what the mechanisms of jet breakup are.

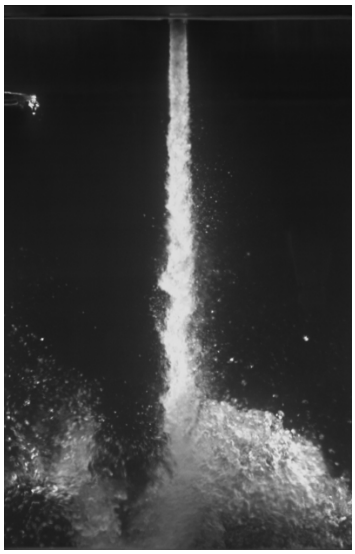

Figure 4.13: Waves caused by a water jet without strainer

4.2.1 Experiments specification

During preliminary tests on jet flow on 26.3.2014 right after the series C was finished, several observations lead to modifications in the basin. Figure 4.13 shows a high speed camera still of a jet flow with 2 kg/s injection mass flow rate. It is visible, that the bulk water below the jet forms high waves that may also influence the jet itself. Since such backlashes are not in scope here, it was decided to introduce a set of three strainers below the standard water level in order to reduce the impulse of the jet into the water (see figure 4.14 in uncovered state and appendix G for details).

Figure 4.14: Strainer at the bottom of the window in series B

At small jet mass flow rates as shown in figure 4.15 for 0.23 kg/s it was observed, that the jet was asymmetric and the directed steam flow is supposed to cause this effect. Therefor a steam guiding shield was built into the basin next to the jet injection nozzle. The drawing can be found in appendix G. It consists of stainless steel sheets guiding the steam upward above the jet nozzle exit and downward to the condenser nozzle. At the top, next to the jet nozzle, there are two well-defined openings (206x36 mm) for the steam to flow to the jet with three strainers each to homogenize the inflow. An experiment comparable to the one, mentioned above, is shown in the right side of figure 4.15. It is visible, that the installation lead to a straight downward flow of the jet as it was expected.

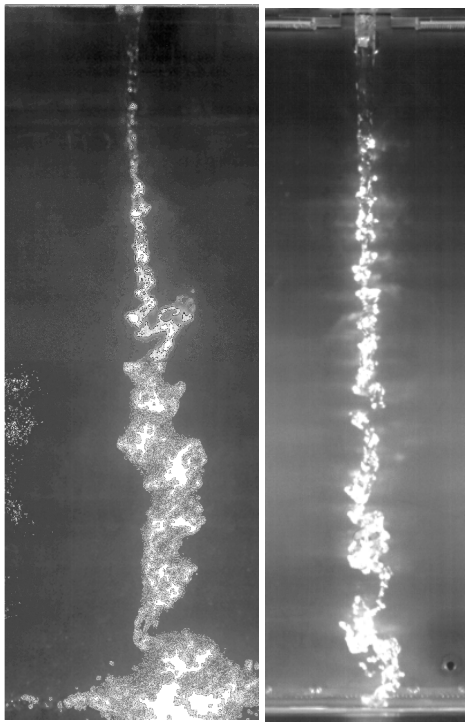

Figure 4.15: Low mass flow rate jet without (left) and with (right) steam guides

Furthermore it was observed, that non-condensable gas gets trapped near the water level, because steam and nitrogen stratifies by buoyancy at high pressure. So a degassing line was installed into the basin near the low water level (see small black circle in figure 4.15 bottom right). This opening is connected to the cooling water collection pipe via a manual operated valve. It was opened when the operator observed nitrogen intake by watching the temperature distribution in the gas phase.

Temperature and pressure sensor lances were installed for series B as described in section 3.5.

4.2.2 Experimental matrix

The distribution of boundary conditions in the matrix is optimized to cover a big range of possible combinations and a dense grid of supporting points. In figure 4.16 the distribution of steam condensation experiments is shown in terms of jet sub-cooling and mass flow rate and in figure 4.17 for the comparison to nitrogen atmosphere. Above T_Sub = 100 K and jet mass flow of 1 kg/s, the jet forms an S-shape and the steam consumption of the experiment is very high, which is supposed to be caused by the strong condensation and the fast gas flow around the jet. So it was decided that the experiments above 1.5 kg/s and 150 K sub-cooling would be too difficult and not useful for modelling.

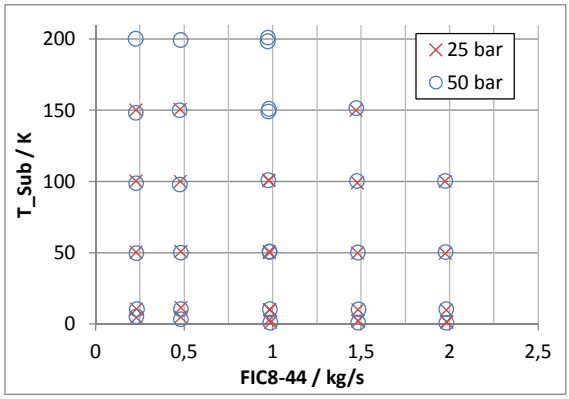

Figure 4.16: Steam-atmosphere

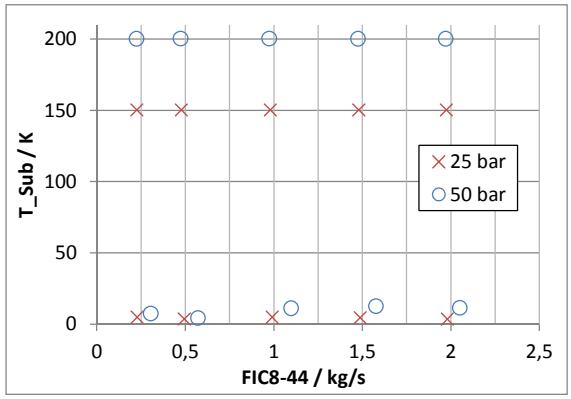

Figure 4.17: nitrogen-atmosphere

In table 4.2 the test matrix of series B is sorted by experimental day, trigger and ExpID as described in section 3.6 above. The columns contain the jet mass flow rate FIC8-44 in kg/s, the water level in mm below the standard-level in series A and C (typically around -650 mm), pressure in the tank PIC8-62 in MPa, temperature in the center of the jet injection nozzle TI8-48 in °C, the time-average of Boolean bGasIsSteam and the difference between injection and steam saturation temperature T_Sub in K.

Table 4.2: List of experiments in series B with measured boundary conditions

date (YYYY_MM_DD)	Trig-ger	ExpID	FIC8_44 / kg/s	LIC8_01 / mm	PIC8_62 / MPa	TI8_48 / °C	bGasIsSteam / time	T_Sub / K
2014_08_25	**9**	B38	1,975	-718,6	2,499	74,0	0%	150,2
2014_08_25	**10**	B39	1,480	-722,5	2,499	74,1	0%	150,1
2014_08_25	**11**	B40	0,981	-724,1	2,499	74,0	0%	150,3
2014_08_25	**12**	B41	0,478	-727,3	2,499	74,1	0%	150,1
2014_08_25	**13**	B42	0,226	-731,2	2,499	73,9	0%	150,3
2014_08_26	**10**	B32	1,980	-819,9	2,501	220,9	0%	3,3
2014_08_26	**13**	B33	1,488	-696,8	2,501	219,9	0%	4,3
2014_08_26	**14**	B34	0,992	-657,7	2,501	219,5	0%	4,8
2014_08_26	**15**	B35	0,495	-848,7	2,500	220,8	0%	3,5
2014_08_26	**16**	B36	0,228	-702,3	2,499	219,5	0%	4,8
2014_08_26	**17**	B26	1,984	-628,2	2,501	222,7	100%	1,6
2014_08_26	**18**	B27	1,485	-641,4	2,501	222,2	100%	2,1
2014_08_26	**19**	B27	1,485	-641,3	2,499	222,1	100%	2,1
2014_08_26	**20**	B28	0,984	-649,9	2,500	221,3	100%	3,0

Table 4.2: List of experiments in series B with measured boundary conditions

date (YYYY_MM_DD)	Trig-ger	ExpID	FIC8_44 / kg/s	LIC8_01 / mm	PIC8_62 / MPa	TI8_48 / °C	bGasIsSteam / time	T_Sub / K
2014_08_26	**21**	B29	0,482	-636,9	2,500	219,6	100%	4,7
2014_08_26	**22**	B30	0,232	-642,5	2,500	219,9	100%	4,4
2014_08_27	**5**	B20	1,982	-637,6	2,501	214,5	100%	9,7
2014_08_27	**6**	B21	1,483	-663,7	2,501	214,4	100%	9,9
2014_08_27	**7**	B22	0,987	-661,5	2,501	214,3	100%	10,0
2014_08_27	**13**	B23	0,484	-623,2	2,501	212,9	100%	11,4
2014_08_27	**15**	B24	0,232	-633,0	2,501	214,0	100%	10,3
2014_08_27	**16**	B14	1,978	-621,6	2,501	174,7	100%	49,6
2014_08_27	**17**	B15	1,481	-624,7	2,500	174,6	100%	49,6
2014_08_27	**18**	B16	0,982	-627,1	2,500	173,5	100%	50,7
2014_08_27	**19**	B17	0,482	-615,9	2,499	173,3	100%	50,9
2014_08_27	**20**	B18	0,231	-636,7	2,499	173,9	100%	50,4
2014_08_27	**21**	B10	0,980	-618,4	2,499	123,7	100%	100,5
2014_08_27	**24**	B11	0,480	-617,7	2,499	124,0	100%	100,2
2014_08_27	**25**	B12	0,230	-644,9	2,499	124,0	100%	100,3
2014_08_27	**26**	B06	0,229	-615,6	2,499	74,0	100%	150,2
2014_08_28	**2**	B05	0,479	-617,5	2,501	73,6	100%	150,6
2014_08_28	**3**	B04	0,978	-619,0	2,501	74,4	79%	149,9
2014_08_28	**4**	B09	1,479	-622,1	2,500	125,2	100%	99,1
2014_08_28	**5**	B08	1,975	-630,5	2,500	124,2	100%	100,1
2014_08_28	**6**	B03	1,474	-622,8	2,500	74,3	100%	150,0
2014_08_28	**7**	B02	1,969	-621,1	2,500	74,0	78%	150,3
2014_08_28	**8**	B02	1,969	-619,7	2,500	74,8	85%	149,5
2014_08_28	**9**	B10	0,980	-617,2	2,501	123,4	100%	100,8
2014_08_28	**11**	B16	0,984	-616,5	2,500	174,2	100%	50,0
2014_08_28	**12**	B22	0,983	-631,0	2,501	214,3	100%	9,9
2014_08_28	**13**	B28	0,989	-633,0	2,501	223,1	100%	1,1
2014_08_28	**14**	B26	1,987	-627,8	2,501	223,2	100%	1,1
2014_09_15	**1**	B86	1,971	-718,4	4,999	63,9	0%	200,3
2014_09_15	**2**	B87	1,475	-719,9	4,999	63,9	0%	200,2
2014_09_15	**3**	B88	0,974	-720,4	4,999	63,8	0%	200,4
2014_09_15	**4**	B89	0,473	-721,3	4,999	63,8	0%	200,4
2014_09_15	**6**	B90	0,223	-726,1	5,000	63,9	0%	200,2
2014_09_16	**4**	B80	2,051	-713,4	5,001	252,7	0%	11,5
2014_09_16	**5**	B81	1,577	-686,5	5,001	251,6	0%	12,6
2014_09_16	**6**	B82	1,097	-649,6	5,000	253,1	0%	11,1
2014_09_16	**7**	B83	0,571	-690,5	4,999	260,0	0%	4,2
2014_09_16	**8**	B84	0,304	-825,1	4,999	256,7	0%	7,5
2014_09_16	**11**	B74	1,982	-684,6	5,001	263,5	100%	0,7
2014_09_16	**12**	B75	1,483	-680,8	5,001	263,3	100%	0,9
2014_09_16	**13**	B76	0,987	-680,8	5,001	263,2	100%	1,0
2014_09_16	**14**	B77	0,482	-642,8	5,001	261,0	100%	3,2

Table 4.2: List of experiments in series B with measured boundary conditions

date (YYYY_MM_DD)	Trig-ger	ExpID	FIC8_44 / kg/s	LIC8_01 / mm	PIC8_62 / MPa	TI8_48 / °C	bGasIsSteam / time	T_Sub / K
2014_09_16	**15**	B78	0,231	-655,3	5,000	258,9	100%	5,3
2014_09_17	**2**	B68	1,981	-702,5	5,001	253,9	100%	10,3
2014_09_17	**5**	B69	1,486	-692,4	5,001	254,0	100%	10,2
2014_09_17	**6**	B70	0,985	-654,4	5,001	253,8	100%	10,4
2014_09_17	**8**	B71	0,481	-649,9	5,001	253,9	100%	10,3
2014_09_17	**9**	B72	0,233	-636,9	5,001	253,8	100%	10,4
2014_09_17	**10**	B62	1,977	-659,8	5,001	213,8	100%	50,4
2014_09_17	**11**	B63	1,481	-665,9	5,000	214,1	100%	50,1
2014_09_17	**12**	B64	0,982	-657,1	4,999	213,5	100%	50,7
2014_09_17	**13**	B65	0,482	-657,7	5,000	214,1	100%	50,1
2014_09_17	**14**	B66	0,231	-617,8	4,999	214,5	100%	49,7
2014_09_18	**3**	B58	0,975	-640,3	5,001	163,3	100%	100,9
2014_09_18	**4**	B57	1,475	-627,8	5,001	163,9	100%	100,3
2014_09_18	**5**	B52	0,977	-645,1	5,001	114,9	100%	149,3
2014_09_18	**6**	B47	0,480	-670,2	5,001	64,8	100%	199,4
2014_09_18	**8**	B46	0,973	-645,5	5,001	65,8	100%	198,4
2014_09_18	**9**	B56	1,975	-642,8	5,001	163,9	100%	100,3
2014_09_18	**11**	B51	1,472	-650,7	5,000	112,7	100%	151,5
2014_09_18	**13**	B46	0,974	-655,6	5,000	63,2	100%	201,0
2014_09_18	**14**	B52	0,978	-644,8	4,999	113,1	100%	151,1
2014_09_19	**1**	B59	0,476	-639,0	5,001	166,3	100%	97,9
2014_09_19	**3**	B60	0,229	-652,2	5,001	165,5	100%	98,7
2014_09_19	**5**	B53	0,474	-636,4	5,001	114,3	100%	149,9
2014_09_19	**7**	B54	0,227	-679,4	5,001	116,0	100%	148,2
2014_09_19	**8**	B48	0,226	-641,3	5,000	64,0	100%	200,2
2014_09_19	**10**	B64	0,982	-607,1	4,999	213,3	100%	50,9
2014_09_19	**11**	B58	0,977	-639,4	4,999	163,9	100%	100,3

4.2.3 Results

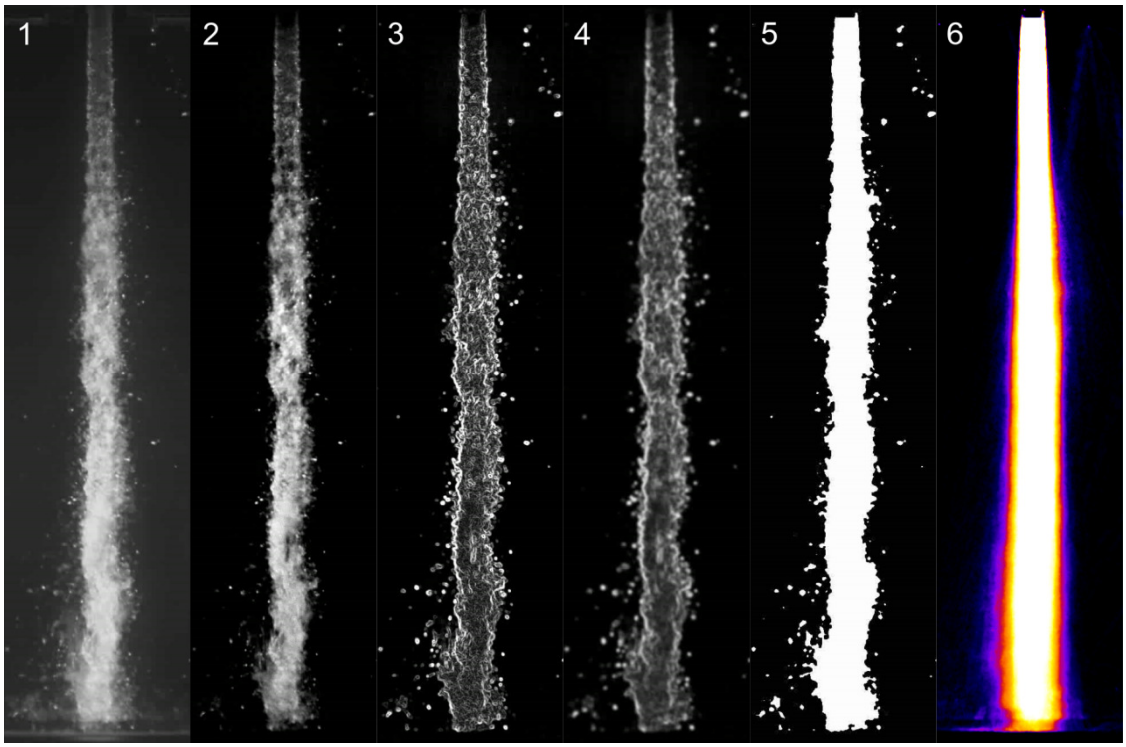

Figure 4.18: Exemplary image processing steps applied to the first frame of experiment 2014_09_19_Tr11_B58 with p=50 bar, m_{in}=1 kg/s and T_{in}=164 °C (100 K sub-cooling)

In order to compare different experiments, image processing as shown in figure 4.18 was used to extract data. The first image shows the original raw image and the images 2 to 5 contain the results of the processing steps: background subtraction, edge filtering, noise filtering and binarization. As a first result, part 5 shows the binary information if there is water visible along the view of the camera in every pixel and one point in time. The last step shows the average value (of the prior) over the whole video. This can be understood as an optical void distribution, since it is related to the average void distribution but it is also an integral value along the camera view. Assuming that the jet is axisymmetric makes it possible to extract the mean jet diameter of the experiment in every position along the jet.

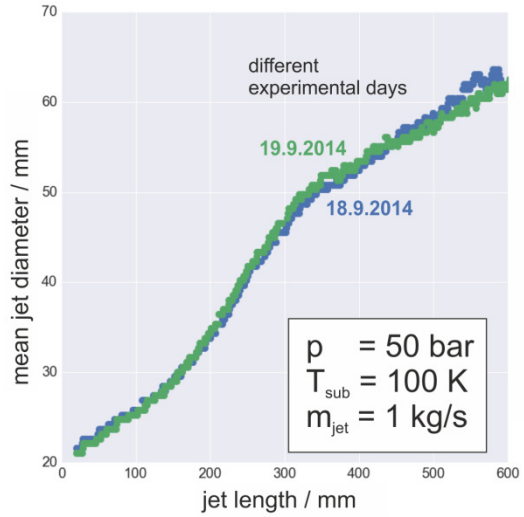

Figure 4.19: Mean jet diameter plotted over jet length for experiments B58

In figure 4.19 the extracted jet diameter is plotted over the jet length for the two repetitions of the experiment B58 (shown in figure 4.18) on two different days. It is visible, that the behavior is similar, so the method gives reproducible results. Furthermore it has to be noted, that the assumption of an axisymmetric shape cannot be valid for diameters over 50 mm since the basin is 50 mm deep and the jet is supposed to touch the outer wall then – so these values are removed for the following analysis. Figure 4.20 shows the comparison of the same boundary conditions with different jet inlet mass flow rate. It is visible that the diameter rises

earlier when the flow rate is higher, which is supposed to be an effect of the initial turbulence which increases the surface roughness and enhances the drag of the jet. A special case is the experiment with 0.25 kg/s jet mass flow rate also shown on the side of the figure. The jet first accelerates because of gravity forces and the roughness increases at the same time. At some point at about 250 mm from the nozzle, the jet expands rapidly because the drag gets too high and the jet inertia are relatively low. The jet breaks up and a spray of single droplets is formed.

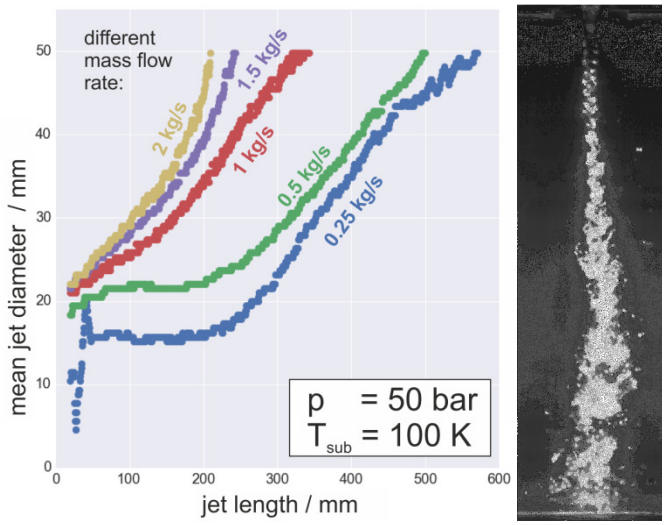

Figure 4.20: Jet diameters over length for different jet inlet mass flow rate and a high speed camera snapshot of the experiment with 0.25 kg/s

The comparison of different jet inlet sub-cooling is shown in figure 4.21. It is evident that the mean jet diameter increases with higher sub-cooling, which may be a coupled effect of the condensation induced turbulence and the relatively high drag forces. Also high temperature gradients in the jet can be responsible for the increase at high sub-cooling. As it is visible in figure 4.22, the diameter increase is also present at the lower pressure of 25 bars but at higher jet lengths. Due to the lower gas density, inertia of the steam is much lower and therefore drag forces are lower at 25 bars.

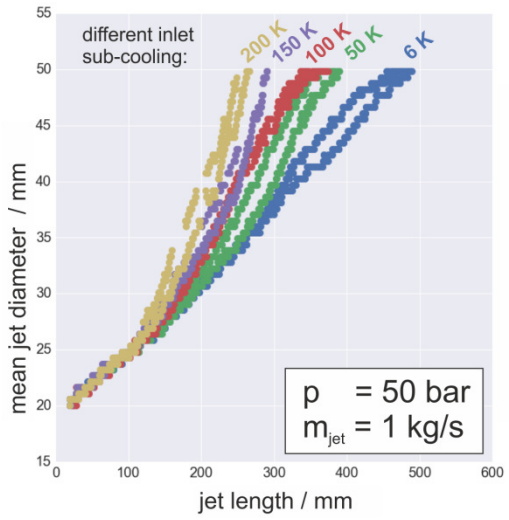

Figure 4.21: Jet diameters over length for different jet inlet sub-cooling

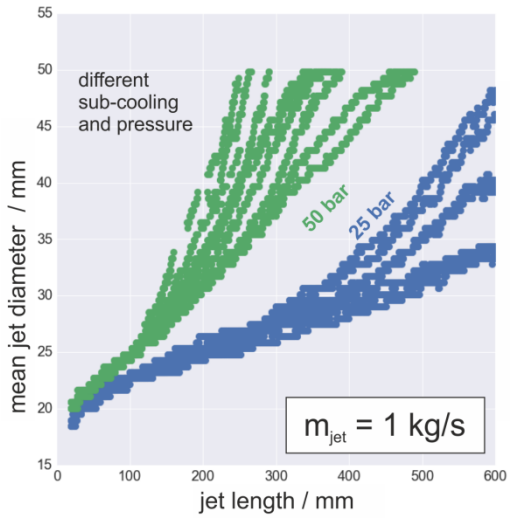

Figure 4.22: Jet diameters over length for different system pressure

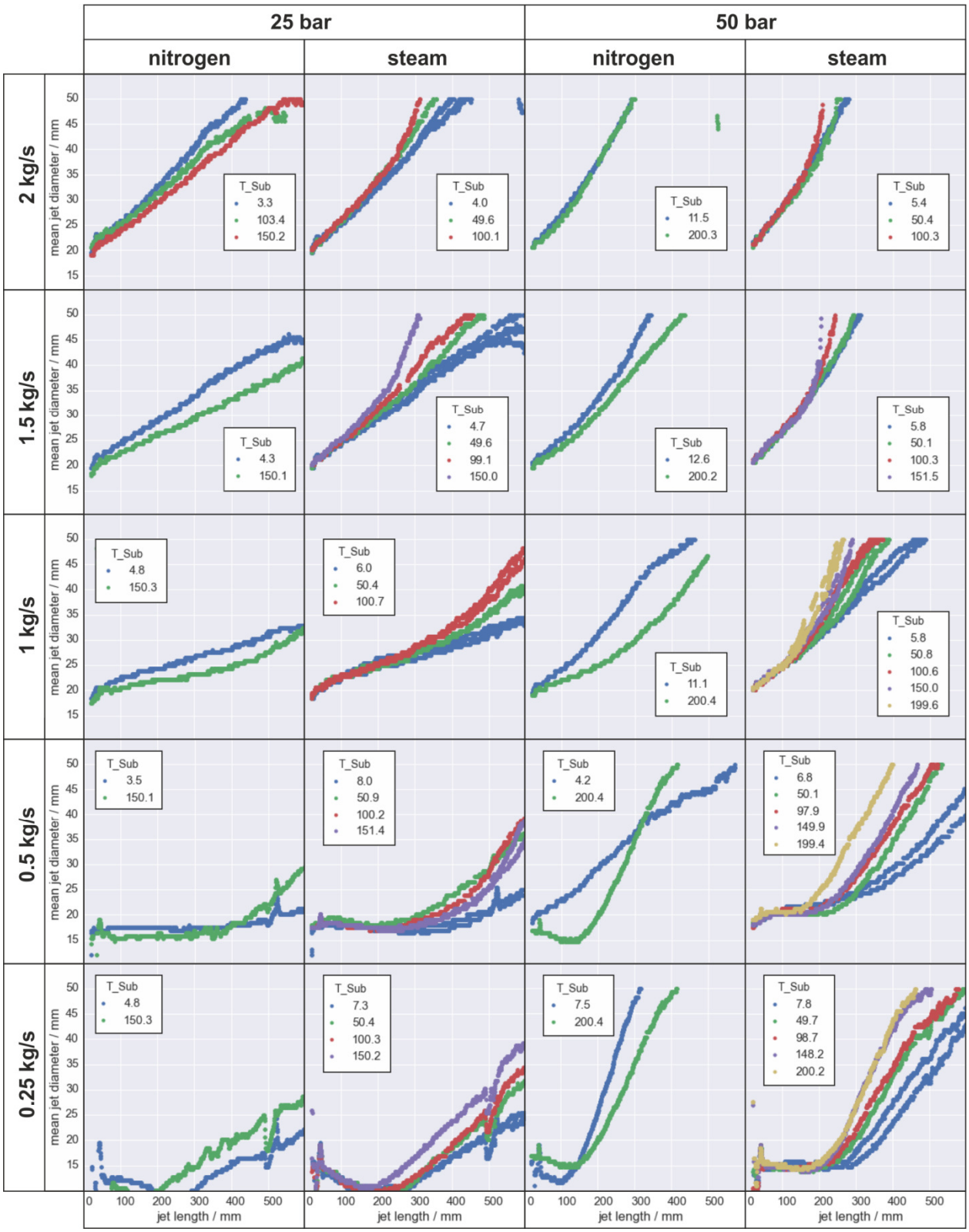

Figure 4.23: Overview of jet diameters plotted over jet length from nozzle for different ambient pressure and gas medium (columns), different jet injection mass flow rate (rows) and different jet inlet sub-cooling in K (color)

Figure 4.23 gives an overview of all the analyzed diameter profiles described above. The phenomena described above can be found in the whole experimental matrix. Furthermore it can be noted, that the temperature dependence of the jet diameter is opposite for most of the experiments with nitrogen as gas atmosphere.

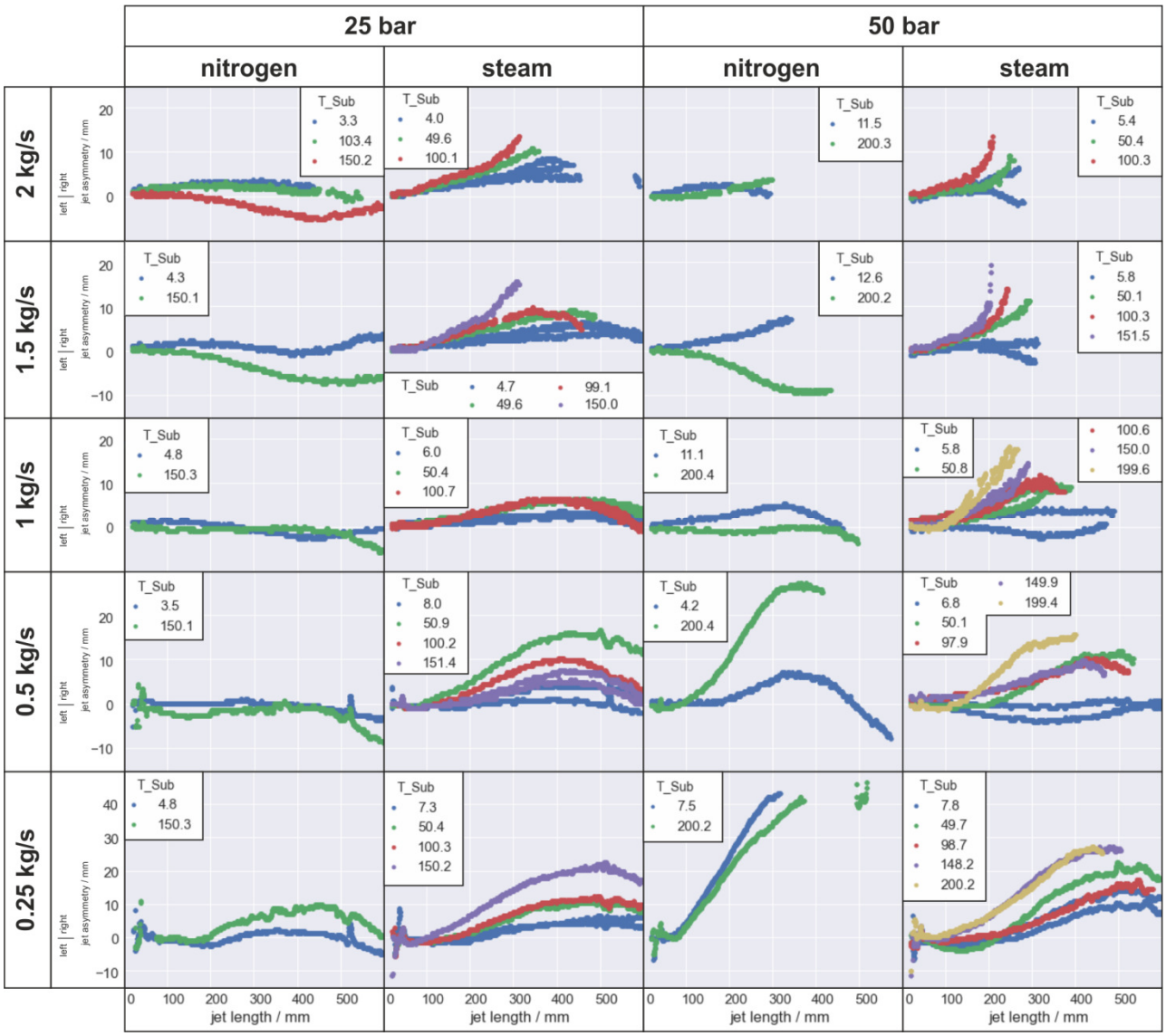

Figure 4.24: Overview of jet asymmetry

Similarly figure 4.24 shows an overview of the asymmetry of the experimental jets extracted from the same images. Basically most jets are symmetric in the range ±10 mm. It can be noted, that most asymmetric jet shapes are directed to the right and that the jets with higher gas pressure are much more asymmetric. Therefore, the asymmetry is supposed to be caused by the flow of the gas, which is induced by the water downward flow itself. When steam condenses on the jet surface, there is an additional flow downwards from the steam inlet strainers described in section 4.2.1 above. It is also possible, that the strainers are not sufficient when gas flow rates are very high and that the steam has an initial flow direction toward the steam condenser near the inlet to the visible test section.

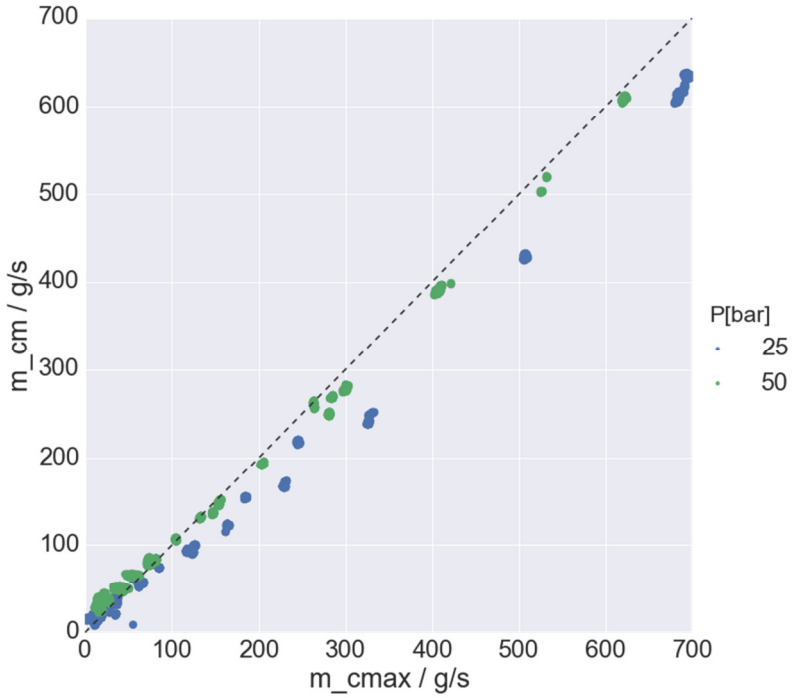

Figure 4.25: Comparison of measured condensation mass flow rate m_cm with maximum possible values m_cmax for all experiments in series B

Figure 4.25 shows the overall measured condensation mass flow rates of the facility plotted over the maximal possible flow rate for the respective injection of cold water as described in section 3.7 above. It can be noted, that the maximum is reached nearly for most experiments and the measured rate is even higher than the maximum for some experiments at low m_cmax. The reason is a combination of measurement uncertainty and parasitic condensation besides the observed direct condensation caused by heat losses. Furthermore the experiments at 50 bars show higher condensation rates than the points at 25 bars. This may be connected to the higher drag between the phases as discussed above with the diameter profiles.

4.3 C – Plunging Jet Experiments

Plunging jet experiments combine the flow situations investigated in the other two test series. The jet first falls through gas atmosphere and the plunges into the basin causing the bulk water to flow and enhancing the condensation on the stratification as well.

The phenomenon that is not present in the previous described experiments is the plunging and the entrainment of gas beneath the water level. The steam condenses during the entrainment process, so it is supposed that it also influences the entrainment process itself.

4.3.1 Experiments specification

In Addition to the setup described for test series A, the jet injection nozzle was installed into the basin for experimental series C. The piping around the pressure tank was changed between series A and C and was the same in series B (see figure 2.7 and appendix C).

4.3.2 Experimental matrix

Similar to the series B, figure 4.26 shows the experimental matrix in terms of sub-cooling and jet mass flow rate for all steam condensation experiments and figure 4.27 shows the same for experiments with nitrogen atmosphere.

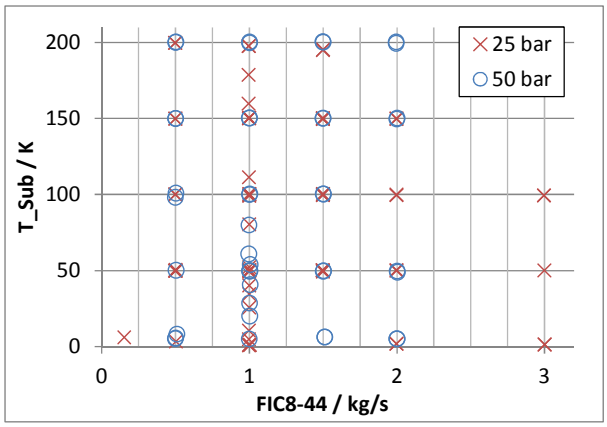

Figure 4.26: Boundary conditions of series B experiments with steam-atmosphere

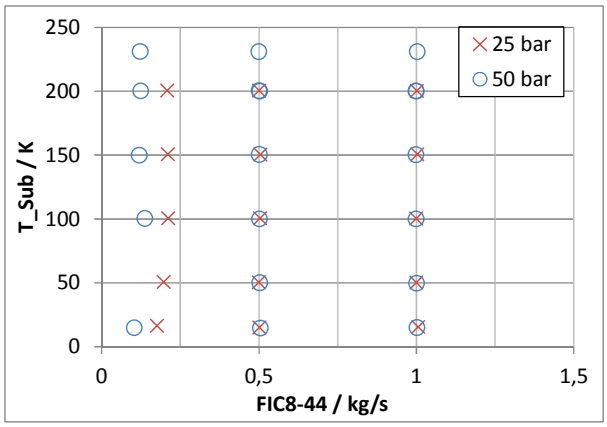

Figure 4.27: Boundary conditions of series B experiments with nitrogen-atmosphere

In table 4.3 the matrix of series C is sorted by experimental day, trigger and ExpID as before. The columns contain the horizontal mass flow rate FI8-41, the jet mass flow rate FIC8-44 in kg/s, the water level in mm, pressure in the tank PIC8-62 in MPa, temperature of the side injection TI8-31, temperature in the center of the jet injection nozzle TI8-48 in °C, the steam mass flow rate FI_Steam, the time-average of Boolean bGasIsSteam and the difference between injection and steam saturation temperature T_Sub in K. Some of the 25 bar steam experiments were repeated on 25.3.2014 with a lower steam flow rate, because in the beginning of series C, the influence of high steam velocity on the jet and the entrainment was underestimated. Also most experiments are repeated at least once, because two different camera settings were applied to the same conditions.

Table 4.3: List of experiments in series C with measured boundary conditions

date (YYY_MM_DD)	Trig-ger	ExpID	FI8_41 / kg/s	FIC8_44 / kg/s	LIC8_01 / mm	PIC8_62 / MPa	TI8_33 / °C	TI8_48 / °C	FI_Steam / kg/s	bGasIs-Steam	T_Sub / K
2014_03_13	**9**	C06	0,000	1,500	3,0	2,499	189,5	174,1	0,301	100%	49,8
2014_03_13	**10**	C06	0,000	1,501	-1,4	2,499	188,4	174,8	0,300	100%	49,1
2014_03_13	**11**	C07	0,000	1,002	0,0	2,499	185,9	174,2	0,302	100%	49,7
2014_03_13	**12**	C07	0,000	1,003	0,8	2,499	185,9	174,8	0,301	100%	49,1
2014_03_13	**15**	C08	0,000	0,504	-0,4	2,499	188,3	174,1	0,302	100%	49,8
2014_03_13	**16**	C08	0,000	0,502	0,4	2,499	188,3	174,3	0,299	100%	49,6
2014_03_13	**17**	C16	0,000	2,000	1,9	2,499	189,3	174,1	0,301	100%	49,8
2014_03_13	**18**	C16	0,000	1,998	-0,3	2,499	188,8	173,6	0,301	100%	50,3
2014_03_13	**19**	C17	0,000	3,000	1,0	2,499	194,5	173,9	0,302	100%	50,0
2014_03_13	**21**	C10	1,000	1,001	-2,8	2,499	182,2	174,4	0,298	100%	49,5
2014_03_13	**22**	C10	1,000	1,000	-1,3	2,499	182,2	174,4	0,301	100%	49,5
2014_03_13	**23**	C05	1,005	1,000	0,1	2,499	148,3	124,5	0,300	100%	99,4
2014_03_13	**24**	C05	1,003	0,998	1,7	2,499	147,0	124,1	0,300	100%	99,9
2014_03_13	**25**	C02	0,000	1,001	-1,8	2,499	148,7	124,5	0,302	100%	99,5
2014_03_13	**26**	C02	0,000	1,001	-1,2	2,499	149,0	124,8	0,299	100%	99,1
2014_03_13	**27**	C01	0,000	1,501	-1,3	2,499	149,8	124,3	0,299	100%	99,7
2014_03_13	**28**	C01	0,000	1,501	-1,4	2,499	150,5	124,4	0,300	100%	99,6
2014_03_14	**2**	C03	0,000	2,000	-1,5	2,499	150,2	124,0	0,300	100%	100,1
2014_03_14	**3**	C03	0,000	2,000	-1,6	2,499	151,7	124,6	0,302	100%	99,4
2014_03_14	**4**	C04	0,000	2,997	0,8	2,499	159,8	124,8	0,303	100%	99,2
2014_03_14	**5**	C04	0,000	2,998	1,4	2,499	160,1	124,6	0,303	100%	99,4
2014_03_14	**6**	C13	0,000	1,998	0,1	2,499	114,6	74,1	0,303	100%	150,0
2014_03_14	**7**	C13	0,000	1,999	1,2	2,499	113,8	74,6	0,304	100%	149,5
2014_03_14	**8**	C12	0,000	1,501	2,0	2,499	111,6	74,6	0,304	100%	149,5
2014_03_14	**9**	C12	0,000	1,500	-0,1	2,499	111,9	74,5	0,303	100%	149,5
2014_03_14	**10**	C11	0,000	1,000	0,3	2,499	112,9	74,1	0,301	100%	150,0
2014_03_14	**11**	C11	0,000	1,000	0,1	2,499	112,7	73,9	0,302	100%	150,2
2014_03_14	**12**	C15	0,998	1,003	-2,8	2,499	114,4	74,6	0,303	100%	149,4
2014_03_14	**13**	C15	0,996	1,000	-0,4	2,499	113,0	74,3	0,304	100%	149,8
2014_03_14	**14**	C18	1,000	1,003	6,7	2,499	219,2	218,0	0,302	100%	6,1
2014_03_14	**15**	C18	0,997	1,002	8,1	2,499	220,1	218,9	0,303	100%	5,2
2014_03_14	**16**	C19	0,000	2,001	-2,8	2,499	222,5	222,4	0,303	100%	1,7
2014_03_14	**17**	C19	0,000	2,000	5,2	2,499	223,0	222,3	0,302	100%	1,8
2014_03_14	**18**	C20	0,000	3,003	8,7	2,499	223,8	222,8	0,303	100%	1,3
2014_03_14	**19**	C20	0,000	3,003	-1,8	2,499	223,7	222,9	0,297	100%	1,2
2014_03_14	**20**	C21	0,000	1,008	2,1	2,499	221,9	223,1	0,302	100%	1,0

Table 4.3: List of experiments in series C with measured boundary conditions

date (YYY_MM_DD)	Trig-ger	ExpID	FI8_41 / kg/s	FIC8_44 / kg/s	LIC8_01 / mm	PIC8_62 / MPa	TI8_33 / °C	TI8_48 / °C	FI_Steam / kg/s	bGasIs-Steam	T_Sub / K
2014_03_14	**21**	C21	0,000	1,001	2,6	2,499	221,8	223,1	0,305	100%	1,0
2014_03_14	**22**	C22	0,000	1,001	-1,5	2,499	221,1	222,8	0,092	68%	1,3
2014_03_14	**23**	C22	0,000	1,001	0,3	2,499	221,2	223,2	0,102	100%	0,9
2014_03_14	**24**	C22	0,000	1,000	-5,9	2,499	221,3	223,3	0,102	100%	0,8
2014_03_14	**25**	C25	0,000	0,505	9,1	2,499	218,5	220,8	0,101	100%	3,2
2014_03_14	**26**	C24	0,000	0,156	-6,7	2,499	215,5	218,1	0,101	100%	6,0
2014_03_14	**28**	C25	0,000	0,999	-10,3	2,499	217,2	219,5	0,102	100%	4,7
2014_03_14	**29**	C25	0,000	0,999	-0,2	2,499	215,6	213,7	0,132	100%	10,4
2014_03_14	**30**	C25	0,000	1,003	-43,4	2,499	206,4	198,6	0,134	100%	25,5
2014_03_14	**31**	C25	0,000	1,002	1,4	2,499	198,4	189,8	0,135	100%	34,3
2014_03_14	**32**	C25	0,000	1,003	2,1	2,499	193,5	184,0	0,132	100%	40,1
2014_03_14	**33**	C25	0,000	1,003	0,1	2,499	186,1	172,0	0,134	100%	52,1
2014_03_14	**34**	C25	0,000	1,002	4,2	2,499	173,2	143,8	0,133	100%	80,3
2014_03_14	**35**	C25	0,000	0,999	1,8	2,499	152,3	112,9	0,132	100%	111,2
2014_03_14	**36**	C25	0,000	0,998	2,2	2,494	138,3	64,3	0,161	100%	159,7
2014_03_14	**37**	C25	0,000	0,998	-2,0	2,489	125,7	45,2	0,158	100%	178,7
2014_03_18	**2**	C26	0,000	0,209	0,6	2,500	23,0	24,0	0,016	0%	200,2
2014_03_18	**3**	C27	0,000	0,501	1,0	2,501	23,0	24,0	0,016	0%	200,2
2014_03_18	**4**	C28	0,000	1,002	-1,5	2,500	23,1	24,1	0,016	0%	200,1
2014_03_18	**6**	C31	0,000	1,003	2,1	2,501	71,8	74,0	0,016	0%	150,2
2014_03_18	**7**	C30	0,000	0,504	4,8	2,501	72,6	74,0	0,016	0%	150,2
2014_03_18	**8**	C29	0,000	0,211	-0,8	2,501	69,3	73,9	0,016	0%	150,3
2014_03_18	**10**	C34	0,000	1,000	-1,7	2,500	121,2	124,1	0,016	0%	100,1
2014_03_18	**11**	C33	0,000	0,503	2,9	2,500	121,1	124,0	0,016	0%	100,2
2014_03_18	**12**	C32	0,000	0,212	0,8	2,500	114,9	123,9	0,016	0%	100,3
2014_03_18	**13**	C37	0,000	1,000	-0,3	2,501	170,4	174,3	0,016	0%	49,9
2014_03_18	**14**	C36	0,000	0,500	1,4	2,500	170,4	174,1	0,016	0%	50,1
2014_03_18	**15**	C35	0,000	0,197	-3,1	2,499	163,1	173,7	0,016	0%	50,5
2014_03_18	**17**	C40	0,000	1,007	4,4	2,501	203,7	208,9	0,016	0%	15,3
2014_03_18	**18**	C39	0,000	0,501	-1,3	2,501	204,1	209,4	0,016	0%	14,8
2014_03_18	**20**	C38	0,000	0,176	2,4	2,499	197,5	208,1	0,016	0%	16,1
2014_03_19	**2**	C43	0,000	1,003	-2,6	5,001	32,6	33,2	0,016	0%	230,9
2014_03_19	**3**	C42	0,000	0,500	2,5	4,999	32,5	33,1	0,016	0%	231,0
2014_03_19	**4**	C41	0,000	0,122	-3,1	4,999	32,0	33,0	0,016	0%	231,1
2014_03_19	**5**	C46	0,000	0,998	-0,4	5,001	62,2	64,0	0,016	0%	200,2
2014_03_19	**7**	C45	0,000	0,500	0,6	4,999	62,6	63,7	0,016	0%	200,5
2014_03_19	**9**	C70	1,003	1,002	-0,9	5,001	176,3	164,5	0,267	100%	99,6

Table 4.3: List of experiments in series C with measured boundary conditions

date (YYY_MM_DD)	Trig-ger	ExpID	FI8_41 / kg/s	FIC8_44 / kg/s	LIC8_01 / mm	PIC8_62 / MPa	TI8_33 / °C	TI8_48 / °C	FI_Steam / kg/s	bGasIs-Steam	T_Sub / K
2014_03_19	**10**	C70	1,003	1,002	0,6	5,001	177,1	164,3	0,268	100%	99,8
2014_03_19	**11**	C72	0,000	1,500	-4,5	5,001	199,3	163,8	0,291	100%	100,4
2014_03_19	**12**	C72	0,000	1,502	-2,4	5,000	192,3	163,9	0,290	100%	100,3
2014_03_19	**13**	C71	0,000	2,000	4,4	5,001	196,2	164,5	0,302	65%	99,7
2014_03_19	**14**	C71	0,000	1,998	-1,2	5,000	200,1	164,2	0,300	0%	100,0
2014_03_19	**15**	C73	0,000	1,001	-0,9	5,000	184,8	164,2	0,237	100%	100,0
2014_03_19	**16**	C73	0,000	1,003	-0,7	5,000	183,1	163,8	0,235	100%	100,4
2014_03_19	**17**	C74	0,000	0,501	1,5	4,999	176,1	163,3	0,221	100%	100,9
2014_03_19	**18**	C74	0,000	0,499	1,8	5,000	178,1	165,9	0,224	100%	98,2
2014_03_19	**19**	C75	1,001	0,996	-3,2	5,001	226,8	214,4	0,224	100%	49,8
2014_03_19	**21**	C75	0,997	0,998	-0,3	5,001	232,1	215,1	0,224	100%	49,0
2014_03_19	**22**	C77	0,000	1,503	-1,8	5,001	228,7	214,4	0,261	100%	49,8
2014_03_19	**23**	C77	0,000	1,501	3,1	5,001	229,3	214,6	0,260	100%	49,5
2014_03_19	**24**	C76	0,000	2,003	8,8	5,001	233,5	215,3	0,294	100%	48,9
2014_03_19	**25**	C76	0,000	2,002	2,9	5,001	232,4	214,4	0,294	100%	49,8
2014_03_19	**26**	C78	0,000	1,002	-2,9	5,000	226,3	214,6	0,270	100%	49,6
2014_03_19	**27**	C78	0,000	1,002	0,9	5,000	222,6	214,2	0,263	100%	50,0
2014_03_20	**2**	C46	0,000	1,000	-0,3	5,001	62,1	64,0	0,019	0%	200,1
2014_03_20	**3**	C45	0,000	0,502	1,6	5,000	61,4	64,1	0,016	0%	200,0
2014_03_20	**4**	C44	0,000	0,124	1,6	5,000	61,0	63,9	0,016	0%	200,3
2014_03_20	**5**	C49	0,000	0,999	-2,3	5,001	109,8	113,9	0,016	0%	150,3
2014_03_20	**6**	C48	0,000	0,501	0,2	5,001	109,9	113,6	0,016	0%	150,5
2014_03_20	**7**	C47	0,000	0,120	2,5	5,001	110,4	114,2	0,016	0%	149,9
2014_03_20	**8**	C51	0,000	0,999	0,5	5,001	159,3	164,2	0,016	0%	100,0
2014_03_20	**9**	C50	0,000	0,502	0,4	5,001	160,0	164,2	0,016	0%	100,0
2014_03_20	**10**	C58	0,000	0,137	2,2	5,001	158,6	163,7	0,016	0%	100,5
2014_03_20	**11**	C54	0,000	1,001	-0,6	5,001	207,4	214,3	0,016	0%	49,8
2014_03_20	**12**	C53	0,000	0,502	3,0	5,001	207,3	214,1	0,016	0%	50,1
2014_03_20	**14**	C57	0,000	1,002	2,1	5,001	240,1	249,2	0,016	0%	15,0
2014_03_20	**15**	C56	0,000	0,505	-1,2	5,000	238,7	249,5	0,016	0%	14,6
2014_03_20	**16**	C55	0,000	0,103	-7,9	4,999	236,7	249,3	0,016	0%	14,9
2014_03_21	**3**	C60	1,008	1,000	-1,3	5,002	107,2	64,5	0,295	100%	199,7
2014_03_21	**4**	C60	1,008	0,999	-0,6	4,981	108,2	63,9	0,299	100%	200,1
2014_03_21	**5**	C62	0,000	1,499	1,4	5,001	120,8	63,6	0,352	100%	200,6
2014_03_21	**6**	C62	0,000	1,500	-0,7	5,001	120,9	64,0	0,348	100%	200,2
2014_03_21	**7**	C61	0,000	1,995	-0,1	5,001	132,4	64,6	0,448	100%	199,6
2014_03_21	**8**	C61	0,000	1,995	-2,4	5,001	134,5	63,8	0,447	100%	200,4

Table 4.3: List of experiments in series C with measured boundary conditions

date (YYY_MM_DD)	Trig-ger	ExpID	FI8_41 / kg/s	FIC8_44 / kg/s	LIC8_01 / mm	PIC8_62 / MPa	TI8_33 / °C	TI8_48 / °C	FI_Steam / kg/s	bGasIs-Steam	T_Sub / K
2014_03_21	**9**	C63	0,000	1,002	1,8	5,000	109,5	64,3	0,297	100%	199,9
2014_03_21	**10**	C63	0,000	1,001	0,2	5,001	110,5	63,8	0,297	100%	200,4
2014_03_21	**11**	C64	0,000	0,501	0,5	4,999	111,5	63,7	0,234	100%	200,5
2014_03_21	**12**	C64	0,000	0,500	0,4	4,999	110,2	64,0	0,239	100%	200,2
2014_03_21	**14**	C65	1,006	0,999	0,6	5,001	138,0	114,3	0,264	100%	149,9
2014_03_21	**15**	C65	1,007	0,998	0,1	5,001	139,1	114,5	0,267	100%	149,7
2014_03_21	**16**	C67	0,000	1,500	-5,0	5,001	168,0	113,9	0,328	100%	150,3
2014_03_21	**17**	C67	0,000	1,498	-1,9	5,001	154,9	114,0	0,329	100%	150,2
2014_03_21	**18**	C66	0,000	2,002	-0,7	5,001	166,7	114,0	0,382	100%	150,2
2014_03_21	**19**	C66	0,000	1,999	0,0	5,001	166,1	114,6	0,383	100%	149,6
2014_03_21	**20**	C68	0,000	1,001	2,1	5,000	146,1	113,7	0,263	100%	150,4
2014_03_21	**21**	C68	0,000	0,999	0,0	5,000	147,3	113,8	0,275	100%	150,3
2014_03_21	**22**	C69	0,000	0,501	-0,1	4,999	143,6	114,1	0,228	100%	150,1
2014_03_21	**23**	C69	0,000	0,501	-0,2	4,999	143,4	114,1	0,229	100%	150,1
2014_03_24	**1**	C79	0,000	0,500	3,3	5,001	213,4	212,8	0,199	17%	51,4
2014_03_24	**2**	C79	0,000	0,503	6,5	5,001	214,7	214,0	0,211	100%	50,2
2014_03_24	**4**	C80	1,003	1,000	1,4	5,001	258,6	259,1	0,214	100%	5,1
2014_03_24	**5**	C80	1,002	0,997	0,5	5,001	258,7	259,2	0,213	100%	5,1
2014_03_24	**7**	C81	0,000	2,000	3,5	5,001	257,2	259,1	0,274	100%	5,1
2014_03_24	**8**	C81	0,000	2,000	-2,4	5,001	258,6	259,1	0,276	100%	5,1
2014_03_24	**9**	C82	0,000	1,511	0,5	5,001	253,3	257,9	0,229	100%	6,3
2014_03_24	**10**	C82	0,000	1,511	4,9	5,001	253,5	258,0	0,225	100%	6,2
2014_03_24	**11**	C83	0,000	1,000	-2,1	4,999	251,6	259,2	0,202	98%	5,0
2014_03_24	**12**	C83	0,000	1,000	2,6	4,999	253,3	259,2	0,202	100%	5,0
2014_03_24	**13**	C84	0,000	0,509	11,0	5,000	253,7	255,9	0,200	100%	8,3
2014_03_24	**14**	C84	0,000	0,500	-4,3	5,001	249,9	258,5	0,198	100%	5,7
2014_03_24	**15**	C84	0,000	0,499	0,6	4,999	252,0	259,0	0,201	100%	5,2
2014_03_24	**16**	C59	0,000	1,003	-6,9	5,000	245,7	244,1	0,238	100%	20,1
2014_03_24	**17**	C59	0,000	1,000	1,3	4,999	239,8	235,6	0,236	100%	28,6
2014_03_24	**18**	C59	0,000	1,005	1,8	4,999	235,3	223,5	0,238	100%	40,7
2014_03_24	**19**	C59	0,000	1,006	-2,4	4,999	227,6	210,2	0,238	100%	53,9
2014_03_24	**20**	C59	0,000	0,997	5,5	4,998	217,1	203,2	0,238	100%	61,0
2014_03_24	**21**	C59	0,000	0,998	-2,0	4,994	210,9	184,2	0,238	100%	80,0
2014_03_25	**3**	C91	0,000	1,503	1,0	2,502	87,5	29,1	0,244	100%	195,3
2014_03_25	**4**	C91	0,000	1,501	-1,9	2,502	74,3	29,3	0,245	100%	195,0
2014_03_25	**5**	C92	0,000	0,999	-1,3	2,501	62,0	26,7	0,182	100%	197,6
2014_03_25	**6**	C92	0,000	0,998	-0,2	2,501	59,1	26,6	0,181	100%	197,7

Table 4.3: List of experiments in series C with measured boundary conditions

date (YYY_MM_DD)	Trig-ger	ExpID	FI8_41 / kg/s	FIC8_44 / kg/s	LIC8_01 / mm	PIC8_62 / MPa	TI8_33 / °C	TI8_48 / °C	FI_Steam / kg/s	bGasIs-Steam	T_Sub / K
2014_03_25	**7**	C89	0,000	0,500	-1,4	2,499	56,1	24,5	0,166	100%	199,7
2014_03_25	**8**	C89	0,000	0,500	-1,3	2,499	57,5	24,4	0,163	100%	199,9
2014_03_25	**9**	C88	0,000	0,500	-0,7	2,501	98,8	74,5	0,163	100%	149,8
2014_03_25	**10**	C88	0,000	0,500	-0,2	2,501	98,7	74,5	0,161	100%	149,8
2014_03_25	**11**	C87	0,000	1,003	-2,3	2,501	104,1	74,1	0,167	100%	150,2
2014_03_25	**12**	C87	0,000	1,001	2,8	2,501	100,5	73,9	0,165	100%	150,4
2014_03_25	**13**	C90	0,000	1,500	-1,8	2,500	103,5	74,2	0,189	100%	150,1
2014_03_25	**15**	C90	0,000	1,500	-2,1	2,499	103,9	74,0	0,187	100%	150,3
2014_03_25	**16**	C85	0,000	1,503	-2,8	2,499	145,5	124,1	0,187	100%	100,2
2014_03_25	**18**	C85	0,000	1,500	2,3	2,499	143,4	124,0	0,185	100%	100,3
2014_03_25	**19**	C89	0,000	1,003	1,0	2,499	135,6	124,2	0,163	100%	100,1
2014_03_25	**20**	C86	0,000	1,003	0,9	2,499	135,5	124,0	0,162	100%	100,3
2014_03_25	**21**	C94	0,000	0,500	-1,1	2,499	137,5	124,3	0,125	100%	100,0
2014_03_25	**22**	C94	0,000	0,500	-1,9	2,499	137,5	124,1	0,126	100%	100,2
2014_03_25	**23**	C95	0,000	1,501	0,0	2,501	175,0	174,3	0,162	100%	50,0
2014_03_25	**24**	C95	0,000	1,499	-0,7	2,501	176,7	174,2	0,162	100%	50,1
2014_03_25	**25**	C96	0,000	1,002	-0,1	2,500	177,9	174,4	0,131	100%	49,9
2014_03_25	**26**	C96	0,000	1,004	1,2	2,500	177,2	174,1	0,134	100%	50,2
2014_03_25	**27**	C97	0,000	0,498	-2,8	2,499	175,6	174,4	0,115	100%	49,9
2014_03_25	**28**	C97	0,000	0,502	-2,0	2,500	177,0	173,9	0,116	100%	50,4

4.3.3 Results

Results of the high speed camera observation can be seen in figure 4.28. It is visible, that the plunging jet leads to entrainment of gas below the water surface in every experiment shown. It depends on the jet-inlet sub-cooling how deep the gas is carried down in the bulk liquid but in every all cases it condenses sooner or later. There is no plume of gas bubbles observed as it is the case when the gas is not condensable as shown in figure 4.29 (please note the different scaling!).

Entrainment - with or without condensation - is a very turbulent and fluctuating process and therefore it is not meaningful to compare single still images. As a first impression of the flow conditions, average images (as described in section 3.3) are shown in

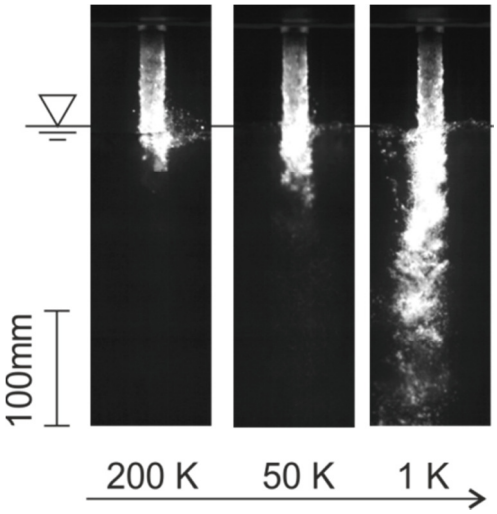

Figure 4.28: High speed camera stills of selected experiments with 1 kg/s jet mass flow rate and 50 bars pressure at different jet-inlet sub-cooling (in K at bottom)

figures 4.30 and 4.31. Here it can be observed, that the gas penetration depth is higher at higher inlet mass flow rate and with lower sub-cooling.

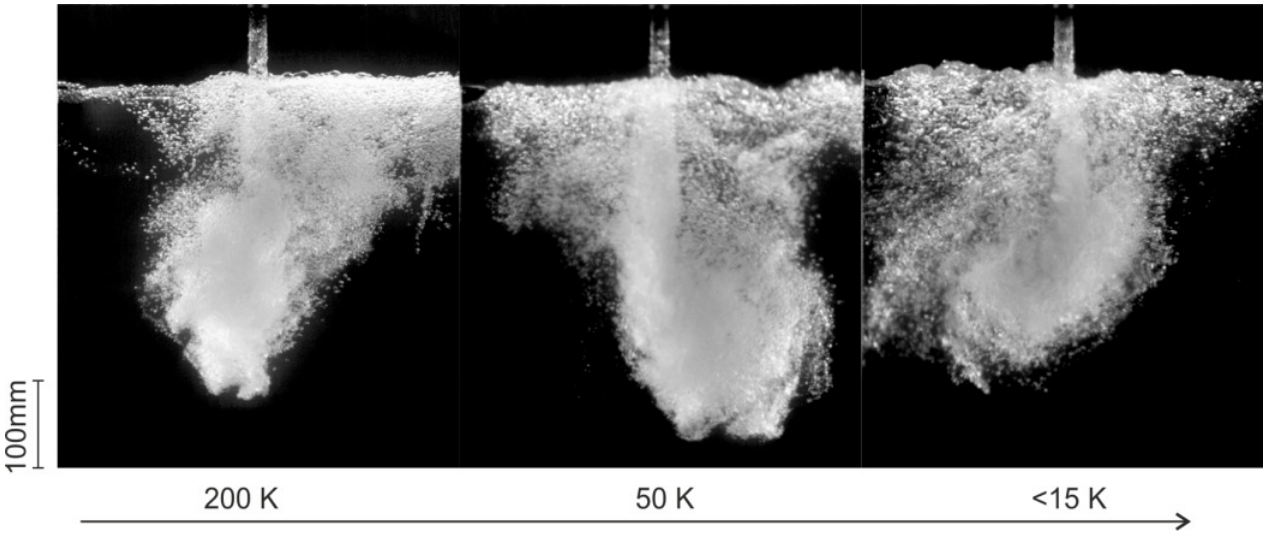

Figure 4.29: High speed camera stills of experiments similar to figure 4.28 but with nitrogen as gas atmosphere

A similar overview is given in figure 4.32 for the experiments with nitrogen atmosphere. Mass flow rates of 0.5 and 1 kg/s are compared and additionally the minimum entrainment mass flow rate was investigated. The latter were found by lowering the inlet mass flow rate stepwise and the corresponding flow rates are given in the figure. When the bubble entrainment stopped, the picture was taken. Only at 50 bars and low sub-cooling it was not possible to reduce the flow rate further, because heat losses in the pipes make setting a combination of low velocity and high temperature difficult and in some cases impossible. But it can be noted, that the onset of entrainment is lower at high pressure, which is due to the higher drag between gas and liquid and the lower density difference.

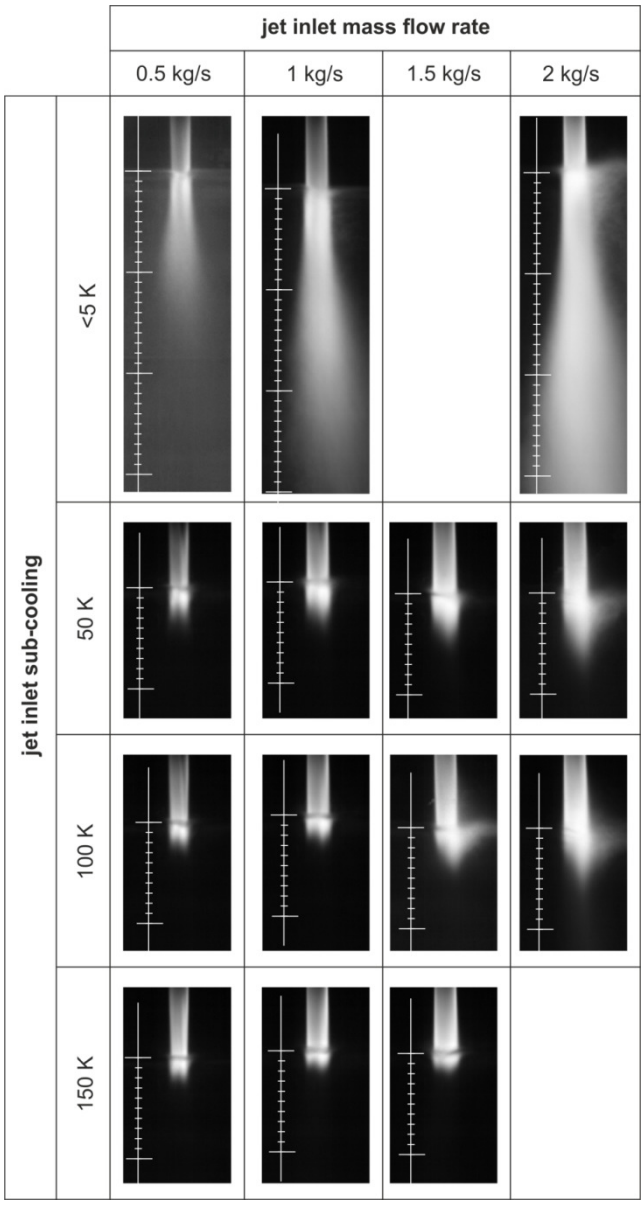

Figure 4.30: Overview of high speed camera average images for different conditions at 25 bar steam-water plunging jet experiments (the supporting scale on the side has a step-width of 1 cm for the small lines and is aligned to the water surface)

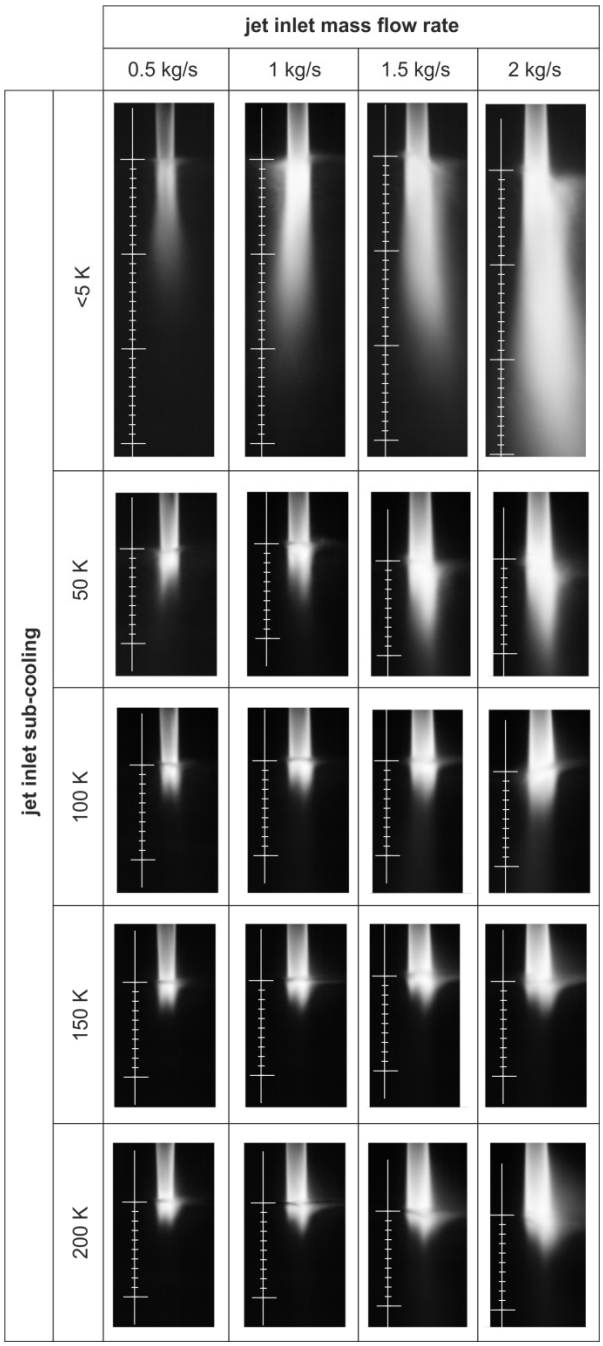

Figure 4.31: Overview of high speed camera average images for different conditions at 50 bar steam-water plunging jet experiments

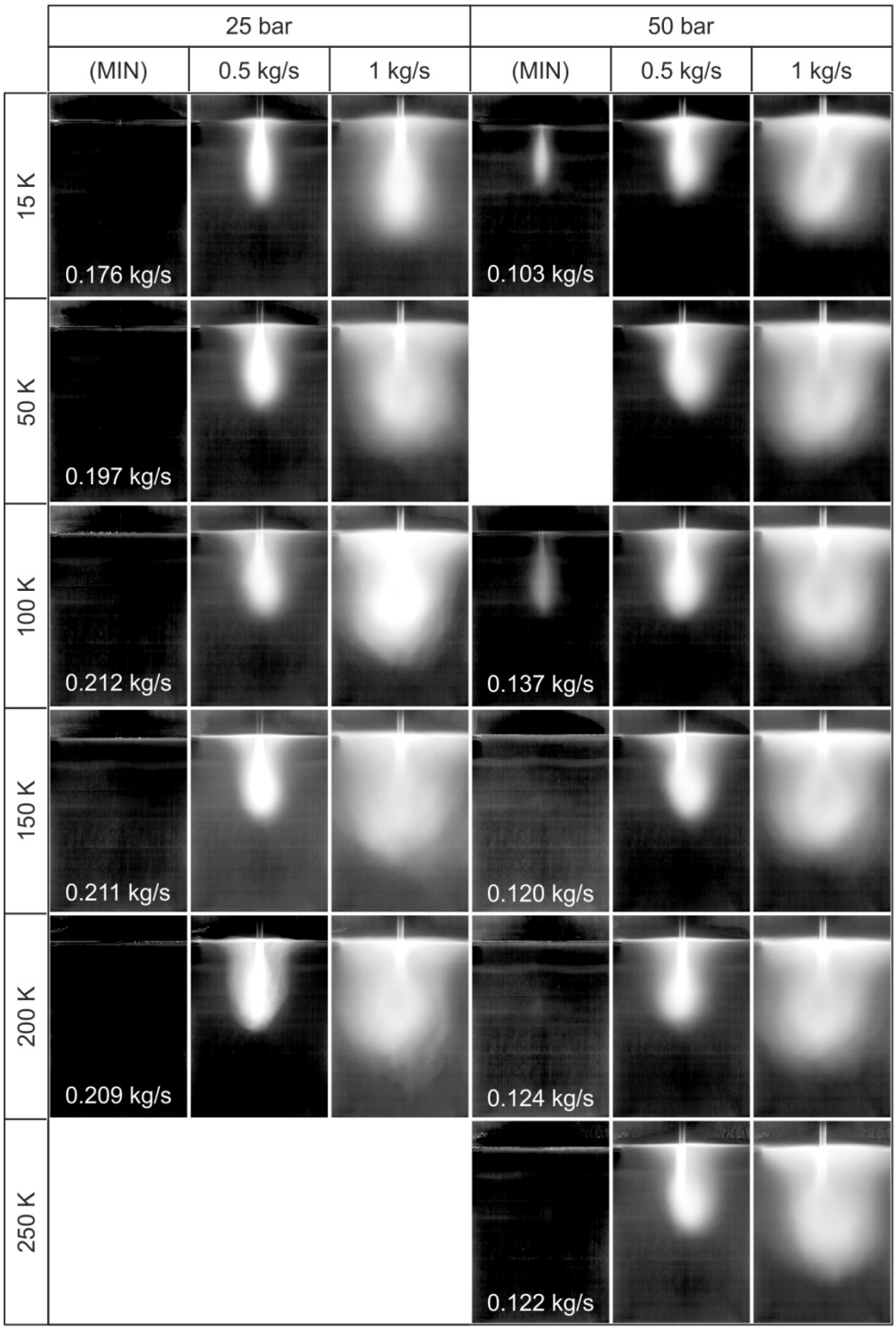

Figure 4.32: Overview of the high speed camera average images for different conditions at nitrogen-water plunging jet experiments (height of one image is about 650 mm)

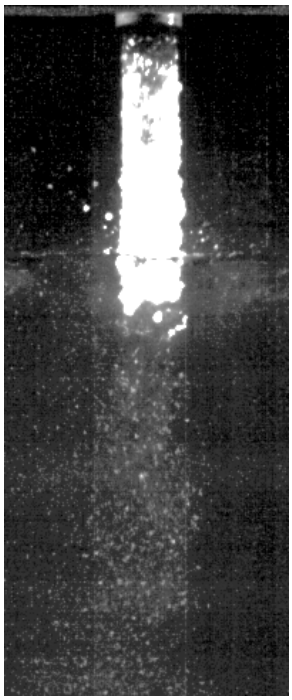

Figure 4.33: Contrast enhanced version of a high speed camera still showing steam condensation around a plunging jet with gas entrainment.

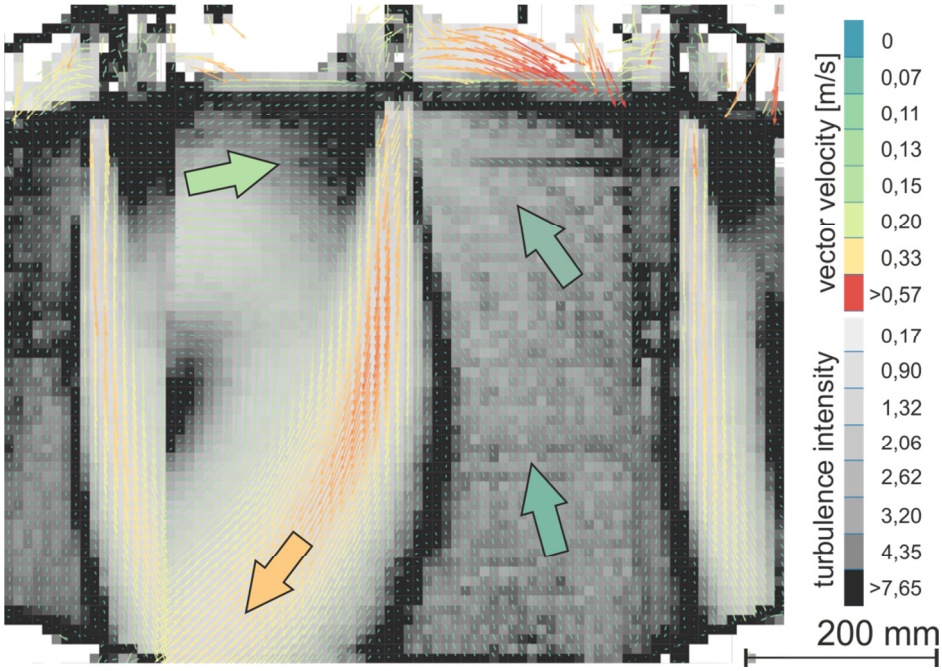

Figure 4.34: Field of liquid velocity and turbulence extracted from micro bubble tracks

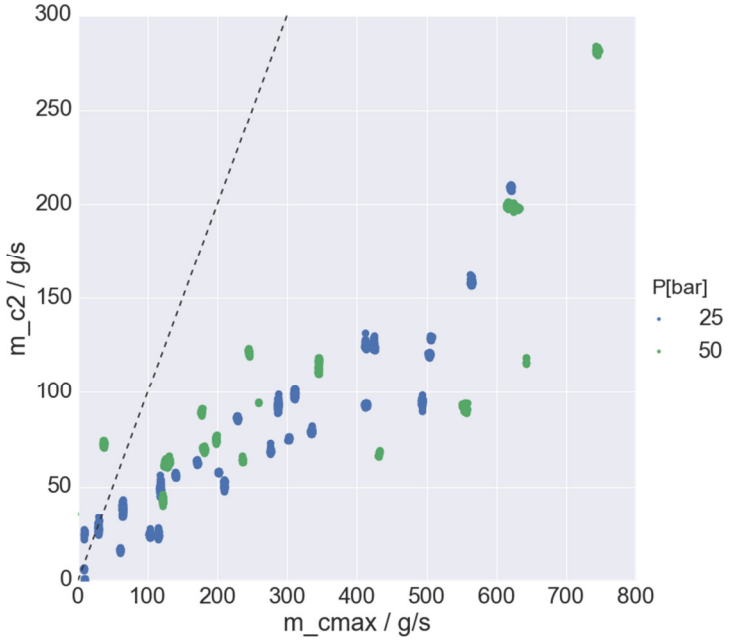

Figure 4.35: Comparison of measured condensation mass flow rate m_cm with maximum possible values m_cmax for all experiments in series C

As it can be seen in figure 4.33, very small gas bubbles are left over after steam bubbles collapse below the plunging point. These bubbles are supposed to be a result of dissolved nitrogen in the water, since they are not subject to further condensation and since the steam saturation temperature showed no signs of non-condensable gases in the steam phase. Because of the very small size, the nitrogen bubbles are dragged by the liquid flow and follow it practically without slip, so they can be used to determine the liquid velocity field by particle tracking. Figure 4.34 shows the result of particle tracking and averaging over time. Since the velocity field is obtained in every point in time, average velocity and turbulence intensity can be extracted from the images.

As presented above for the other experimental series already, figure 4.35 shows the distribution of measured condensation mass flow rates compared to the maximal possible rates. It is visible, that there is a broad distribution around 25%. So the effect is not too small to be measured as in series A and not too big to reflect the boundary conditions in the result as in series B.

5 Summary

Three different experimental series were presented with condensation at high pressures. The measurement technique and the procedures are explained in detail and the results of the three series are discussed separately.

Basically, it was observed, that the condensation process is relatively weak in stratified flow, strong in jet flow and intermediate in plunging jet flow. Interesting observations were the dependency of the jet flow diameter on the ambient pressure and the jet inlet sub-cooling.

How to access the raw data and the diverged data is explained in the appendix.

Acknowledgement

This work was carried out in the frame of a research project funded by the German Federal Ministry of Economic Affairs and Energy under project number 150 1411.

The authors thank the TOPFLOW operational team and workshop for their work regarding the building and operation of the experimental facility.

HZDR
HELMHOLTZ ZENTRUM DRESDEN ROSSENDORF

Bautzner Landstr. 400
01328 Dresden, Germany
Tel. +49 351 260-2047
Fax +49 351 260-12047
d.lucas@hzdr.de
http://www.hzdr.de

HZDR-066